RETARDATION OF CORROSION AND TRIBOLOGICAL DEGRADATION OF AUTOMOTIVE MATERIALS IN PALM BIODIESEL

SAZZAD BIN SHARIF

FACULTY OF ENGINEERING
UNIVERSITY OF MALAYA
KUALA LUMPUR

2016

RETARDATION OF CORROSION AND TRIBOLOGICAL DEGRADATION OF AUTOMOTIVE MATERIALS IN PALM BIODIESEL

SAZZAD BIN SHARIF

THESIS SUBMITTED IN FULFILMENT OF THE REQUIREMENTS FOR THE DEGREE OF DOCTOR OF PHILOSOPHY

FACULTY OF ENGINEERING
UNIVERSITY OF MALAYA
KUALA LUMPUR

2016

UNIVERSITY OF MALAYA
ORIGINAL LITERARY WORK DECLARATION

Name of Candidate: **Sazzad Bin Sharif**

Registration/Matric No: **KHA130054**

Name of Degree: **Doctor of Philosophy**

Title of Thesis: **RETARDATION OF CORROSION AND TRIBOLOGICAL DEGRADATION OF AUTOMOTIVE MATERIALS IN PALM BIODIESEL**

Field of Study: **Materials Engineering**

I do solemnly and sincerely declare that:

(1) I am the sole author/writer of this Work;
(2) This Work is original;
(3) Any use of any work in which copyright exists was done by way of fair dealing and for permitted purposes and any excerpt or extract from, or reference to or reproduction of any copyright work has been disclosed expressly and sufficiently and the title of the Work and its authorship have been acknowledged in this Work;
(4) I do not have any actual knowledge nor do I ought reasonably to know that the making of this work constitutes an infringement of any copyright work;
(5) I hereby assign all and every rights in the copyright to this Work to the University of Malaya ("UM"), who henceforth shall be owner of the copyright in this Work and that any reproduction or use in any form or by any means whatsoever is prohibited without the written consent of UM having been first had and obtained;
(6) I am fully aware that if in the course of making this Work I have infringed any copyright whether intentionally or otherwise, I may be subject to legal action or any other action as may be determined by UM.

Candidate's Signature Date:

Subscribed and solemnly declared before,

Witness's Signature Date:

Name:

Designation:

ABSTRACT

Biodiesel has been promoted as a potential candidate to replace fossil fuel partially or completely. However, unstable fuel properties of biodiesel hinders its commercialization in automobile sector. Several remedial studies have been done to reduce material degradation by means of fuel alteration and metal surface modification. Recent studies with different additives doped biodiesel in reducing corrosion and tribological degradation are found to be more feasible. However, inhibition mechanism of additives are still unexplored and remain a further scope of study. The present study aims to investigate the effect of additives along with the inhibition mechanism in reducing corrosion and tribological degradation of automotive materials in palm biodiesel. Static immersion tests were conducted for corrosion study by exposing cast iron and low carbon steel coupons in palm biodiesel at 300 K and 353 K for 50 days in the presence and absence of additives (tert-butyylamine (TBA), Benzotriazole (BTA), Butylate-dhydroxytoluene (BHT), Pyrogallol (PY)). Tribological study was performed using ball-on-plate (steel ball and cast iron plate) high frequency reciprocating rig (HFRR) at 300 K with applied load of 75 N and frequency of 33 Hz. Tert-butyylamine (TBA), Benzotriazole (BTA), Butylated hydroxyamisole (BHA) and Tert-butyl hydroxyl quinine (TBHQ) were used for reducing tribological degradation. Effects of additive-doped biodiesel and its blends on exposed metals surfaces were examined by corrosion rate, inhibition efficiency, adsorption isotherm, thermodynamic function for corrosion study and specific wear rate, frictional coefficient, specific film thickness, lubrication regime, adsorption for tribological study. Metal surface characterization was done by Atomic Force Microscopy (AFM), Scanning Electron Microscope (SEM)/ Energy Dispersive Spectroscopy (EDS), X-ray Diffraction (XRD) and X-ray Photoelectron Spectroscopy XPS. The result shows that TBA doped biodiesel has fairly good corrosion inhibiting properties and increases with increasing TBA concentration.

The higher inhibition efficiency could be attributed to the dominant physical adsorption which makes a protective layer over metal surface and prevents corrosion. In tribological study, results exhibit that TBHQ doped biodiesel derives a physicochemically adsorbed layer which suppresses the coefficient of friction and wear.

ABSTRAK

Biodiesel telah dinaikkan pangkat sebagai calon berpotensi untuk menggantikan bahan api fosil sebahagian atau sepenuhnya. Walau bagaimanapun, ciri-ciri bahan api tidak stabil biodiesel menghalang memperdagangkannya dalam sektor automobil. Beberapa kajian pemulihan telah dilakukan untuk mengurangkan degradasi bahan melalui pengubahan bahan api dan pengubahsuaian permukaan logam. Kajian baru-baru dengan bahan yang berbeza didopkan biodiesel dalam mengurangkan hakisan dan degradasi tribological didapati tidak lebih layak. Walau bagaimanapun, mekanisme perencatan bahan tambahan masih belum diterokai dan kekal sebagai skop lanjut pengajian. Kajian ini bertujuan untuk mengkaji kesan bahan tambahan bersama-sama dengan mekanisme perencatan dalam mengurangkan hakisan dan degradasi tribological bahan automotif di biodiesel sawit. ujian rendaman statik telah dijalankan untuk kajian kakisan dengan mendedahkan besi tuang dan kupon keluli karbon rendah di biodiesel sawit pada 300 K dan 353 K selama 50 hari di hadapan dan ketiadaan bahan tambahan (tert-butyylamine (TBA), Benzotriazole (BTA), Butylate -dhydroxytoluene (BHT), Pyrogallol (PY)). kajian Tribological dilakukan dengan menggunakan bola-on-plat (bola keluli dan membuang plat besi) pelantar salingan frekuensi tinggi (HFRR) pada 300 K dengan beban yang dikenakan 75 N dan kekerapan 33 Hz. Tert-butyylamine (TBA), Benzotriazole (BTA), BUTYLATED hydroxyamisole (BHA) dan tert-butil hidroksil kuinina (TBHQ) telah digunakan untuk mengurangkan degradasi tribological. Kesan biodiesel tambahan-didopkan dan campuran pada logam terdedah permukaan telah diperiksa oleh kadar kakisan, kecekapan perencatan, penjerapan isoterma, fungsi termodinamik untuk kajian hakisan dan kadar haus tertentu, pekali geseran, ketebalan filem tertentu, rejim pelinciran, penjerapan untuk kajian tribological. pencirian permukaan logam yang dilakukan oleh Atomic Force Microscopy (AFM), Mikroskop Imbasan Elektron (SEM) / Tenaga serakan Spektroskopi (EDS), X-ray Diffraction

(XRD) dan X-ray fotoelektron Spektroskopi XPS. Hasilnya menunjukkan bahawa biodiesel TBA didopkan mempunyai kakisan yang agak baik menghalang sifat dan meningkat dengan peningkatan kepekatan TBA. kecekapan perencatan yang lebih tinggi boleh dikaitkan dengan penjerapan fizikal yang dominan yang menjadikan lapisan perlindungan ke atas permukaan logam dan menghalang hakisan. Dalam kajian tribological, keputusan pameran yang biodiesel TBHQ didopkan berasal a physicochemically lapisan terjerap yang menyekat pekali geseran dan haus.

ACKNOWLEDGEMENT

At the outset, it is worth to express my profound gratitude and bow to the endless grace and mercy of the Almighty Allah without Whose desire I could not have materialized my dream to complete this thesis. At the same time, I take great pride to acknowledge my sincere gratitude to my respected supervisor Dr. Mohammad Abul Fazal, for his continuous unstinting and untiring inspiration, encouragement and valuable guidance towards the write up of this thesis. Without his scholastic and constructive criticisms, whole-hearted assistance, unfailing interest, continuous supervision and valuable suggestions throughout the period of this research, I could not conclude this thesis.

I would like to convey my deepest appreciation to my reverent grandmother Zaheda Begum, beloved parents (Md. Amin Sharif and Shakila Begum), Saila Sharmin, Ibrahim Khalilullah and Sameeha Najat who played a role model for giving me mental support and courage. Their ever-welcoming attitude and insatiable thirst for progress and excellence have been a limitless source of motivation for me.

I would also like to express my deepest gratitude and indebtedness for the kind cooperation of my co-supervisors Prof. A.S.M.A. Haseeb and Prof. H.H. Masjuki in the successful completion of this study.

I would also like to appreciate University Malaya Research Grant (RP013A-13AET) for financial support.

Last but not the least, there are many other people to whom I would like to thank for their help and support during study in University of Malaya especially Arafat Mahmood, Moin Quazi, Arslan Ahmed, Zaharuddin, Shariful Islam and Fayeka Mansura.

TABLE OF CONTENTS

LIST OF FIGURES

LIST OF TABLES

LIST OF SYMBOLS AND ABBREVIATIONS

B0 = Petroleum diesel

B20 = 20% Biodiesel in petroleum diesel

B100 = Biodiesel

A = Area

ASTM = American Society for Testing and Materials

BHT = Butylate-dhydroxy-toluene

BTA = Benzotriazole

C = Additive concentration

C_{Addi} = Concentration of additive

CI = Cast iron

C_R = Corrosion rate

C_{Ri} = Corrosion rate in presence of additive

D = Density

E = Average modules of elasticity

E_a = Activation energy

E_{ball} = Elastic modules of ball material

EDS = Energy dispersive X-ray spectrocopy

E_{plate} = Elastic modules of plate material

FAME = Fatty acid methyl ester

ISO - Organization of Standardization

ΔG_{addi} = Gibbs energy

HFRR = High frequency reciprocating rig

h_{min} = Minimum film thickness

k = Specific wear rate

K_{eqi} = Equilibrium constant

L = Load

LCS = Low carbon steel

m_{loss} = Mass loss

PY = Pyrogallol

R = Universal gas constant

$R_{a.ball}$ = Roughness of ball

$R_{a.plate}$ = Roughness of plate

R_c = Radius of curvature

SEM = Scanning electron microscopy

s = Sliding distance

T = Temperature

TBA = Tert-butylamine

t = Time

V = Surface velocity

W = Weight loss

XPS = X-ray photoelectron spectroscopy

XRD = X-ray diffraction

μ_{ac} = Frictional coefficient of doped biodiesel

μ_{bc} = Saturated frictional coefficient of doped biodiesel

μ_{blend} = Frictional coefficient of biodiesel blend

η = Inhibition efficiency

η_0 = Dynamic viscosity

θ = Surface coverage

ρ = Density of material

λ = Specific film thickness

ν_{ball} = Poisson ratio of ball material

ν_{plate} = Poisson ratio of plate material

CHAPTER 1: INTRODUCTION

1.1 Research Background

Increasing demand of biodiesel pave the way to use it as potential alternative fuel (De Silva et al., 2011; Demirbas & Ayhan, 2007; Lenauer et al., 2014). However, biodiesel as a substitute has to be technically feasible and similar properties to that of diesel fuel (Deng et al., 2011; Fazal, MA, et al., 2011a; Hoekman et al., 2012; Thamsiriroj & Murphy, 2011). Pure biodiesel (B100) significantly minimizes polycyclic aromatic hydrocarbons emissions by 19.4% (Chao He et al., 2010). B100 inherently offers better lubricity because of having high affinity of esters to metal. Polar group of ester forms protective layer on tribo-contact surface which is advantageous for engine wear and friction (Goodrum & Geller, 2005; Kalam, MA., & Masjuki., 2008; Knothe, 2005; Knothe & Steidley, 2005b; Masjuki, HH., & Maleque, 1996). Conversely, susceptibility of biodiesel to oxidation is the major drawback due to its unsaturated hydrocarbon like oleic acid, linoleic acid and linolenic acid (Fazal, MA, et al., 2011b; Sarin et al., 2009). Double bonded carbon atoms presence in unsaturated fatty acid also responsible for the easy formation of a peroxide (ROO) or hydro-peroxides (ROOH) compound. This oxidative nature leads to oxidative wear in the presence of biodiesel (Yaakob et al., 2014). Hygroscopic nature of biodiesel leads to hydrolysis of ester bonds and forms free fatty acid molecules (Haseeb et al., 2010; Sørensen, Gitte, et al., 2011). This unstable fuel properties of biodiesel and its blends seems to be more aggravated when fuel comes in contact of automotive materials.

Currently, automobile companies are not offering a warranty for more than 5% blends of biodiesel with diesel. According to Kousoulidou et al. and Shahir et al. (Kousoulidou et al., 2012; Shahir, K., et al., 2015), maximum blending ratio of saturated biodiesel can be 30% which reduces emissions without significantly affects vehicle parts. It has been reported that B20 (20% biodiesel and 80% diesel) significantly minimizes polycyclic aromatic hydrocarbons emissions 13.1% (Chao He et al., 2010). Lower blended biodiesel yields reduced knock of residual oxygen in combustion chamber especially for B20. B20 has very little impact on power and torque which is not noticeable by the user (Lin et al., 2009). B20 still could be the reason for higher corrosion and oxidative wear which throws a challenge against compatibility of material-fuel interface (Kousoulidou et al., 2010).

Quite a number of studies on tribology (Fazal et al., 2013b; Fazal & MA. Haseeb, 2014; Morris et al., 2013; Tung & McMillan, 2004) and corrosion (Chew et al., 2013; Cursaru et al., 2014; Fazal et al., 2010, 2012, 2013a; Haseeb A.S.M.A et al., 2010; Hu et al., 2012; Singh et al., 2012) of automotive materials exposed to various biodiesel and their blends have been conducted to quantify the compatibility. Their research studies are mostly on lower percentage of biodiesel blend (Shahabuddin et al., 2012). Higher percentage of biodiesel aroused compatibility issue and causes some other technical problems. Therefore, remedial measures are great issues of concern in order to enhance the performance and life span of automotive material while using biodiesel. Various synthetic additives against the corrosion and tribological degradation have been investigated by a few researchers (K. A. Sorate & Bhale, 2015). Yıldırım et al. (Yıldırım & Cetin, 2008) reported that the effectiveness of inhibitors depends on the adsorption capability on metal surfaces. Scholars have used an adsorption isotherm model to describe the mobility of different components in the aquatic environment (adsorbate) attached to the solid surface (adsorbent) via physical or chemical bonds (Foo & Hameed, 2009, 2010). Adsorbent with large porous surface area, high thermostability and degree of affinity, and low acid/base reactivity plays vital roles in binding of organic and inorganic components (El Qada et al., 2008). Adsorption occurs through electrostatic attraction between the charged molecules and the charged metal (spontaneous physical adsorption) or interaction of the unshared electron pairs with the molecule or π-electrons of nitrogen atom or with the metal (chemisorption) (Li et al., 1997). In these processes, inhibitors can function as the adsorbate medium to initiate the bond formation of different components in the adsorbent to the adsorbate. In case of corrosion inhibitors (bearing N, O, or S heteroatoms), amine-based inhibitors show improved corrosion inhibition by either physical or chemical adsorption mechanism (Li et al., 1997). While, for lubricity (Y.-C. Lin et al., 2013), physical adsorption of OH containing additives and local hydrodynamic factor of lubricant dominate the tribological behavior.

Some efforts have already been given by researchers to characterize the corrosion and tribological behavior of different metals in biodiesel. However, there is very limited information on its remedial measure and did not reveal the related inhibition mechanism. Therefore, based on the motivation of previous studies, this study is undertaken to investigate the effect of additives on reducing the corrosiveness and improve the lubricity of biodiesel. The effect of corrosion inhibitors in reducing corrosion of ferrous metals was determined through analysis of adsorption isotherms and thermodynamic parameters. The underlying mechanism of adsorption also discussed to some extent. Meanwhile, effect of additives on the lubricity improvement was studied and related mechanism was also explained.

1.2 Objective

1. To examine the effect of additives on the corrosion of automotive materials in palm biodiesel.
2. To investigate the inhibition mechanism in reducing corrosion.

3. To examine the effect of additives on the tribological degradation of automotive materials in palm biodiesel.
4. To investigate the inhibition mechanism in reducing tribological degradation.

1.3 Scope of the study

Immersion test was conducted in order to assess the corrosiveness of biodiesel and its blends. Tribological test by high frequency reciprocating test rig (HFRR) was conducted for evaluation of biodiesel lubrication. Atomic Force Microscopy (AFM), Scanning Electron Microscope (SEM)/ Energy Dispersive Spectroscopy (EDS), X-ray Diffraction (XRD) and X-ray Photoelectron Spectroscopy XPS.

1.4 Organization of Thesis

This thesis organized with five chapters. First chapter is about research background and objective of this study. In chapter 2, elaborated literature review is presented about effect of different factors on fuel stability, material degradation and their remedies. Chapter 3 contains materials and methods for this study with detail experimental setup. Chapter 4 includes experimental results and discussions of obtained results respectively. Conclusion of this research work is drawn in chapter 5 along with constructive recommendation and potential possibilities for further study.

CHAPTER 2: LITERATURE REVIEW

2.1 Introduction

The hike in petroleum diesel consumption in the automobile sector has led to a rapid depletion of fossil fuels (Höök & Tang, 2013; Shafiee & Topal, 2009). This alarming growing demand for fuel has led to the consideration of alternative energy sources. Exhaust emissions after burning of gasoline and diesel also pose a significant threat to the environment (Lapuerta et al., 2008). Stringent regulations such as EN-590 and ASTM D 975 have been legislated to reduce diesel emissions (Ghazali et al., 2015; Lapuerta et al., 2008). Hydro-treatment of diesel reduces emission, but its poor contents of sulfur and polar nitrogen compounds cannot provide adequate lubricity. The European Union (EU) has improved the lubricity of diesel by allowing the 5.75% blend of biodiesel into petro-diesel, which also provides minimum emissions (Cursaru et al., 2014; Shahir, A., et al., 2015). Thus, biodiesel received widespread acceptance as an anti-wear additive and emission inhibitor for diesel engines (Ashnani et al., 2014). The increasing demand for biodiesel established it as a potential alternative fuel (De Silva et al., 2011; Demirbas & Ayhan, 2007; Lenauer et al., 2014). However, biodiesel as a substitute must be technically feasible and should exhibit properties similar to those of diesel fuel (Deng et al., 2011; Fazal, MA, et al., 2011a; Hoekman et al., 2012; Thamsiriroj & Murphy, 2011). Pure biodiesel (B100) significantly minimizes polycyclic aromatic hydrocarbon emissions by 19.4% (Chao He et al., 2010). B100 inherently offers enhanced lubricity because of the high affinity of esters to metals. The polar group of esters forms a protective layer on the tribo-contact surface, which is advantageous in reducing engine wear and friction (Goodrum & Geller, 2005; Kalam et al., 2008; Knothe, 2005; Knothe & Steidley, 2005b; Masjuki et al., 1996). Conversely, the susceptibility of biodiesel to oxidation is a major drawback because of its unsaturated hydrocarbons, such as oleic acid, linoleic acid, and linolenic acid (Fazal, MA, et al., 2011b; Sarin et al., 2009). The presence of double-bonded carbon atoms in mono- (C_nH_{2n-1}-COOH), di- (C_nH_{2n-3}-COOH), tri- (C_nH_{2n-5}-COOH), and poly-unsaturated fatty acids are also responsible for the easy formation of a peroxide (ROO) or hydro-peroxide (ROOH) compound. This oxidative nature of biodiesel may lead to oxidative wear in automotive materials (Yaakob et al., 2014). The hygroscopic nature of biodiesel leads to the hydrolysis of ester bonds and the formation of free fatty acid molecules (Gitte Sørensen et al., 2011).These unstable fuel properties of biodiesel and its blends appear more aggravated when fuel comes in contact with automotive materials. At present, automobile companies do not offer a warranty for diesel with >5% blends of biodiesel (Haseeb et al., 2011). According to Kousoulidou et al. (Kousoulidou et al., 2012; Shahir, K., et al., 2015), the maximum blending ratio of saturated biodiesel can reach 30%, which reduces emissions without significantly affecting the vehicle parts. B20 (20% biodiesel and 80% diesel) significantly minimizes polycyclic aromatic hydrocarbons emissions by 13.1% (Chao He et al., 2010). Low yields of blended biodiesel reduced the knock of residual oxygen in the combustion chamber, particularly for B20. However, B20 slightly influences the power and torque, and this effect is unnoticeable to the user (Lin et al., 2009). Moreover, B20 is the possible reason for the increased corrosion and oxidative wear, which challenges the compatibility of material–fuel interface (Kousoulidou et al., 2010). Several studies on tribology (Fazal et al., 2013b; Fazal & MA. Haseeb, 2014; Morris et al., 2013; Tung & McMillan, 2004) and corrosion (Chew et al., 2013; Cursaru et al., 2014; Fazal et al., 2010, 2012, 2013a; Haseeb A.S.M.A et al., 2010; Hu et al., 2012; Singh et al., 2012) of automotive materials exposed to various biodiesel and their blends have been conducted to quantify the compatibility. These studies are mostly focused on the low percentage of biodiesel blend (Shahabuddin et al., 2012). The high percentage of biodiesel has elicited compatibility issues and other technical problems. Therefore, remedial measures are of considerable concern to enhance the performance and life span of automotive materials while using biodiesel. Various synthetic additives to prevent corrosion and tribological degradation have been investigated by different researchers (K. A. Sorate & Bhale, 2015). For the sake of scope, this chapter summarizes the recently published data on the corrosion and tribological degradation studies along with the corresponding solutions. This review also intended to focus on the physical and chemical aspects of various biodiesel feedstocks.

2.2 Major feed-stocks and production of biodiesel

The use of biodiesel is increasing worldwide. In many countries, depending on their climate and soil condition, various vegetable oils have been emphasized in feedstock production to produce biodiesel (Barnwal & Sharma, 2005). Table 2.1 lists the major biodiesel-producing countries, the percentage of total biodiesel production from various feedstocks, the biodiesel yielding ratios, and the corresponding costs. To address the rising demand of biodiesel, the production of feedstocks with high biodiesel yielding ratio should be increased. Among the feedstocks, palm is ranked first, followed by soybean and rapeseed. Malaysia and Indonesia produce the highest amounts of palm feedstock with low cost, among other feedstock-producing countries.

Table 2.1: Major biodiesel-producing countries, percentage of total biodiesel production from various feedstocks, biodiesel yielding ratio, and corresponding costs (Ghazali et al., 2015; Mosarof et al., 2015)

Feed-stocks	% of total biodiesel production	Country of origin	Production (kg/ha)	Catalyst	Biodiesel yield (wt%)	Cost ($/ton)
Palm	39	Indonesia, Malaysia	5000	NaOH KOH	42-45	478
Soybean	26	China, Argentina, Brazil, Russia, USA	375	NaOH KOH CaO/Silica	20	684
Rapeseed	16	Finland, France, Germany, Russia, Sweden, UK, Italy	1000	No	37-50	683
Sunflower	9	Russia, Spain, Russia, EU, Ukraine	952	CaO/SBA-14 NaOH	35-45	200-300
Peanut	3	China, India	1059	-	45-55	-
Coconut	2	Philippine, Thailand	2689	NaOH	63-65	-
Jatropha	-	China, India, Philippine, Thailand, Indonesia	1590	H2SO4/KOH NaOH	40-60	400

Biodiesel is produced from either vegetable oils or animal fats, which comprises triglycerides consisting of three long-chain fatty acids (Barnwal & Sharma, 2005; S. Singh & Singh, 2010). Fatty acids themselves are carboxylic acids with long unbranched aliphatic chains (with 4 to 28 carbon atoms), composed of hydrogen atoms attached to the carbons. Compared with petroleum diesel, biodiesel is more acidic in nature and may cause enhanced degradation of exposed metal surfaces. Therefore, the use of alkaline catalysts in producing biodiesel would be more logical. The presence of a residual alkaline catalyst may help to neutralize or reduce the acidic nature of biodiesel, thereby decreasing its affinity to a metal surface (Johari et al., 2015).

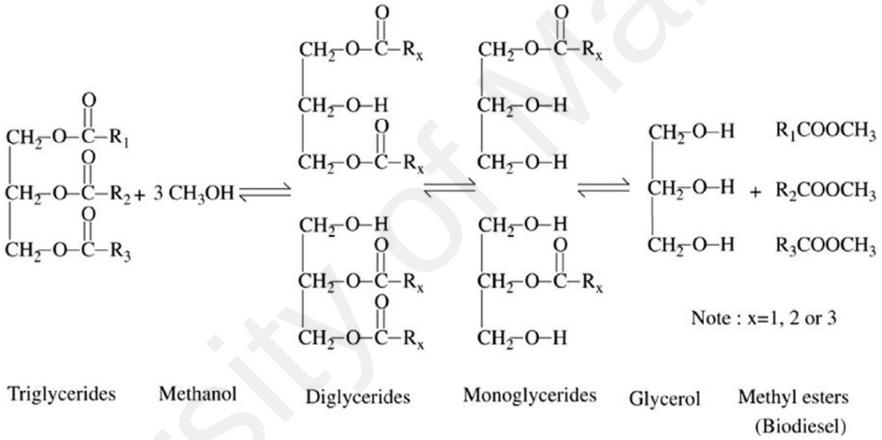

Figure 2.1: Biodiesel (methyl esters) prepared by trans-esterification from vegetable oils (triglyceride) with alcohol at 60 °C to 70 °C in the presence of a catalyst (R1,2,3: Alkyl group) (Ashnani et al., 2014; Mofijur et al., 2013).

2.3 Properties of biodiesel

2.3.1 Physical properties

Pure biodiesel derived from different feedstocks can significantly affect the unique physical properties, which are listed in Table 2.2 The structural formula of individual fatty acid methyl esters (FAMEs) can significantly influence the biodiesel properties (Gopinath et al., 2015). Properties such as total acid number, viscosity, density, induction period, flash point, and cetane number crucially affect the friction, material surface wear, biodiesel lubricity, performance, and emission (Knothe, 2008; C.-Y. Lin

& Lin, 2006; Rizwanul Fattah et al., 2013; Szybist et al., 2007). Therefore, different standards such as ASTM and EU have fixed the range of each property. The consequences of using a biodiesel outside the ASTM and EU standards can cause severe complications such as corrosion, fuel degradation, filter clogging, poor combustion, and low performance. Table 2.2 indicates that biodiesel with higher viscosity achieves higher lubricity, but the value remains below the standard. Only palm biodiesel showed the highest lubricity among the other feedstocks. A possible reason is its higher degree of unsaturated fatty acid, which demonstrates superior lubricity compared with its saturated fatty acid percentage. The longer carbon chain of saturated fatty acids existing in palm biodiesel is the major cause of its higher lubricity. The value of the kinematic viscosity of biodiesel remains less than that of diesel fuel because of its sulfur content. Table 2.2 shows that biodiesel from all feedstocks yielded higher cetane numbers than those of diesel fuel, and such values result in reduced knock and emission. The presence of O_2 (11%) ensures that complete combustion results in reduced emissions (Shahabuddin M et al., 2013). Qi et al. (Qi et al., 2009) further showed improved results by using 10% methanol containing 50 wt% O_2 in biodiesel. Furthermore, biodiesel exhibits low CO_2 emission because of lower elemental carbon to H_2 ratio (Kegl et al., 2013; Lin et al., 2011). The almost zero content of sulfur in biodiesel indicates a benefit over mineral diesel because of its desulfurization behavior (Kegl et al., 2013; Pehan et al., 2009).

Despite the number of favorable physical properties of biodiesel, direct uses of pure methyl ester (B100) as fuel without blends are not suitable. Given that physical properties such as high viscosity, low volatility, and moisture absorption, natural gum (phosphatides) reactivity of unsaturated hydrocarbon chains (K. A. Sorate & Bhale, 2015) poses poor atomization, carbon deposition, ring sticking, injector coking, injector pump failure, lubricating oil dilution, and crank-case polymerization in diesel engine

(Agarwal & Das, 2001; Knothe & Steidley, 2005a; Sarin et al., 2009; K. A. Sorate & Bhale, 2015). Though Shahabuddin et al. reported that the presence of O_2 in pure biodiesel ensures complete combustion (Shahabuddin M et al., 2013), all biodiesels demonstrate lower oxygen stability compared with diesel, which causes rapid oxidation. Oxidized biodiesel reduces the flash point and cetane number by increasing its degree of unsaturation (C.-Y. Lin & Chiu, 2010). In addition, the presence of O_2 decomposes unsaturated fatty acids; such decomposition is responsible for the low heating value (Agarwal, 2007; Arkoudeas et al., 2003). The low values of flash point and cetane number are responsible for incomplete combustion, thereby increasing the brake-specific fuel consumption (BSFC) (Habibullah et al., 2015). Considering the disadvantages of these physical properties, researchers proposed the following simple solution after long-term comparative endurance tests: partially substituted mineral diesel with biodiesel can overcome most operational and durability concerns.

Table 2.2: Physical properties of biodiesel from major feed-stocks and mineral diesel

Feed stocks	Density (g/cm^3)	Kinematic viscosity (cSt)	Lubricity (µm)	Cloud point (°C)	Pour point (°C)	Flash point (°C)	Sulfur Content mg/kg	Cetane number	Oxidation stability (h)	Calorific value (MJ/kg)	Ref.
Coconut	0.93	3.08	-	5	-	-	0.009	70	8.1	38.16	(Jayadas & Prabhakaran Nair, 2007; Kalam et al., 2003)
Palm	0.88	5.7	460	13	-	164	-	62	7.2	38.69	(Benjumea, Agudelo, & Agudelo, 2008; Shiotani & Goto, 2007)
Jatropha	0.85	4.72	-	-	3	182.5	0.02	53	3.7	-	(Palash et al., 2014)
Peanut	0.848	4.42	-	5	-8	166	-	53.59	-	33.6	(Kaya et al., 2009)
Soybean	0.913	4.5	375	2	-1	171	-	53	1.28	39.6	(Ali et al., 1995; Hu et al., 2005; Murugesan et al., 2009)
Sunflower	0.916	4.6	123	7.2	- 15.0	274	-	52	2.7	39.6	(Cursaru et al., 2014; Hill, 2002)
Rapeseed	0.884	4.5	310	-2	-9	84	5	54.7	4.5	39	(Goodrum & Geller, 2005; Sulek et al., 2010)
Diesel	0.82	3.4	535	-15	-33	52	10	45	110	43.2	(Benjumea et al., 2008)
Standard range	[a]0.860-0.900	[b]3.5-5.0	[c]400-520	[d]-	[e]-6	[f]120	[g]10	[i]51	[j]6	[k]-	(Knothe, 2006)

Note: a- EN ISO 3675/12185, b- EN ISO 3104/ 3105, c- ASTM D-6079, d-ASTM D2500, e- ASTM D 97, f- EN ISO 3679, g- EN ISO 20846/ 20884, i- EN ISO 5165, j- EN 14112, k- DIN 51900-2

2.3.2 Chemical properties

Petroleum diesel normally contains 75% aliphatic hydrocarbon and 25% aromatic hydrocarbon with no oxygen. By contrast, biodiesel comprises of 40% unsaturated components with the presence of 11% oxygen. Naturally, biodiesel is less stable and more corrosive than diesel; biodiesel is also very sensitive to light, temperature, and metal ions. It can be attributed to the unstable degree of functionality which refers to the number of reactive polar groups present in the biodiesel molecule. The compositional stability of biodiesel can be affected by its hygroscopic and auto-oxidative nature, microbial growth, interaction with metals, temperature, and so on. (Fazal, MA, et al., 2011b; Jakeria et al., 2014). It is seen in Figure 2.2 that saturated fatty acids, with the general formula $C_nH_{2n+1}COOH$, consist of single carbon–carbon bonds; hence, saturated fatty acids do not readily accept any additional hydrogen atoms. By contrast, unsaturated fatty acids consist of more than one carbon–carbon double bonds (Gopinath et al., 2015). Double-bonded unsaturated fatty acids in biodiesel are reactive, making biodiesel chemically unstable (Kajdas & Majzner, 2001; Yamane et al., 2007). However, biodiesel in pure form has been reported to be chemically stable (Melero et al., 2010). During storage, transportation, and utilization, biodiesel degrades and becomes corrosive (Lee et al., 2010). The degradation of composition also depends on different feedstocks and their susceptibility to various metals.

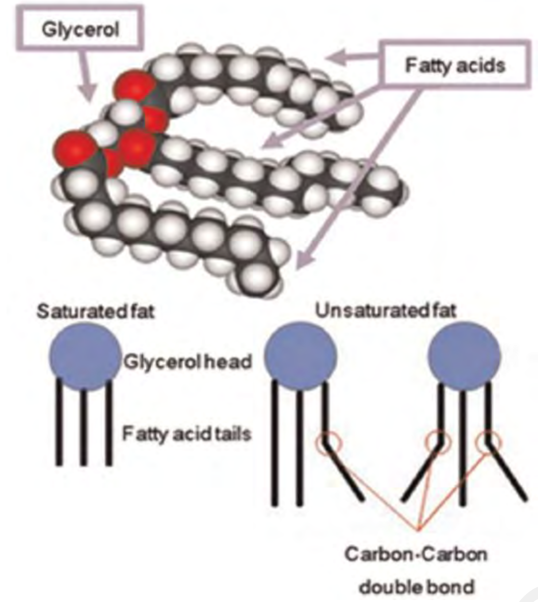

Figure 2.2: Diagram represents a triglyceride, a saturated fat and an unsaturated fat (Gopinath et al., 2015)

Table 2.3: Chemical properties of fatty acid and susceptibility to automotive materials

Feed-stocks		Saturated fatty acid mass %	Mono-unsaturated fatty acid mass %	Poly-unsaturated fatty acid mass %		Oxidiz-ability %	Susceptibility to metal	Ref.
		(Plamitic and Stearic acid) $R(CH_2)_{14}$-COOH and $R(CH_2)_{16}$-COOH	(Oleic acid) $R(CH_2)_7$-CH=CH-$(CH_2)_7$COOH	(Linoleic acid) $R(CH_2)_4$-CH=CH- CH_2 –CH=CH-$(CH_2)_7$COOH	(Linolenic acid) $R(CH_2)_4$-CH=CH- CH_2 –CH=CH- CH_2 –CH=CH-$(CH_2)_7$COOH			
	Lipid number	C16:0 and C18:0	C18:1	C18:2	C18:3			
	Degree of unsaturation	1	2	3	4			
Coconut		92.4	6.2	1.4	0	0.015	-	(Jakeria et al., 2014; Yaakob et al., 2014)
Palm		47.7	41.9	10.4	0	0.112	Cu>Brass>Al> Cast iron>Mild-steel> Stainless steel	(Atadashi et al., 2012; Fazal et al., 2010; Fazal et al., 2014; Fazal & MA. Haseeb, 2014)
Jatropha		21.3	44.7	32.8	0.2	0.340	Cu>Co>Mn>Ni>Fe	(A. Kumar & Sharma, 2008; Pasqualino, C., et al., 2006)
Peanut		19.3	47.1	33.6	0	-		(Pasqualino, C, et al., 2006)
Soybean		15.6	18.8	56.1	8.5	0.734	Carbon steel>galvanized steel	(Jakeria et al., 2014)
Sunflower		9.3	43.7	47	0	0.478	Cu> Mild carbon steel>Al	(Cursaru et al., 2014)
Rapeseed		5.6	21.9	72.5	0	-	Cu> Carbon steel>Al>Stainless steel	(Hu et al., 2012)

Note: $R=CH_3$

As shown in Table 2.3, feedstocks achieve different values of saturated fatty acids. Coconut and palm yield higher amounts of saturated fatty acids than those obtained by *Jatropha*, soybean, sunflower, and rapeseed. The degree of saturation does not always determine the oxidation stability. For instance, despite the higher degree of saturation than those in sunflower and rapeseed, soybean shows lower oxidation stability because of the highly reactive bis-allylic hydrogen in poly-unsaturated linoleic acid methyl ester. The oxidation stability index (OX) can provide further clarification. Soybean presents the highest value of oxidizability because of the high percentage of oleic (O), linoleic (L), and linolenic (Ln) acid methyl esters (Cosgrove et al., 1987). Various blends of biodiesel (B5-B20) have been adopted to improve its service life (Fazal, MA, et al., 2011a; C.-Y. Lin & Lin, 2006). Although conventional petroleum diesel is projected to be replaced partially by biodiesel, certain chemical issues hinder its potential commercial applications (Stedile et al., 2015); these issues will be described later. These limitations can be solved by either material modification or chemical alteration of biodiesel.

2.4 Benefits of biodiesel

As a potential alternative to petroleum diesel, biodiesel often elicits research attention. The properties of biodiesel are identical to those of petroleum diesel. More importantly, biodiesel is a renewable and nontoxic fuel, which significantly reduces toxic emissions when burned. During combustion, biodiesel liberates lower levels of hydrocarbons, carbon monoxide, polycyclic aromatic hydrocarbons, sulfur dioxide, and smoke than those of regular diesel (Ryu, 2009). Thus, biodiesel is considered an environmentally friendly and sustainable alternative to fossil fuels. The combustion of biodiesel can ensure 90% decrement in total unburned hydrocarbons and polycyclic aromatic compounds compared with diesel (Mohsin et al., 2014). Biodiesel offers excellent lubricity properties compared with diesel because it contains free fatty acids made of hydrocarbon; these acids contain polarity-imparting oxygen atoms (Ryu, 2009). Thus, biodiesel often acts as an additive to improve the lubricity of ultra-low sulfur diesel (ULSD) (Ryu, 2009). Biodiesel can be well mixed with diesel, thereby helping to improve diesel properties. For example, biodiesel blends can benefit ULSD by improving its flash point, lowering the overall exhaust emissions and toxicity (B. R. Moser & Vaughn, 2010). The higher cetane number of biodiesel produces less noise and shortens the ignition delay (Ryu, 2009). From the perspective of combustibility, the higher flash point of biodiesel makes it one of the safest alternative fuels to replace diesel.

2.5 Nature of biodiesel

Although biodiesel exhibit properties very similar to those of petroleum diesel, the major concerns of using biodiesel in diesel engines persist. These concerns include corrosiveness, hygroscopic nature, and auto-oxidation (Jakeria et al., 2014). When the oxidation rate increases, the total acid number increases and can cause corrosion in metal parts (Sarin et al., 2009). Oxidation can indirectly increase wear and reduce the lubricity of engine parts (Fazal et al., 2013b). During long-term storage, the compositions can be changed because of the presence of air, sunlight, temperature, or material of storage container. Storage instability can degrade fuel properties such as induction period, acid value, and viscosity. If the storage duration is extended, the acid value, peroxide value, density, and viscosity will increase (Jakeria et al., 2014).

2.5.1 Oxidation

Biodiesel is chemically degraded by oxidation, which occurs because of aerobic contact during storage. The degradation of biodiesel also occurs by hydrolysis and thermal decomposition. Auto-oxidation is responsible for the formation of hydro-peroxides

(ROOH) (Fattah et al., 2014). The situation becomes more complicated in case of metal-assisted secondary oxidation reaction, which finally results in products such as organic acids, aldehydes, dimers, and polymers (Muik et al., 2005). The oxidation of biodiesel also depends on the solubility of water in it. During storage, transportation, and application, water can be condensed and interpose a thin layer of water-biodiesel mixture between the biodiesel and the metal surface (Wang et al., 2011). This water reconverts esters into long chain fatty acids via hydrolysis, thereby increasing the degree of unsaturation and causing auto-oxidation (DeMello et al., 2007). The oxidation rate of biodiesel can be determined by the number of allylic and bis-allylic methylene moieties adjacent to C=C bonds of oleic acid, linoleic acid, and linolenic acid (Figure 2.3) (Bouaid et al., 2007). Relative oxidation susceptibility among the common unsaturated esters are ordered as linolenates > linoleates > oleates (Jain & Sharma, 2012). The OX index determines a clear picture of relative oxidation rate (Neff et al., 1992). This index depends on the coefficients of oleic (O), linoleic (L), and linolenic (Ln) acid methyl ester, which can be determined by the formula of oxidizability (OX=(0.02%O+%L+2%Ln)) (Cosgrove et al., 1987).

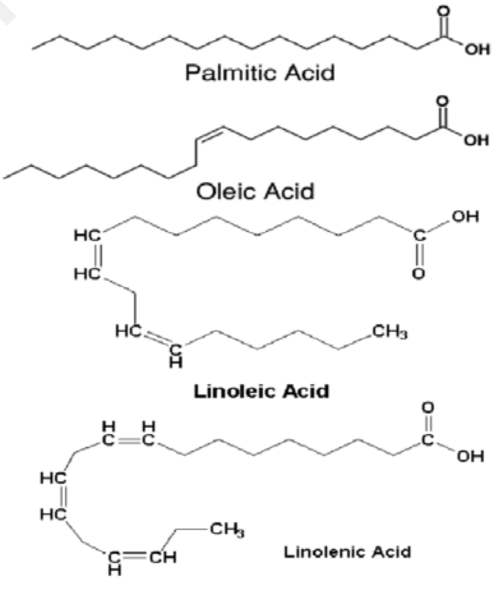

Figure 2.3: Common fatty acid methyl ester biodiesel molecules with increasing C=C bonds (Yaakob et al., 2014)

Bis-allylic methylene moieties induce greater effects on oxidation than allylic methylene moieties. The presence of poly-unsaturated methyl esters in biodiesel is more vulnerable than monounsaturated methyl esters to oxidation. Oxidation is a three-part process of radical chain reaction, consisting of initiation, propagation, and termination, as shown in Figure 2.4. This process initiates with the removal of hydrogen from polyunsaturated fatty acid (bis-allylic acid) to form carbon-based free charged (ROO·) radicals. These radicals react with dissolved O_2 and forms peroxide (ROO) and hydro-peroxide (ROOH) radicals; this reaction is known as the propagation reaction. Compared with hydro-peroxides, peroxide radicals demonstrate higher affinity with O_2; this affinity results in auto-oxidation and increases the percentage of hydro-peroxides. Consequently, this auto-oxidation results in the formation of decomposed compounds, such as acids, aldehydes, esters, ketones, peroxides, and alcohols (K. A. Sorate & Bhale, 2015). These decomposed compounds are responsible for the high total acid number (TAN) and the formation of insoluble gums and sediments, which reduce the quality of fuel and engine performance (Monyem & H Van Gerpen, 2001; Tang et al., 2008).

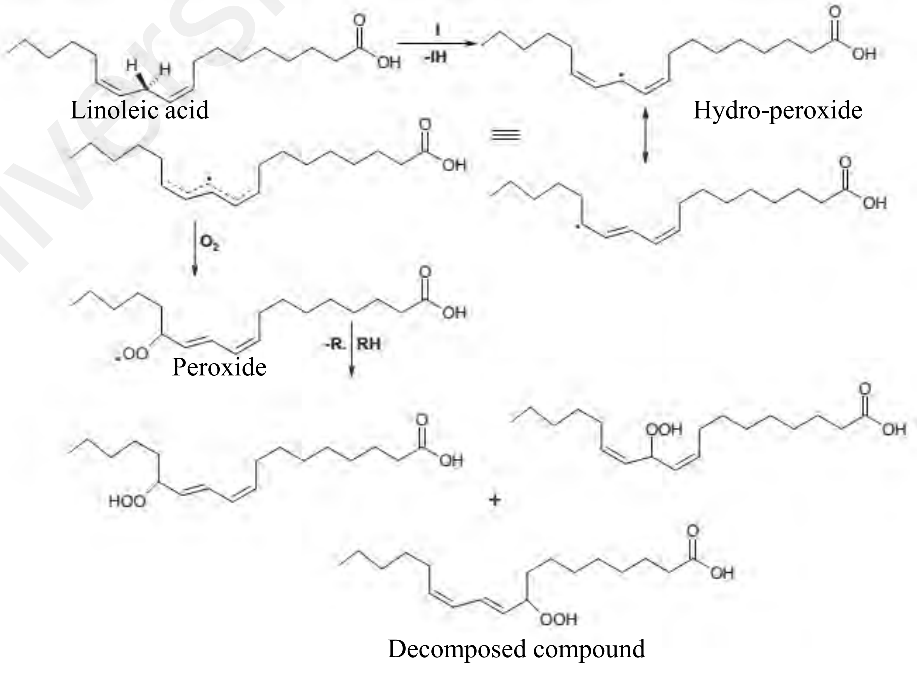

Figure 2.4: Oxidation mechanism of poly-unsaturated linoleic acid methyl ester (Yaakob et al., 2014)

2.5.2 Hydrolysis

The degradation of biodiesel occurs through hydrolysis and thermal decomposition. The hydrolysis of biodiesel occurs with the presence of moisture, whereas thermal decomposition is caused by elevated temperature (Barnwal & Sharma, 2005; Jain & Sharma, 2010; Yaakob et al., 2014). Hydrolysis is a reaction in which the molecular bonding of esters is broken by the reaction with water. According to ASTM D6751, the maximum allowable amount of water in biodiesel is 0.05%. The hygroscopic and polar nature of biodiesel makes the water molecules attracted to the esters; thus, the water content in biodiesel may become reactive with time. This attraction initiates the hydrolysis of esters, as shown in Eqation 2.1 (Atadashi et al., 2013). The hydrolysis of esters alters the properties and composition of fuels. Fazal et al. (Fazal, MA, et al., 2011a) indicated that the water content in biodiesel increased significantly after the immersion test; they found that the tendency of biodiesel to absorb water is roughly 30 times higher than that of petroleum diesel. Water found in biodiesel may exist in either dissolved or dispersed form. Phase separation remains often imperfect, and water tends to stay in the final biodiesel product in a finely dispersed form (Kovács et al., 2015). The presence of water accelerates its corrosive interactions with the metal surface.

$R_1\text{–COOR}_2$ (ester) + H–OH (water) = $R_2\text{–OH}$ (alcohol) + $R_1\text{–COOH}$ (fatty acid)... (2.1)

The existence of water in biodiesel also enhances the microbial growth, which in turn may accelerate fuel degradation (Sharma et al., 2008). Microbial growth rate is comparatively faster than hydrolysis (De Mello et al., 2007). The moisture absorption of biodiesel can reach up to 150 ppm (Burton & Biofuels, 2008), which sufficiently decreases the heat of combustion (A. Demirbas, 2009). This moisture also affects the engine respiratory system via microbe colonization and gel formation, which in turn may lead to fuel system plugging and injector coking. Biodiesel with high amounts of secondary products (mono- and di-glycerides) is more prone to moisture absorption

(Srivastava & Prasad, 2000), whereas water-contaminated biodiesel exhibits enhanced corrosiveness (Fazal et al., 2010; Felizardo et al., 2006). During the distillation and purification of biodiesel, natural antioxidants are destroyed, making biodiesel susceptible to degradation (Sharma et al., 2008).

2.5.3 Thermal decomposition

High temperature significantly affects the accelerated oxidation of biodiesel by yielding polymerized compounds and increasing the weight of biodiesel (Robert O Dunn, 2007; Jain & Sharma, 2010). At elevated temperatures, the oxidation temperature decreases along with increasing amounts of bis-allylic hydrogens in biodiesel (dos Reis Albuquerque et al., 2012). At thermal instability, the poly-unsaturated linoleic acid methyl ester initially forms a cyclohexene ring via isomerization and then forms a dimer via thermal dimerization; this process is known as the Diels–Alder reaction, which is illustrated in Figure 2.5 (Yaakob et al., 2014). In such manner, the elevated temperature and degree of unsaturation lead to thermal oxidation, which may produce aldehydes, ketones, and carboxylic acids, as well as limit the commercial use of biodiesel in automotive applications (Haşimoğlu et al., 2008).

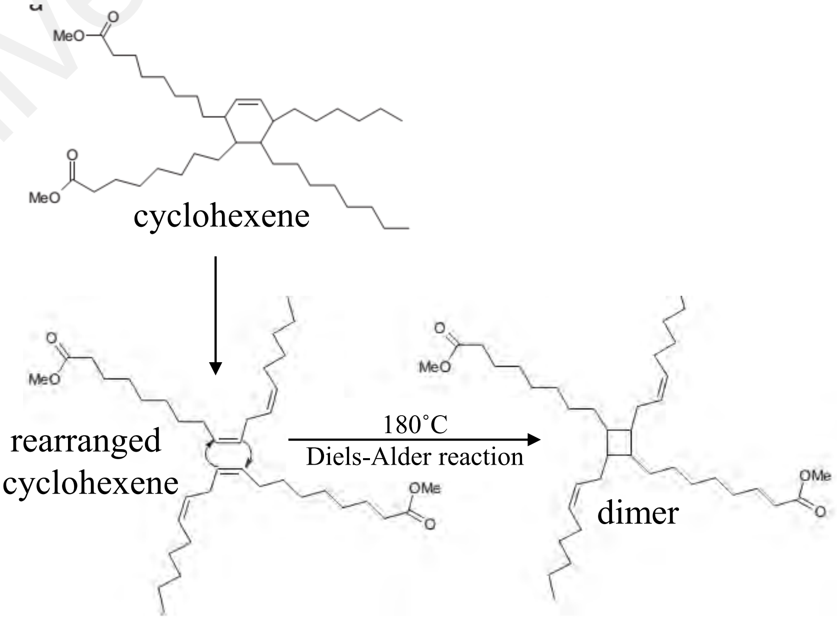

Figure 2.5: Formation of dimer via Diels-Alder reaction (Yaakob et al., 2014)

Elevated temperatures considerably influence the alteration of biodiesel properties, including oxidation, lubricity, corrosiveness, composition, induction period, viscosity, and density. According to Horel (Horel, 2009), the formation of CO_2 in the presence of O_2 (i.e., respiration) increases along with temperature. Severe corrosion is attributed to the presence of a higher acid number owing to oxidation. Photo-oxidation occurs as a result of exposed duration with intense light. In addition, various impurities, such as chloride ions in water, facilitate the anodic reaction and then degrade themselves and the metal surface in contact.

2.5.4 Co-metabolic biodegradation

Co-metabolic biodegradation (Zhang et al., 1998) refers to the alteration of biodiesel and petroleum diesel by microorganisms, such as bacteria (*Pseudomonas fluorescens, Bacillus sp., Bacillus subtilis, Alcaligenes sp., P. aeruginosa, Acinetobacter lwoffi, Flavobacterium sp., Micrococcus roseus,* and *Corynebacterium sp.*), fungi (*Amorphoteca, Neosartorya, Talaromyces,* and *Graphium*), and yeast (*Candida, Yarrowia,* and *Pichia*) (Adebusoye et al., 2007; Daugulis & McCracken, 2003). Biodiesel is more active than petroleum diesel because of its fatty acid with a hydrocarbon chain and two oxygen atoms. Moreover, fatty acids present great affinity to the abovementioned microorganisms (Sørensen, , et al., 2011). The acid is oxidized at the position of β-carbon attached to the functional group and degraded to acetic acid. Afterward, the newly formed fatty acid with two fewer carbons breaks down to CO_2 and H_2O in the presence of microorganisms by a series of reactions (Cole, 1994). Biodiesel is more prone to degradation than petroleum diesel because the latter contains aliphatic cyclic hydrocarbon, benzene, and other complex hydrocarbons with strong chemical stability and requiring more energy for microorganisms to penetrate the structure (Cole, 1994). By contrast, biodiesel contains oxygenated moieties that can be easily attacked by microorganisms and promotes further degradation (Von Wallbrunn et al., 2003).

These factors induce significant effects on the chemical stability of biodiesel and the long-term durability of the automotive component, thereby limiting the commercialization of biodiesel as a transportation fuel. The chemical stability of biodiesel can be improved by applying some preventive measures or alterations, such as modifying or curing with additives (Fazal & MA. Haseeb, 2014).

2.5.5 Remedial measures

The auto-oxidative stability of biodiesel can be improved by reducing the degree of poly-unsaturation and blending the biodiesel with diesel fuel (Yaakob et al., 2014). Auto-oxidation forms hydro-peroxides that decompose and cause secondary oxidation known as polymers (Fernandes et al., 2013; Rizwanul et al., 2014). Sorate & Bhale (K. A. Sorate & Bhale, 2015) reported that the oxidation stability of biodiesel was inversely proportional to the percentage of linoleic and linolenic acids. Such limitations can be addressed by reducing the affinity of oxygenated moieties to the metal surface.

The deoxygenation of biodiesel is another concurrent remedial measure that poses a high atomic ratio of hydrocarbon with a remarkable reduction in O/C ratio and ensures a higher energy density. Biodiesel without deoxygenation contains oxygenated compounds, such as carboxylic acids (C_7–C_{10}) and esters that threaten the engine components (Ben Hassen-Trabelsi, Kraiem, Naoui, & Belayouni, 2014). Among the various deoxygenation methods, the application of semi-batch intermediate liquid fraction by using CaO and treated hydrotalcite (MG70) as catalysts at 400 °C achieved 85% to 88% of hydrocarbons (Romero et al., 2015). Bio-oil was deoxygenated by promoting the reactions of decarboxylation and decarbonylation to remove oxygen atoms via the formation of CO_2 and CO byproducts. The successfully deoxygenation-converted biofuel mainly comprised hydrocarbons with a high atomic ratio H/C and a low atomic ratio O/C. With less oxygen content, biodiesel is considered a suitable candidate as a transportation fuel. Moreover, a remarkable reduction in oxygen ensures the high chemical stability of biodiesel, thereby inhibiting its corrosiveness and improves its tribological compatibility against automotive materials. Fuel modification with additives is another popular method for minimizing the auto-oxidation of biodiesels (Fernandes et al., 2013). Among the most commonly used corrosion inhibitors are imidazolines, primary amines, diamines, amino-amines, oxyalkylated amines, naphthaneic acid, phosphate esters, and dodecyl benzene sulfonic (Singh et al., 2012). The use of additives or inhibitors, such as tert-butyl hydroxyl quinine (TBHQ), butylated hydroxytoluene (BHT), butylated hydroxyamisole (BHA), propyl gallate (PrG), pyrogallol (PY), tert-butylamine (TBA), ethylenediamine (EDA), n-butylamine (nBA), and benzotriazole (BTA), achieves chemical stability by procrastinating auto-oxidation. These feasible remedial measures against the auto-oxidation of biodiesel motivate researchers to rethink biodiesel as an alternative fuel in automotive applications.

2.6 Materials used in automotive engine and fuel system

The automobile application of biodiesel was first tested by Rudolf Diesel in the 18th century (Shay, 1993). Numerous endeavors have followed to make biodiesel as a suitable alternative fuel because of its favorable tribological and environmental benefits (Knothe, 2005). The engine and fuel systems in automobiles comprise various static and dynamic components, such as piston, piston ring, cylinder liner, exhaust valve, injector needle, filter plunger, fuel tank, feed pump, fuel filter, and fuel line (Figure 2.6). Table 2.4 describes these components, the materials, and the types of material degradation. All these components are made of either ferrous or nonferrous materials, and their alloys are exposed to biodiesel under different operating conditions (Haseeb et al., 2011; K. Sorate & Bhale, 2013). When the chemical properties are changed, the biodiesel becomes susceptible to those metals. Therefore, a suitable blend of biodiesel and metal must be selected for both the static and dynamic parts of automobiles.

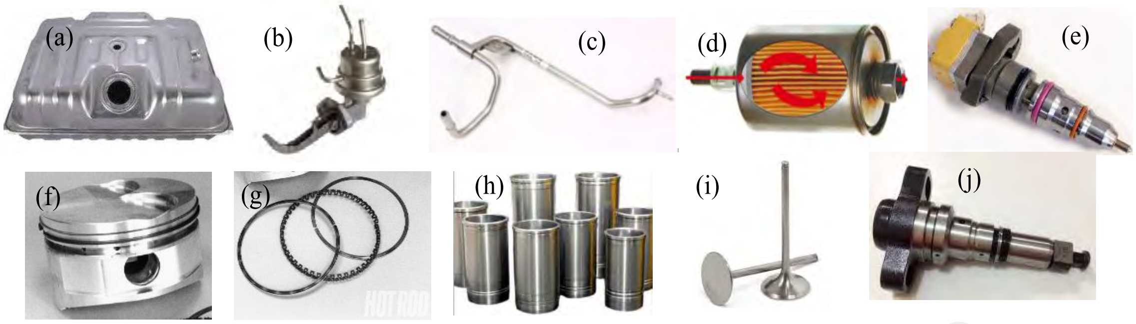

Figure 2.6: Automotive components in engine and fuel systems: (a) Fuel tank, (b) fuel pump, (c) fuel line, (d) fuel filter, (e) fuel injector, (f) piston, (g) piston ring, (h) cylinder liner, (i) valve, and (j) fuel filter plunger.

Table 2.4: Typical diesel engine and fuel system components, material and type of material degradation

Component	Types of alloy used	Major type of degradation	Ref.
Fuel tank	Iron, nickel, manganese, cobalt, copper, leaded bronze	Corrosion	(Bessee & Hutzler, 2009; Haseeb A.S.M.A et al., 2010; K. A. Sorate & Bhale, 2015)
Fuel pump	Aluminum alloy, iron-based alloy, copper-based alloy	Corrosion	(Sarvi et al., 2008; K. A. Sorate & Bhale, 2015)
Fuel lines	Steel, copper	Corrosion	(Crouse & Angle, 1993; Haseeb et al., 2011; Haşimoğlu et al., 2008)
uel filter housing	Aluminum	Corrosion	(Crouse & Angle, 1993; Stanfel, 2009)
Fuel injector plunger and barrel	18CrNi8 steel: (Cr: 16% to 18%, Ni: 10% to 14%, C: 0.03%, Mn: 2%, Si: 0.75%, P: 0.045%, S: 0.03%, N: 0.10%, and Mo: 2% to 3%).	Tribology	(Blau & Pollard, 2009; Crouse & Angle, 1993; Hardalupas et al., 1992; Karamangil & Taflan, 2013)
Piston	Aluminum alloy: (Si: 11% to 13% Cu: 3% to 5%, Mg: 0.5% to 1.2%, Ni: 1% to 3%, Fe: 0.3%, Mn: 0.3%, Ti: 0.2%, Zn: 0.3%, Zr: 0.2%, V: 0.18%, Cr: 0.05%, and Al: remaining)	Tribology	(Haque & Sharif, 2001)
Piston ring	CrMoV18 steel: (C: 0.85% to 0.95%, Si: 1%, Mn: 1%, P: 0.04%, S: 0.015%, Cr: 17% to 19%, Mo: 0.9% to 1.30%, V: 0.07% to 0.12%, and Fe: remaining)	Tribology	(De Silva et al., 2011)
Cylinder liner	Gray cast iron: (C: 3.40% to 3.70%, Si: 2.30% to 2.80%, Mn: 0.50% to 0.80%, S: 0.15%, P: 0.25%, and Fe: remaining)	Tribology and corrosion	(Lenauer et al., 2015) (De Silva et al., 2011)
Valve	Austenitic stainless steel: (C: 0.03% to 0.10%, Si: 0.50%, Mn: 0.50%, P: 0.015%, S: 0.015%, Cr: 14.0% to 17.0%, Mo: 0.50%, and Fe: remaining)	Tribology	(Grzesik et al., 2013)

Although biodiesel has attracted a very high acceptance in automobile applications because of its environmental and tribological benefits, the corrosiveness of this material remains controversial. In (Tyson, 2009), the automotive components made of ferrous and nonferrous metals were damaged because of the accelerated oxidation or moisture absorption of biodiesel, as shown in Figure 2.7. The hygroscopic nature of biodiesel leads to microorganism contamination and enhances the corrosion process (Klofutar et al., 2010; Tsuchiya et al., 2006). Therefore, the corrosive nature of biodiesel poses a serious concern for the long-term durability of automotive components and requires a rigorous investigation. The following sections discuss the degradation of automotive materials exposed to a biodiesel environment.

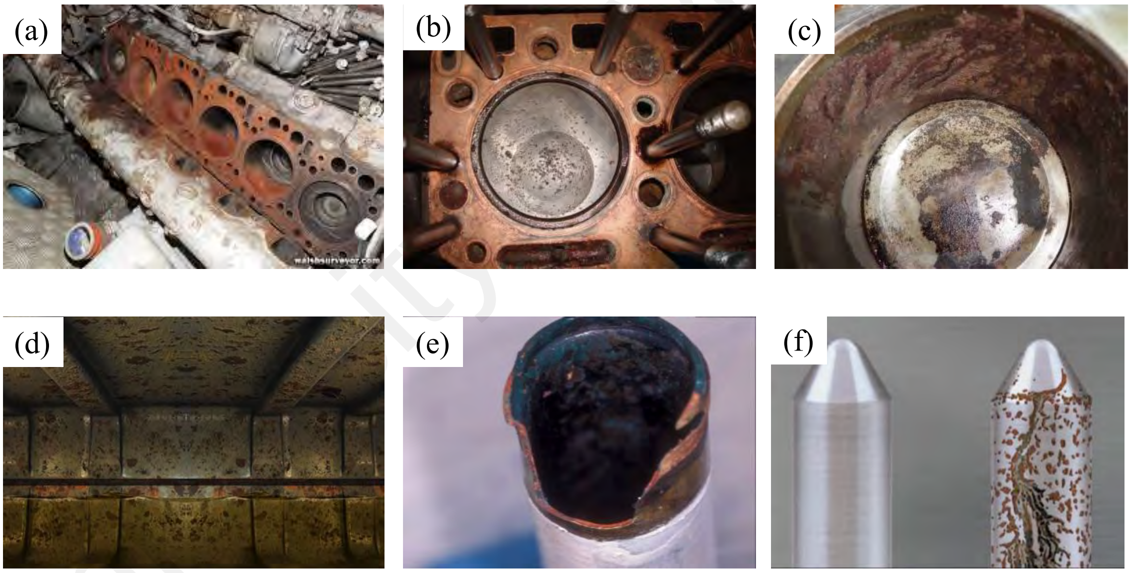

Figure 2.7: Corroded automotive components in engine and fuel systems: (a) Engine block, (b) piston head, (c) cylinder liner, (d) fuel tank, (e) fuel line, and (f) fuel injector

2.7 Corrosion behavior of automotive materials

Automotive materials mostly comprise ferrous and non-ferrous metals, such as iron, iron-based alloys, steel, copper, copper-based alloys, aluminum, and aluminum-based alloys, which are more or less corrosive in biodiesel. The corrosion compatibility of these materials exposed to biodiesel presents a key research issue. According to Sakae et al. (Fujita & Mizuno, 2007), the corrosion of automotive materials can be classified into perforation corrosion, cosmetic corrosion, and edge corrosion, of which perforation corrosion is the most common problem (Fujita & Mizuno, 2007). Agarwal et al. (Agarwal, 2007) introduced general corrosion, dry corrosion, and wet corrosion when the automotive materials were exposed to ethanol. Ionic impurities (chloride ions and acetic acid) and polar molecules are responsible for general and dry corrosion, respectively, whereas oxidized compounds and azeotropic water are responsible for wet corrosion. Prieto et al. (Prieto et al., 2008) introduced galvanic corrosion, which was attributed to the very low conductivity of biodiesel as an electrolyte (4.06×10^{-9} miliSemence/cm) and the polarized covalent bond compound in between hydrogen–oxygen and carbon–oxygen bonds. Biodiesel is slightly more polar than diesel fuel because of the electron negativity of oxygen with enhanced corrosion (Balat & Balat, 2010; Maru et al., 2009). The O_2, H_2O, CO_2, and $RCOO^-$ radicals in biodiesel act as leading factors in enhancing the corrosiveness of biodiesel. During storage, the generation of aerobic and anaerobic microorganisms promotes bacterial activities and increases acidity (pH = 3.5) (M Bento & C Gaylarde, 2001). Chemical- or microbiological-influenced corrosion may occur in automotive materials, as discussed in the following.

2.7.1 Corrosion of ferrous metal

Corrosion generally occurs on the sample surface in a uniform or localized manner. For corrosion, Kaul et al. performed a 300-day static immersion test of piston and cylinder liner metal in biodiesel for various feedstocks (Kaul et al., 2007). They found that *Salvadora* and *Jatropha* feedstocks were more corrosive than the biodiesel from other feedstocks (Table 2.5). The biodiesels from Karanja and Mohua feedstocks showed similar corrosion behavior as diesel. Table 2.5 shows that stainless steel demonstrates the best corrosion resistance among all ferrous metals, which may be attributed to its low carbon content (Cao et al., 2007). However, the effect of elevated temperature on the corrosion of metal and the degradation of biodiesel remains unknown.

Table 2.5: Corrosion of ferrous metals under different operating conditions

Ferrous metal	Biodiesel	Duration (h)	Temperature (°C)	Corrosion rate (mpy)	Ref.
Cast iron	B0	7200	RT	0.006	(Kaul et al., 2007)
	B100	1200	RT	0.077	(Fazal, MA, et al., 2011b)
	B100	2880	RT	0.112	(Fazal et al., 2012)
	Jatropha	7200	40	0.078	(Kaul et al., 2007)
	Kanarja, Mahua	7200	40	0.006	
	Salvadora	7200	40	0.132	
	FB-80	7200	38	0.192	(Geller et al., 2010)
Mild steel	B0 B100	1200	27	0.046, 0.052	(Fazal, MA, et al., 2011b)
	B0 B100	1200	80	0.05, 0.059	(Fazal, MA, et al., 2011b)
	B0 B100	720	27	0.0015, 0.004	(Jin et al., 2015)
	B0 B100	1440	50	0.0014, 0.055	(Jin et al., 2015)
	B0 B100	2880	80	0.027, 0.08	(Jin et al., 2015)
Carbon steel	Rapeseed oil and methanol	1440	43	0.018	(Hu et al., 2012)
	Sunflower	3000	RT	0.170	(Cursaru et al., 2014)
	Sunflower	3000	60	0.336	
Stainless steel	Rapeseed oil and methanol	1440	43	0.001	(Hu et al., 2012)
	B100	1200	80	0.015	(Fazal et al., 2010)

B100: Palm biodiesel, PB50: 50% biodiesel in diesel, FB80: 80% fat-based bio-fuel blend, and RT: room temperature

Tsuchiya et al. (Tsuchiya et al., 2006) studied the corrosion of steel immersed in diesel and 5% FAME blended diesel at 80 °C for 500 h. The pitting corrosion even for 2% FAME biodiesel confirmed that the extremely corrosive free fatty acids, such as formic acid, acetic acid, propionic acid, and caproic acid after oxidation, are responsible for such pitting corrosion. Fazal et al. (Fazal, MA, et al., 2011b) later investigated the corrosion behavior of cast iron and mild steel at different elevated temperatures in 50% palm biodiesel for 1200 h. Jin et al. (Jin et al., 2015) recently investigated ASTM 1045 mild steel at different temperatures and exposure times in palm biodiesel and diesel. Figure 2.8 shows the corrosion behavior model of mild steel in diesel and palm biodiesel with the functions of time and temperature. In both kinds of fuels, the corrosion rate increases along with temperature and duration.

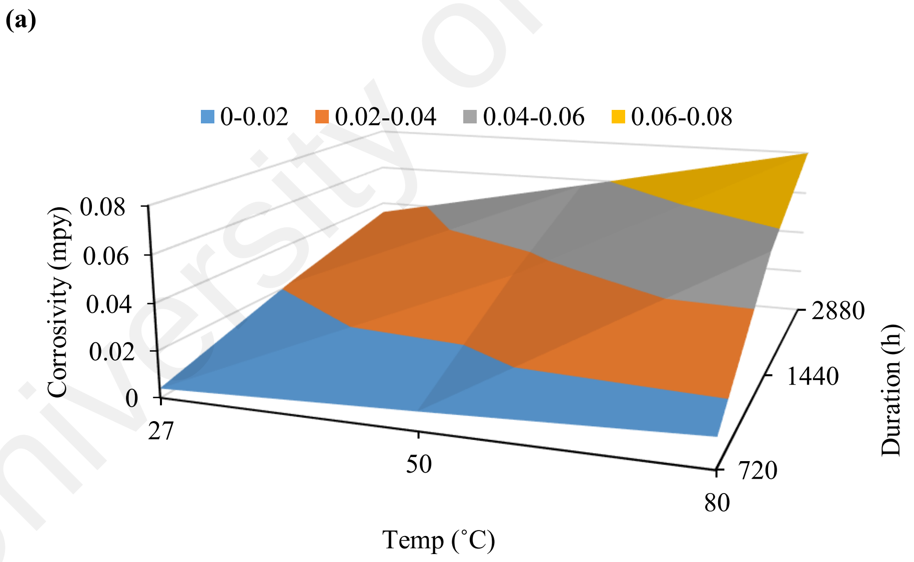

Figure 2.8: Corrosion behavior of ASTM 1045 mild steel exposed to (a) B100 and (b) B0 with different temperatures and exposure times (Jin et al., 2015).

(b)

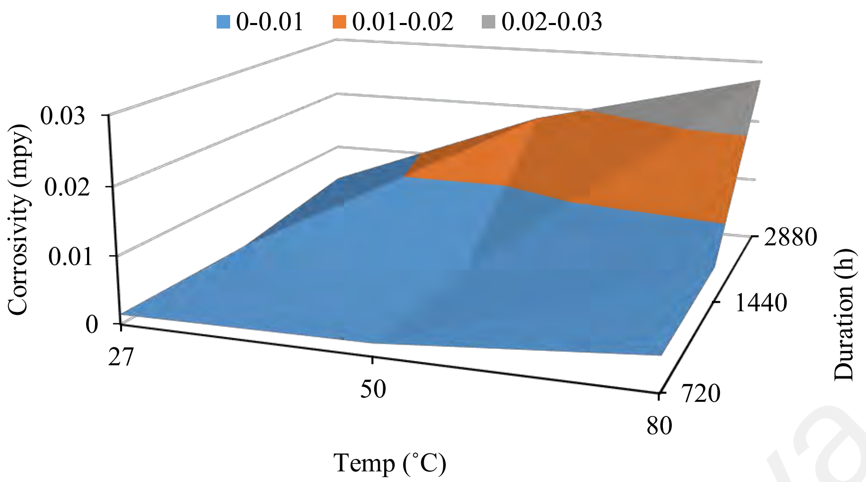

Figure 2.8, continued

The corrosion of metal and the degradation of fuel both increase along with temperature. An increasing temperature is also accompanied by an increasing presence of oxygen in the form of compounds, such as iron carbide or iron oxides. The subsequent dissolution of these compounds degrades the metal surfaces. Cast iron is highly vulnerable to corrosion mostly in palm biodiesel, followed by mild steel and carbon steel. The higher temperature and relatively higher duration in the metal–fuel interface may also contribute to the increasing corrosion (Fazal et al., 2010). Guthrie et al. (Guthrie et al., 2002) clarified the corrosion mechanism of these ferrous metals, as discussed in the following section.

2.7.2 Corrosion mechanism of ferrous metal

According to Guthrie et al. (Guthrie et al., 2002), oxidation generates iron ions that form hydrated oxide with hydroxide ions in the presence of moisture and oxygen. The further reaction of iron hydroxide initiates the corrosion of iron or iron alloy. Cast iron forms a small concentration of Fe_2O_3 and $Fe(OH)_2$ in diesel, whereas relatively higher amounts of $FeCO_3$, Fe_2O_3, $Fe(OH)_2$, and $Fe_2(OH)_2CO_3$ are formed in biodiesel. Fazal et al. (Fazal, MA, et al., 2011b; Fazal et al., 2012) investigated the cast iron and mild steel surface degradation when exposed to biodiesel (Figure 2.9), and their XRD report ensured the formation of iron compounds (e.g., $FeCO_3$, Fe_2O_3, and $Fe(OH)_2$) at higher concentrations. Recently, D. Jin et al. (Jin et al., 2015) examined the corrosion behavior of ASTM 1045 mild steel in palm biodiesel and reported that on the basis of the relative area ratio, the quantity of Fe^{+3} in the corrosion product was higher than that of Fe^{+2}. Such finding is attributed to the presence of higher oxygen in biodiesel, thereby improving the interaction of biodiesel with metal to form metal compounds. For ferrous metals, the compound results from the following chemical reactions (2.2):

$$\begin{aligned} &4Fe + 4H_2O + 2O_2 \rightarrow 4Fe(OH)_2 \\ &4Fe(OH)_2 + O_2 \rightarrow 2Fe_2O_3.H_2O + 2H_2O \qquad (2.2) \\ &Fe^{2+} + 2RCOO^{\bullet} \rightarrow FeCO_3 + R - R + CO_2 \end{aligned}$$

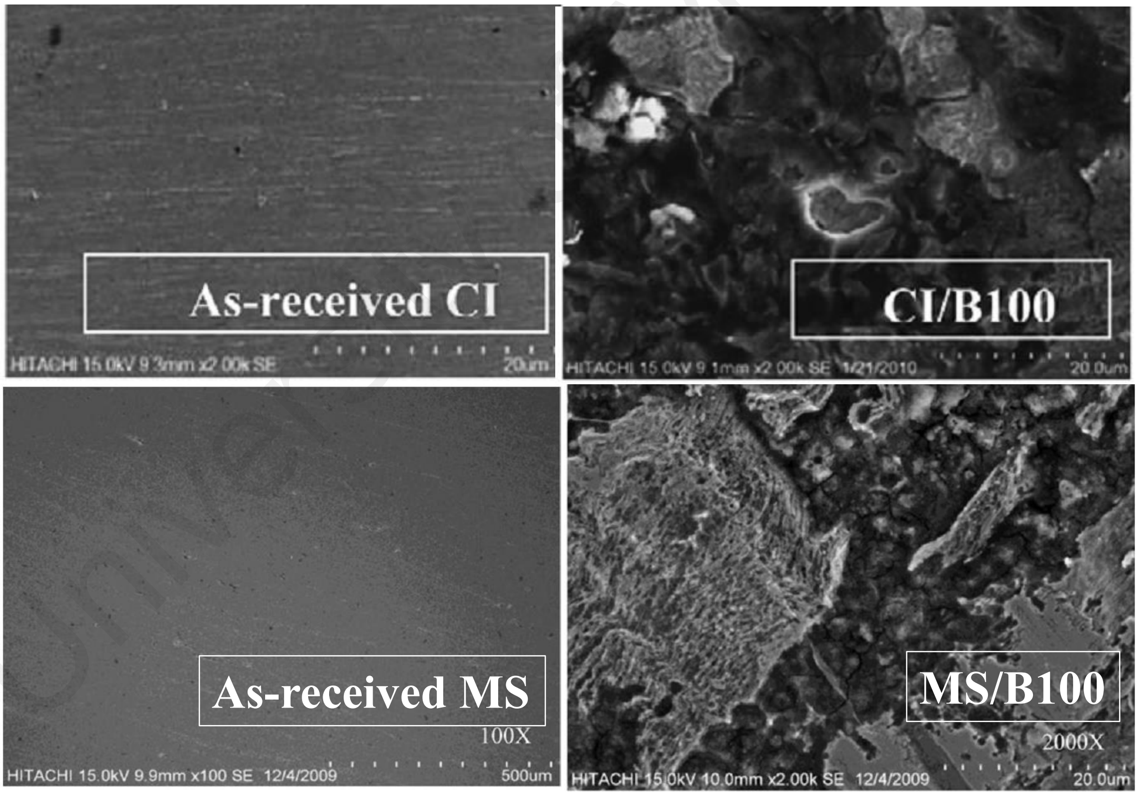

Figure 2.9: SEM micrographs of cast iron (CI) and mild steel (MS) surface before and after exposure in biodiesel (B100) (Fazal, MA, et al., 2011b; Fazal et al., 2012)

2.7.3 Corrosion of non-ferrous metal

After a 10-month immersion test at 38 °C, Geller et al. (Geller et al., 2010; Geller. et al., 2008) observed that copper and brass demonstrated the highest and second highest weight loss because of pitting corrosion (Mankowski et al., 1997). Fazal et al. performed a similar study on palm biodiesel (Fazal, MA, et al., 2011b; Fazal et al., 2012) and reported that copper was not corroded in biodiesel but also acted as a catalyst to degrade fuel properties. Table 2.6 shows that copper is very much aggressive in rapeseed methyl ester (0.915 myp corrosion rate) compared with palm and sunflower. Palm and sunflower show almost similar corrosion behavior for copper and aluminum. Chew et al. (Chew et al., 2013) conducted a similar experiment on magnesium, which was 35% lighter than aluminum yet exhibited almost similar strength. Magnesium yielded a significantly higher corrosion rate than aluminum and copper. Magnesium, copper, and copper-based alloys are the most vulnerable to corrosion among all non-ferrous metals, whereas leaded bronze shows the best corrosion resistance capability among all copper-based alloys. Aluminum and its alloys demonstrate higher corrosion resistance than all non-ferrous materials in all kinds of biodiesel tests and can be used as benchmarks for the corrosion of other materials (Kaul et al., 2007). The compatibility of different ferrous and non-ferrous materials has been reported, and the following section will discuss the corrosion mechanism for non-ferrous materials as clarified by Amin et al. (Amin et al., 2009) and Fazal et al. (Fazal et al., 2012).

Table 2.6: Corrosion of non-ferrous metals in different operating conditions

Non-ferrous metal	Biodiesel	Duration (sec)	Temperature (°C)	Corrosion rate (mpy)	Ref.
Copper	Rapeseed oil and methanol	1440	43	0.023	(Hu et al., 2012)
	B100	2640	RT	0.042	(Haseeb A.S.M.A et al., 2010)
	B100	2880	RT	0.392	(Fazal et al., 2012)
	B100	1200	80	0.586	(Fazal et al., 2010)
	B100 (oxidized)	840	60	0.053	(Haseeb A.S.M.A et al., 2010)
	FB80	7200	38	0.557	(Geller. et al., 2008)
	RME 100	600	80	0.915	(Norouzi et al., 2012)
	Sunflower	3000	RT	0.323	(Cursaru et al., 2014)
			60	0.640	
Leaded bronze	B100	2640	RT	0.018	(Haseeb A.S.M.A et al., 2010)
	B100 (oxidized)	840	60	0.023	
Aluminum	B100	720	RT	0.123	(Chew et al., 2013)
		1440		0.052	
	B100	2880	RT	0.173	(Fazal et al., 2012)
	Rapeseed oil and methanol	1440	43	0.003	(Hu et al., 2012)
	B100	600 to1200	80	0.202	(Fazal et al., 2010)
	RME 100	600	80	0.35	(Norouzi et al., 2012)
	Sunflower	3000	RT	0.162	(Cursaru et al., 2014)
			60	0.316	
Aluminum alloy	Jatropha	7200	40	0.011	(Kaul et al., 2007)
	Kanarja, Salvadora	7200	40	0.005	
	Mahua	7200	40	0.012	
Magnesium	B100	720	RT	3.091	(Chew et al., 2013)
		1440		2.656	
Brass	B100	2880	RT	0.209	(Fazal et al., 2012)

Note: B100: Palm biodiesel, PB50: 50% biodiesel in diesel, FB80: 80% fat-based biofuel blend, RME 100: 100% rapeseed methyl ester

2.7.4 Corrosion mechanism of non-ferrous metal

The surface of the material exposed to biodiesel was characterized via SEM to illustrate clearly the corrosion attack (Figure 2.10). Fazal et al. (Fazal et al., 2012, 2013a) investigated the corrosion mechanisms for copper, brass, and aluminum. Their rigorous study on the corrosion mechanism of Cu clearly illustrated the corrosion phenomenon, whereas their XRD pattern on the copper surface indicated the presence of comparatively higher concentrations of $CuCO_3$ along with other copper compounds, such as CuO, Cu_2O, $Cu(OH)_2$, and $CuCO_3.Cu(OH)_2$. These results suggest that for copper and copper-based alloys, copper carbonate ($CuCO_3$) and cuprite oxide (Cu_2O) are the dominant compounds formed in biodiesel and diesel, respectively. According to equation (2.3), the O_2 and CO_2 dissolved from the atmosphere (Squarcialupi et al., 2002) or the $RCO\dot{O}$ radical generated from esters play important roles in the formation of copper compounds. Fazal et al. (Fazal et al., 2013a) concluded that the ion concentration in biodiesel and the Cu acted as catalysts for enhanced corrosion. Amin et al. (Amin et al., 2009) investigated the degradation of aluminum exposed to biodiesel and found that a trihydroxide film was formed when the aluminum was exposed to OH^- ion. They added that an increase in pH would accelerate the corrosion by damaging the film.

$$
\begin{aligned}
&2Cu + \tfrac{1}{2}O_2 \rightarrow Cu_2O && (2.3)\\
&Cu_2O + \tfrac{1}{2}O_2 \rightarrow 2CuO\ ;\ Cu_2O + 2CO_2 + \tfrac{1}{2}O_2 \rightarrow 2CuCO_3 &&\\
&CuO + CO_2 \rightarrow CuCO_3 &&\\
&2Cu + O_2 + 2H_2O \rightarrow 2Cu(OH)_2 &&\\
&CuO + H_2O \rightarrow Cu(OH)_2 &&\\
&Cu^{2+} + 2RCOO^{\bullet} \rightarrow CuCO_3 + R - R + CO &&\\
&2Cu(OH)_2 + CO_2 \rightarrow Cu(OH)_2.CuCO_3 + H_2O &&
\end{aligned}
$$

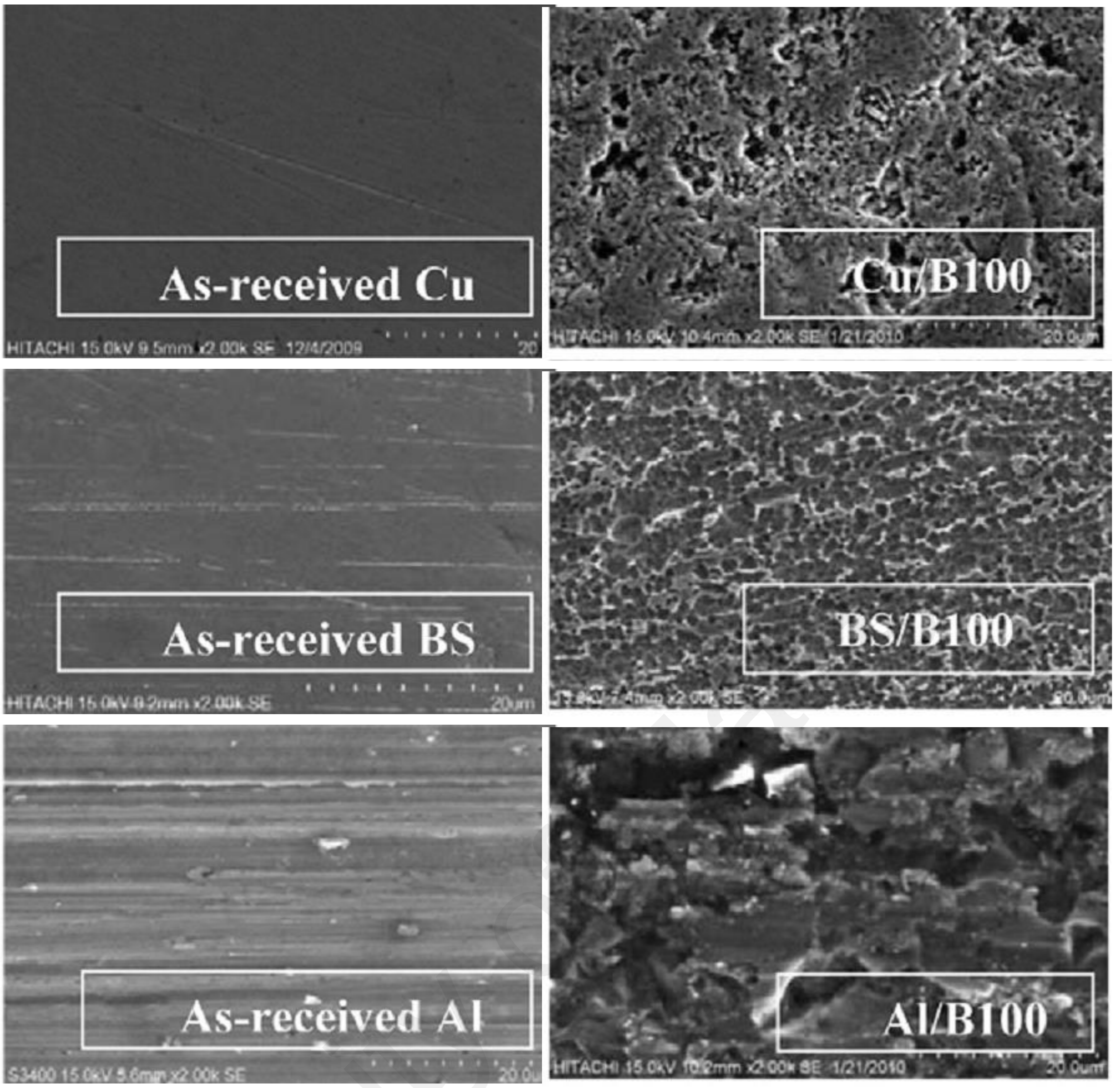

Figure 2.10: SEM images of Cu, BS, and Al surfaces before and after exposure to biodiesel (B100) (Fazal et al., 2012).

2.7.5 Remedial measures for corrosion of automotive materials

Most studies show that metals are more corrosive in biodiesel than in diesel. Material susceptibility always follows an order of corrosion rate, where magnesium > copper > brass > cast iron > mild carbon steel > aluminum > stainless steel (Hu et al., 2012). Hu et al. argued that copper, cast iron, and mild carbon steel were significantly more susceptible than aluminum and stainless steel because of their higher presence of carbon. Although stainless steel is the best corrosion-resistant automotive material in biodiesel, this material remains corrosive in biodiesel and is not economically viable to use for automotive components.

Some characteristics of biodiesel, such as oxygen-containing functional groups (moieties), free fatty acids, unsaturation degree, and hygroscopic nature, challenge the compatibility of the material–fuel interface. Therefore, the retardation of engine material part degradation and biodiesel corrosiveness is a main topic of concern that can be mitigated by corrosion inhibitors (Moser et al., 2011). The inhibitor is not used to prevent corrosion but to extend the time of corrosion (Maru et al., 2009). According to Yıldırım et al. (Yıldırım & Cetin, 2008), the effectiveness of corrosion inhibitors depends on their adsorption capabilities on reactive sample surfaces. As shown in Figure 2.11 a to Figure 2.11c, the adsorption on the metal surface inhibitor successively forms a protective layer over the metal surface and prevents the direct contact between the reactive metal and corrosive biodiesel.

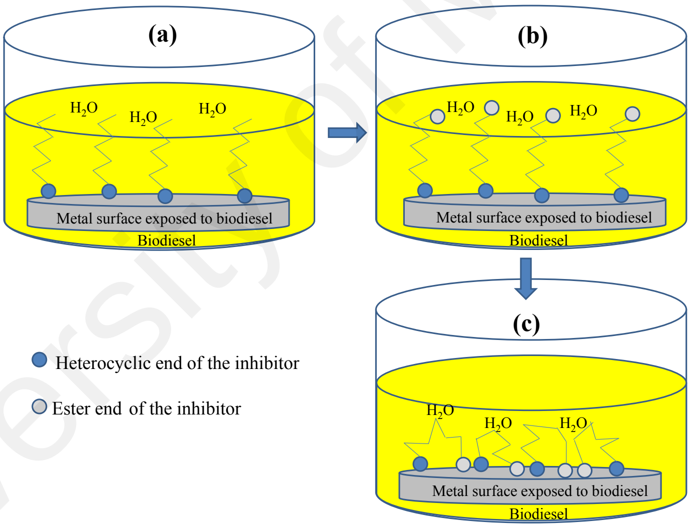

Figure 2.11: Possible orientation of inhibitor on the metal stripe surface exposed to biodiesel

Yıldırım et al. also added that among all corrosion inhibitors (i.e., bearing nitrogen (N), oxygen (O), or sulfur (S) heteroatoms), amine-based inhibitors showed the best corrosion inhibition because the adsorption of molecules on the metal surface via heterocyclic moiety increased the interaction of N atoms (protonated amine) much higher than that of other heteroatoms that prevented the direct contact between the active metal and fuel. Amine-based corrosion inhibitors, such as TBA, EDA, nBA, and BTA, demonstrate excellent corrosion prevention performance through adsorption on the metal surface. Such adsorption may be classified into two major types, namely, (1) electrostatic attraction between the charged molecules and charged metal (spontaneous physical adsorption) and (2) interaction of unshared electron pairs in the molecule, the π-electrons of the nitrogen atom, or the metal (chemisorption) (Li et al., 1997). Fazal et al. (Fazal, M.A, et al., 2011) investigated the effects of EDA, TBA, and nBA on the corrosion of copper, brass, aluminum, and cast iron and found that 100 ppm TBA-doped biodiesel was an effective corrosion inhibitor with 49.41% inhibition efficiency. The existence of a new phase ($Fe(NO_3)_3 \cdot 9H_2O$) on the metal surface that may be formed via TBA contributes to corrosion retardation. Nevertheless, further studies with different additive concentrations and elevated temperatures must be conducted to identify the inhibition action and adsorption type of additives on different automotive materials. Deyab (M. Deyab, 2016; M. A. Deyab, 2014) investigated the adsorption of ascorbyl palmitate (AP) and butylated hydroxytoluene (BHT) on exposed carbon steel, ethanol-blended gasoline, and blended biodiesel by using the weight-loss method and electrochemical impedance spectroscopy (EIS). They confirmed that the concentration inhibition efficiency increases at a specific temperature, whereas the temperature inhibition efficiency decreases at a specific concentration. M. A. Deyab (M. A. Deyab, 2014) also justified the adsorption isotherm model of inhibitors with the help of thermodynamic functions, such as activation energy (E_a), free Gibbs energy (ΔG_{addi}), and standard enthalpy (ΔH_{addi}). The following section discusses the inhibition mechanism in detail.

Table 2.7: Corrosion inhibition in diesel and biodiesel

Corrosion inhibitors	Structural formula	Medium	Concentration	Material	Corrosion rate	Inhibition efficiency	Ref.
Tert-butylamine (TBA)	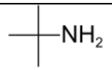	B100	100ppm	Cast iron	0.039mpy	49.41%	(Fazal, M.A, et al., 2011)
Ethylenediamine (EDA)	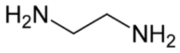	B100	100ppm	Cast iron	0.053mpy	31.38%	(Fazal, M.A, et al., 2011)
n-Butylamine (nBA)	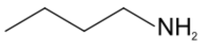	B100	100ppm	Cast iron	0.068mpy	12.06%	(Fazal, M.A, et al., 2011)
Ascorbyl palmitate (AP)	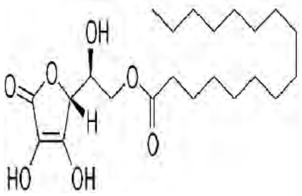	Ethanol blended gasoline	120 mg/l	Carbon steel	1.6×10^{-5} mg $cm^{-2}h^{-1}$	98.8%	(M. A. Deyab, 2014)
Butylated hydroxytoluene (BHT)	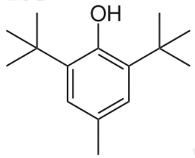	20% wost cooking oil blended diesel	150mg/l	Carbon steel	1.38×10^{-5} mg $cm^{-2}h^{-1}$	94.4%	(M. Deyab, 2016)

2.7.6 Corrosion inhibition mechanism

The inhibition mechanism of additives through adsorption can be investigated by the weight loss of degraded materials. The measured weight loss can be converted into corrosion rate and inhibition efficiency as follows (M. A. Deyab, 2014; Fazal et al., 2013a):

$$Corrosion\ rate\ (C_R) = \frac{8.76\times10^{9}W}{D\,t\,A} \qquad (2.4)$$

$$Inhibition\,efficiency\ (\eta) = \left[\frac{C_R - C_{Ri}}{C_R}\right]\times100\% \qquad (2.5)$$

where corrosion rate (C_R) is expressed in micrometer per year (µm/y); W, D, t, and A denote weight loss (kg), density of material (kg/m^3), immersion time (hr), and exposed area (m^2), respectively. In equation (2.5), C_R and C_{Ri} represent the corrosion rates in biodiesel and additive-doped biodiesel, correspondingly.

2.7.6.1 Adsorption isotherms for the inhibition system

The performance of the additive was investigated using the recently proposed adsorption isotherms (M. Deyab, 2015; M. Deyab & Abd El-Rehim, 2013; M. A. Deyab, 2014, 2016). Previous research provides basic information on the interaction between the additive and metal surface. The best-fitted experimental data for the isotherm model are determined and can be used to develop a suitable model of adsorption. The Langmuir model is the easiest and widely used isotherm (Ćurković et al., 2011). Langmuir hypothesized that a surface contains a certain number of sites where species can adhere through physisorption or chemisorption. Surface coverage (θ) is needed to determine the characteristic curve of the adsorption isotherm. For different concentrations of the additive, θ can be calculated using the inhibition efficiency equation ($\theta = \eta/100$). The calculated values help in plotting a graph and finding a suitable adsorption isotherm. The Langmuir mathematical relationship is used to fit the θ values (Foo & Hameed, 2010) as follows:

$$C_{Addi}/\theta = 1/K_{eqi} + C_{Addi} \qquad (2.6)$$

where C_{Addi} is the concentration of the additive, and K_{eqi} is the equilibrium constant of the adsorption and denotes the strength between the adsorbate (biodiesel) and adsorbent (material surface). The reciprocal of the intercept of the isotherm line represents the equilibrium constant of the adsorption. High values of $\mathrm{K}_{\mathrm{eqi}}$ indicate the stronger adsorption of the inhibitor (M. Deyab & Abd El-Rehim, 2013). The K_{eqi} value is employed to determine the separation factor (K_{L}) and energy of the adsorption as follows (Mall et al., 2005):

$$K_L = \left[1 + K_{eqi} C_{Addi}\right]^{-1} \qquad (2.7)$$

The above equation identifies the type of isotherm under the following conditions: (i) favorable adsorption if $0 < K_{\mathrm{L}} < 1$ and (ii) unfavorable adsorption if $K_{\mathrm{L}} > 1$ (Mall et al., 2005). The standard free energy of adsorption (ΔG_{addi}) must be determined to identify whether the adsorption process is spontaneous. The ΔG_{addi} of the inhibitor on the material surface can be calculated as follows (X. Li, Deng, & Fu, 2012):

$$\Delta G_{addi} = -RT\ln(55.5 \times 10^{6} K_{eqi}) \qquad (2.8)$$

where ΔG_{addi}, R, T, and K_{eqi} denote the adsorption energy of the inhibitor (kJ mol^{-1}), the universal gas constant (8.314472 J/mol·K), the operating temperature (K), and the equilibrium constant of the adsorption process, respectively. Depending on the value of ΔG_{addi}, the adsorption process can be classified as (i) chemical adsorption (if $\Delta G_{addi} < -40$ KJmol^{-1}), (ii) physicochemical adsorption (if $-40 \leq \Delta G_{addi} \leq -20$ KJmol^{-1}), or (iii) physical adsorption (if $\Delta G_{addi} > -20$ KJmol^{-1}) (M. Deyab & Abd El-Rehim, 2013).

2.7.6.2 Thermodynamic functions of corrosion inhibition mechanism

The effect of elevated temperature on corrosion inhibition can be identified by several thermodynamic functions, such as activation energy (E_a) and standard enthalpy (ΔH_{addi}), for adsorption processes. These functions help define the adsorption nature of different concentrations of additives on the metal surface that is exposed to biodiesel at elevated temperatures as well as the nature of adsorption reaction. The following equation computes the activation energy (E_a) of the corrosion process in different additive concentrations (Connors, 1990):

$$E_a = \frac{2.303R \times \log \frac{C_{R@RT}}{C_{R@ET}}}{\left(\frac{1}{T_{ET}} - \frac{1}{T_{RT}} \right)} \qquad (2.9)$$

where $C_{R@RT}$ and $C_{R@ET}$ denote the inhibited corrosion rates at room temperature (T_{RT}) and elevated temperature (T_{ET}) (K), respectively. The endothermic or exothermic process in adsorption can be distinguished by considering another thermodynamic parameter, namely, the standard enthalpy of adsorption (ΔH_{addi}), which can be calculated by the linear regression between $\Delta G_{adddi} / T$ and $1/T$ of the following Gibbs–Helmholtz equation (Atkins, 1978):

$$\frac{\Delta G_{addi}}{T} = \frac{\Delta H_{addi}}{T} + C \qquad (2.10)$$

In the exothermic process, the absolute value of ΔH_{addi} is lower than 40 kJ/mol. However, in the endothermic process, the absolute value of ΔH_{addi} approaches 100kJ/mol or above (Herrag et al., 2010). This process for biodiesel requires further study.

2.8 Tribological degradation

In automobiles, 48% of the total energy that is developed by an engine is lost because of friction (Spearot, 2000). The United States Department of Energy reported that reducing the friction and wear in the tribological components of engine can save US$ 120 billion per year (Holmberg et al., 2012). Therefore, the importance of reducing tribological degradation has been increasingly acknowledged. Several studies have also been conducted to understand the lubricity of biodiesel for automotive materials (Fazal et al., 2013b; Fazal & MA. Haseeb, 2014; Morris et al., 2013; Tung & McMillan, 2004).

In the global lubrication market, the rise in biodiesel as lubricants is a result of new environmentally friendly initiatives that are less toxic, renewable, and alternatives to traditional petroleum-based lubricants (W. Li et al., 2012). Biodiesel consists of a complex mixture of fatty acids (FA) with different chain length and unsaturation content (Ashnani et al., 2014). Hydrophilic polar head and nonpolar hydrophobic chain make it amphiphilic in nature (Adhvaryu et al., 2000). The chemical composition of its polar and nonpolar groups is beneficial for tribological application (A. Adhvaryu, Erhan, & Perez, 2004). Lubricant with the long chain or tail molecules attaching itself to the solid surface and provide layer. Polar end (carboxyl group-COOH) of fatty acid is an intermediate link to connect alkyl chain (-CH_3) with the surface. Longer hydrocarbon chain provides more effective separation between solid surfaces (Adam, 1928; Brophy & Zisman, 1951). This lubrication also provides a high degree of slip and low COF. Excellent properties make biodiesel attractive alternatives to petroleum for use as lubricants and industrial fluids (Knothe & Steidley, 2005b). Amphiphilic properties of biodiesel play a vital role in the performance of lubricant that occurs in the boundary, hydrodynamic, or elastohydrodynamic lubrication regimes (A. Adhvaryu et al., 2004). Biodiesel cannot always satisfy the demands of a high performance lubricant by themselves (Reeves et al., 2012) because of oxidation instability and reactivity of unsaturated hydrocarbon chain (Fazal & MA. Haseeb, 2014; Goodrum & Geller, 2005; Sarin et al., 2009). Hydroperoxides and organic acids are products of oxidation which forms an insoluble residue and decrease the lubricity (Fazal et al., 2013b; Haseeb et al., 2010; N. Kumar & Chauhan, 2014). In tribology, this oxidative deterioration of biodiesel introduces oxidative wear (Xu et al., 2013). Some other factors such as moisture absorption, deposit formation, corrosivity, contaminants, elevated temperature, reduced viscosity, etc. have also a negative impact on biodiesel lubricity (Fazal et al., 2013b; Haseeb et al., 2010). Through various chemical manipulations are done for the enhancements of lubricity (C. J. Reeves, 2013), still other researchers are interested to investigate the stability of biodiesel when doped with antioxidants (Kapilan et al., 2009; Saad et al., 2008). For this reason, additives are doped with biodiesel to improve the lubricant's ability to reduce friction and wear. Biodiesel oxidation cannot be fully eradicated but remarkably minimized by means of antioxidant which retardate reconversion of free fatty acids to triglycerides. An antioxidant is needed for improvement of oxidation stability of biodiesel and reduce oxidative wear. Search for suitable antioxidant became imperative for the researchers over lubricity improver. Generally, antioxidants are divided into two types which are hydro-peroxides decomposer and chain breaker. Phenolic types are most commonly used as a chain-breaking antioxidant. Generally, the active hydroxyl group present in phenolic antioxidant provides protons that intercept the peroxide radical ($RCOO^{\cdot}$) to prevent it from creating another radical. Thus, retarding the chain reaction of auto-oxidation as follows.

Radical tapping stage: $R\text{-}COO^{\cdot} + AO = R\text{-}COOH + A^{\cdot}$

Radical termination stage: $A^{\cdot} + A^{\cdot} = A\text{-}A$ or non-radical material

The lubricity of phenolic antioxidants can be determined by the number of hydroxyl/ phenolic groups found in its molecular structure. Tert-Butylhydroquinone (TBHQ), Propyl Gallate (PG), and Pyrogallol (PY) have two OH groups, while 3, 5-di-butyl-4-hydroxytoluene (BHT) and (BHA) have only one OH group attached to the aromatic ring. By using the theory of electro-negativity, TBHQ, PG, and PY provide more locations to react with the free radical thus terminating the auto-oxidation chain reaction without forming any acidic products (Jakeria et al., 2014). TBHQ, PrG and PY have more than one hydroxyl groups attached to the aromatic ring thereby more effective antioxidant compared to BHT and BHA (Albuquerque et al., 2012; K. A. Sorate & Bhale, 2015). Several research has been attempted in order to quantify the respective lubricity for specific biodiesel. Accordingly, this portion of the study aimed to search the impact of different additives doped palm biodiesel on lubricity.

2.8.1 Wear and friction

Friction and wear play important roles in defining the durability of mating components against tribological degradation where the sliding contact takes place. Diesel engine and its fuel systems comprise numerous dynamic tribo-pairs, such as piston and piston ring to cylinder liner, valve to valve guide, injector needle to injector inner chamber, and filter plunger to plunger guide. Most of these tribo-pairs are directly exposed to fuel, which solely provides the lubricity of these mating components (K. Sorate & Bhale, 2013). Biodiesel shows excellent lubricity by reducing friction and wear through its unsaturated hydrocarbon content (R. Fattah et al., 2014; Fazal, MA, et al., 2011b; K. A. Sorate & Bhale, 2015). Several experiments using reciprocating motion, rotating motion with four-ball, pin-on-disk, and ball-on-plate arrangements were performed to evaluate the wear behavior in the metal and biodiesel interface. For example, Xu et al. (Xu et al., 2013) investigated the effect of different biodiesels on automotive materials in relative motion. They found a better lubricity yet a rough surface texture in surface morphology because of the oxidation of biodiesel. The main wear mechanism was identified as oxidative wear. In (Tsuchiya et al., 2006), a black corrosive organic product was observed adjacent to the worn surface because of the oxidation of biodiesel, thereby creating corrosive acid at a higher temperature (N. Kumar & Chauhan, 2014; Yufu Xu et al., 2010). However, this oxidation creates an inorganic oxide layer or lubrication film and provides less abrasive wear (Lu et al., 2005), which can be attributed to the higher oxidation rate of fresh biodiesel, which in turn forms relatively higher molecular weight compounds and increases viscosity or lubricity (Fox & Stachowiak, 2007). In their analysis of the tribological performance of biodiesel (Jatropha), Kumar et al. (N. Kumar & Chauhan, 2014) found high coefficients of friction and wear at a high temperature and load because of the accelerated oxidation of biodiesel at high temperature as shown in Figure 2.12. These findings indicated that temperature and load individually and collectively affected the tribological performance of biodiesel. Blends with lower concentrations of biodiesel showed a higher frictional coefficient because of the non-uniformity of heteroatom (Fazal et al., 2013b). Abrasive wear, which is observed for pure diesel fuel and lower concentrations of biodiesel, can be identified by the particle sizes of extruded debris of less than 20 µm (Sperring & Nowell, 2005). These third body abrasions may exist if the debris size ranges from 1 µm to 4 µm with less than 20 µm clearance. In actual practice, the debris rolls within the clearance and grooves, thereby resulting in less friction and no further abrasive wear

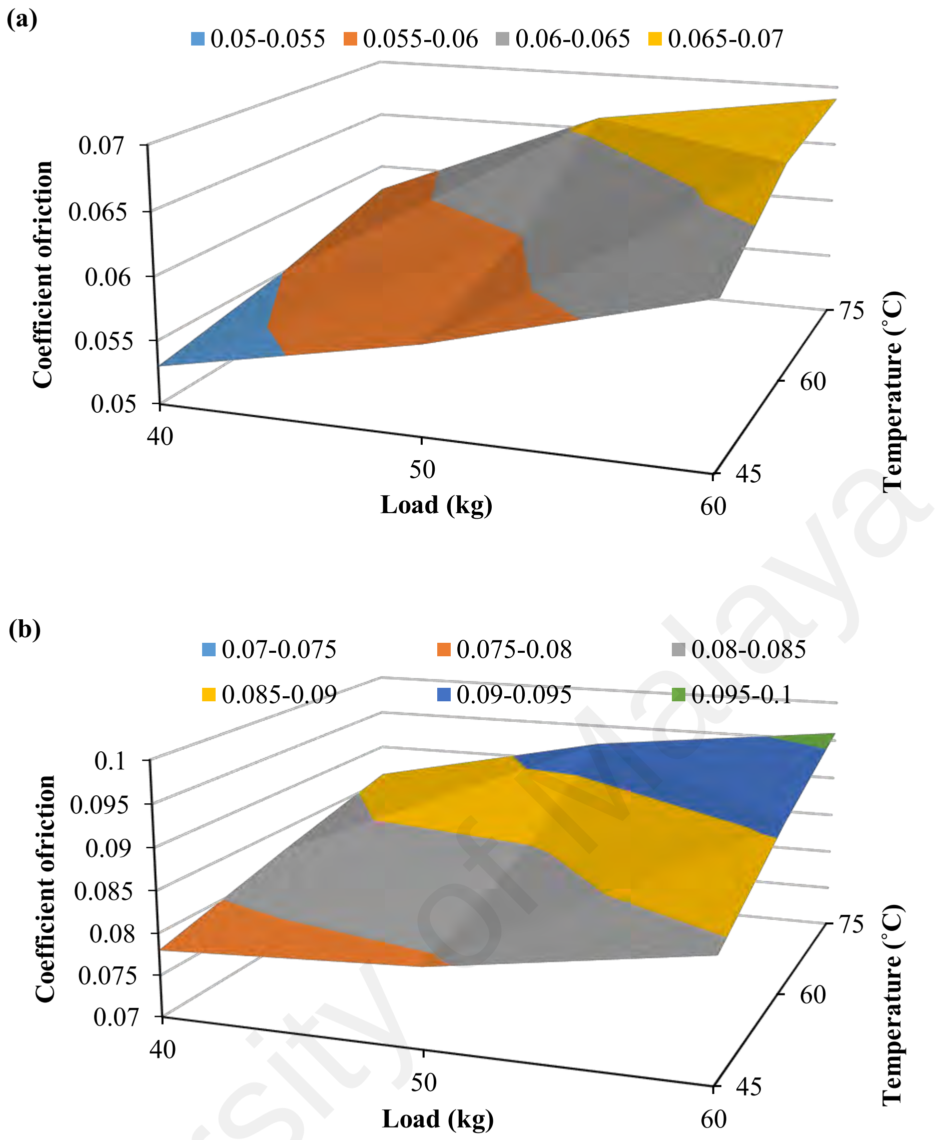

Figure 2.12: Tribological behavior of steel exposed to (a) Jatropha and (b) B0 with different temperatures and load (N. Kumar & Chauhan, 2014).

The lubricity of diesel or biodiesel protects a tribo-pair from friction and wear. The reduction of friction and wear reduces fuel consumption with increased torque, improves durability, increases reliability with a low maintenance cost, and extends the life service interval (Nakasa, 1995). Given the poor lubricity of conventional diesel, the pure biodiesel or its blends may present promising alternatives that can address the challenges in lubricity. To improve lubricity, ASTM-D7467 has mandated biodiesel blends, such as B10 (10% biodiesel and 90% diesel) and B20 (20% biodiesel and 80% diesel) (Kousoulidou et al., 2012). The standard mixture of biodiesel (B20) can reduce particulate emissions by 15% to 20% (McCormick et al., 2001). The presence of sulfur in diesel provides a favorable lubricity, but the high sulfur content of diesel negatively affects the thermal and thermo-oxidative stability as well as the SO_2/SO_3 emission (Sulek et al., 2010). Conversely, biodiesel offers better lubricity than diesel fuel with extremely low sulfur content (Rashid et al., 2008). Such better lubricity can be attributed to the elements in biodiesel (i.e., ,unsaturated components, free fatty acids, oxygenated molecules, and long chain molecules), the polarity, moderate viscosity, and oxidative nature of ester molecules, and the contaminants (i.e., glyceride and triglycerides) (Fazal et al., 2013b; Fazal & MA. Haseeb, 2014). The lubricity of biodiesel mainly depends on methyl esters and mono-glycerides, whereas free fatty acids, diglycerides, and triglycerides almost have no effects on lubricity. Drown et al. (Drown et al., 2001) argued that long chain fatty acids and the residual glycerin rate of oleic acid in biodiesel can behave favorably with better lubricity. Sharma et al. (Sharma et al., 2009) explained that each molecule of the aliphatic fatty acid ($C_nH_{2n+1}COOH$) contained a polar long covalently bonded hydrocarbon chain. The long chain ends have high affinity to partially positive-charged metal surfaces and align themselves normally to the surface to create a monolayer film for the sliding surface. This sliding layer provides a favorable lubricity because of the absence of direct metal-to-metal contact and the reduced thermal energy (Knothe & Steidley, 2005a). Minami and Mitsumune (Minami & Mitsumune, 2002) reported that the anti-wear properties of biodiesel depended on the amount of peroxide, which can decompose the anti-wear additives and introduce higher wear. The presence of oleic acid rate in biodiesel also has a vital role on the lubricity property (Oğuz et al., 2011).

2.8.2 Metal surface degradation

The fuel properties of biodiesel are affected during auto-oxidation. Figure 2.13 shows that the changes in fuel properties can lead to degradation or damage the automotive components, thereby affecting the lubricity of biodiesel. Some products, such as hydroperoxides and organic acids, are formed during oxidation, create an insoluble residue, and decrease lubricity.

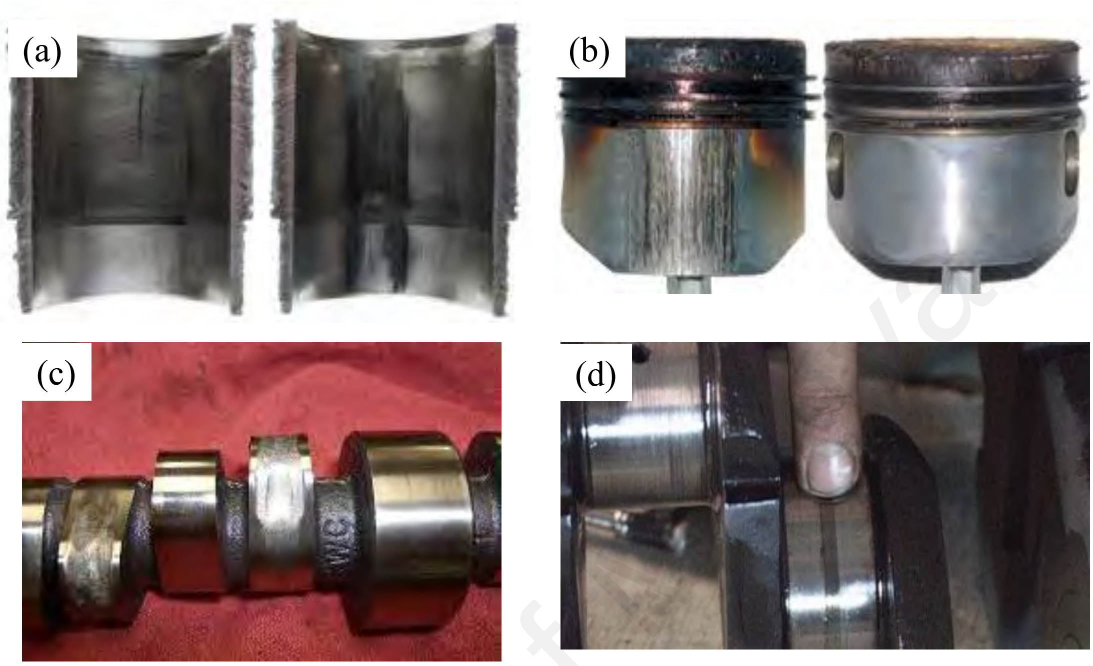

Figure 2.13: Tribological degradation of automotive component (a) cylinder liner (b) piston (c) cam (d) crank shaft

Table 2.9 presents the results of the biodiesel lubricity tests on HFRR (ASTM D6079) and four ball wear machine (ASTM D4172) under different biodiesel blends. These tests reveal that temperature friction and wear both increase along with decreasing lubricity (Fazal et al., 2013b; Haseeb et al., 2010; N. Kumar & Chauhan, 2014), which may be attributed to the reduced thickness of the film created at the contact surface as a result of the increased temperature. This phenomenon may also be explained as the fragmentation of film through polymerization, cross linking, and decomposition at elevated temperatures (Knothe & Steidley, 2005a; Maleque et al., 2000; Salaheldeen et al., 2015). Generally, the tables indicate that all blends of different feedstocks behave better than diesel fuel with better lubricity, less friction, and less wear without engine modifications. From the tribological perspective, coconut oil achieves the best results in the rigorous test followed by sunflower and palm biodiesel because a higher percentage of saturated fatty acid can ensure better lubricity by preventing the reconversion of unsaturated fatty acid. These results may also be attributed to the fact that the carbon chains of fatty acids in coconut oil are longer than those of fatty acids in sunflower and palm oil.

Table 2.8: Wear scar diameter and friction coefficient at various operation parameters

Biodiesel	Blends	Tribo-pair	Load (N)	Speed/ frequency/ rotation	Temp (˚C)	WSD (mm)	COF	Duration (h)	Ref.
Coconut	B100	CI	1226	50 km/h	-	0.54	0.07	2	(Jayadas & Prabhakaran Nair, 2007)
Palm	B0 B10 B20 B50 B100	Cr-alloy steel	392	1500rpm	75	0.95 0.927 0.848 0.82 0.76	0.09 0.0892 0.08775 0.086 0.0857	1	(Fazal et al., 2013b)
Jatropha	B0 B20/B40/B100	Steel	588	1500rpm	45-75	1 0.5-0.7	0.08-0.1 0.055-0.075	1	(N. Kumar & Chauhan, 2014)
Soybean	B0 B20	Low C-steel	100	-	60	0.4 0.27	0.11 0.10	1	(Wain et al., 2005)
Sunflower	B100	Steel	392	1200 rpm	75	0.3	-	1	(Minami & Mitsumune, 2002)
Rapeseed	B100	Steel	2	50 Hz	60	0.217	0.125	1.5	(Sulek et al., 2010)

Although additive-free biodiesel lubrication film is superior to additive-free diesel, the former has a higher wear rate than commercial lubricants (Jayadas & Prabhakaran Nair, 2007). The hydrodynamic and/or boundary lubrication film thickness can be reduced by the high temperature, load, and frequency, as well as the low viscosity and concentration (Maleque et al., 2000; Masjuki et al., 1999). Oxidation instability, as a consequence of temperature, moisture absorption, and reactivity of the unsaturated hydrocarbon chain, has negative effects on the lubricity and wear for different blended fuels (Goodrum & Geller, 2005; Sarin et al., 2009). Moreover, oxidation increases viscosity and demonstrates better lubricity in the short-term test, but the degradation of fuel reduces lubricity in the long-term study (Tsuchiya, Shiotani, Goto, Sugiyama, & Maeda, 2006). The degradation of fuel enhances corrosion and subsequently leads to the rapid tribological degradation of automotive materials. Therefore, the remedial measures with inhibitors must be investigated to improve the lubricity of biodiesel and its blends.

2.8.3 Remedial measures for wear reduction

Antioxidants are naturally present in triglyceride which is neutralized through transesterification, thereby deteriorating oxygen stability (Yaakob et al., 2014). In tribology, the oxidative deterioration of biodiesel introduces oxidative wear (Xu et al., 2013). Some other factors, such as moisture absorption, deposit formation, corrosiveness, contaminants, elevated temperature, and reduced viscosity, have negative effects on biodiesel lubricity (Fazal et al., 2013b; Haseeb et al., 2010). Biodiesel oxidation cannot be fully eradicated yet can be significantly minimized by using antioxidants that can retardate the reconversion of free fatty acids to triglycerides. Therefore, antioxidants are needed to improve the oxidation stability of biodiesel and reduce oxidative wear. Small percentages of hydroxylated and unsaturated components can be used to improve the lubricity of low-sulfur diesel fuels (Munson et al., 1999). However, a higher percentage of biodiesel is currently used as an alternative to petro diesel to reduce emission. Such percentage must be free from hydroxylated and unsaturated components to prevent oxidation, which can lead to poor atomization, sticking, and coking. Therefore, researchers must search for a suitable antioxidant to improve lubricity. Antioxidants are generally divided into hydro-peroxide decomposers and chain breakers. Phenolic types are most commonly used as chain-breaking antioxidants. The active hydroxyl group in phenolic antioxidant provides protons that intercept the peroxide radical ($RCOO^{\cdot}$) to prevent the creation of another radical as illustrated in Figure 2.14. Therefore, the chain reaction of auto-oxidation is hampered as follows:

Radical tapping stage: $R\text{-}COO^{\cdot} + AO = R\text{-}COOH + A^{\cdot}$

Radical termination stage: $A^{\cdot} + A^{\cdot} = A\text{-}A$ or non-radical material

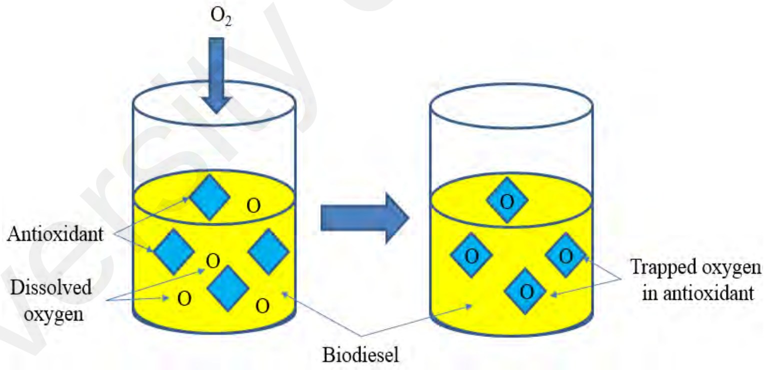

Figure 2.14: Retardation mechanism of the chain reaction of auto-oxidation

The inhibition efficiency of phenolic antioxidants can be determined by the number of hydroxyl/phenolic groups that are found in the molecular structure. The inhibition efficiency of several additives can be explained based on the number of hydroxyls and OH groups that are attached to the aromatic ring. TBHQ, PG, and PY contain two or more OH groups, whereas BHT and BHA only contain one OH group that is attached to the aromatic ring. Based on theory of electro-negativity, TBHQ, PG, and PY provide more locations to react with the free radical, thereby terminating the auto-oxidation chain reaction without forming any acidic products (Jakeria et al., 2014; K. A. Sorate & Bhale, 2015). Moreover, decomposer antioxidants (i.e., sulfides and phosphides) convert hydro-peroxides into alcohols and become stable after transforming into an oxidized form.

Table 2.9: Antioxidants used for wear reduction

Name	Structural formula	Suitable medium	Ref.
Tert-butyl hydroxyl quinine (TBHQ)	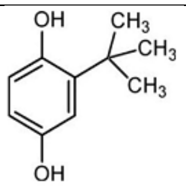	Palm biodiesel, Soybean, Sunflower	(Albuquerque et al., 2012)
Butylated hydroxyamisole (BHA)	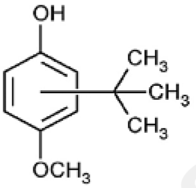	Castor oil, Methyl soyate	(Jakeria et al., 2014)
Butylated hydroxytoluene (BHT)	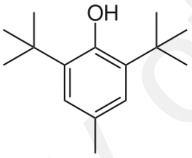	Soyabean oil ethyl este, Tallow	(Jain & Sharma, 2010)
Propyl gallate i.e. 3,4,5-trihydroxybenzoate (PrG)	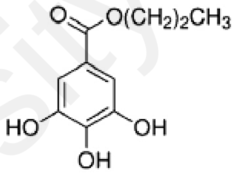	Soyabean	(Robert O. Dunn, 2005)
Pyrogallol i.e. 1,2,3-trihydroxybenzene (PY)	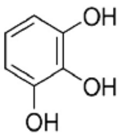	Rapeseed oil, Cooking oil, Tallow, Karanja oil, Jatropha oil, Croton oil	(K. A. Sorate & Bhale, 2015)

Table 2.9 shows the commonly used synthetic antioxidants, with each antioxidant behaving differently for various feedstocks and fatty acid ester compositions (Chen & Luo, 2011). TBHQ, AP, PrG, and PY have more than one hydroxyl groups that is attached to the aromatic ring; therefore, these antioxidants are more effective than BHT and BHA. TBHQ is considered a more active antioxidant for palm biodiesel, soybean, and sunflower because this antioxidant can rapidly form a complex bond with the free

radicals of these feedstocks than those of other feedstocks. By contrast, PY and PrG have also been reported as the best antioxidants because of their molecular structures, which have a larger number of hydroxyl groups attached to their rings (Karavalakis et al., 2011). Table 2.9 shows that PY is the most effective antioxidant for biodiesel, whereas TBHQ is the best antioxidant for palm biodiesel. Several studies have attempted to quantify the inhibition effectiveness of specific biodiesels as shown in Table 2.9. However, the inhibition mechanism of additives on the tribological degradation of different automotive materials has attracted limited research. The following section discusses the materials and methods for identifying the retardation mechanism of degradation because of wear and friction.

2.8.4 Retardation mechanism of tribological degradation

The lubrication regime must be determined to characterize the retardation mechanism, whereas the minimum film thickness to surface ratio must be identified to determine the lubrication regime or specific lubrication film thickness.

2.8.4.1 Film thickness

Specific lubrication film thickness can be determined as follows (Williams, 2005):

$$\lambda = \frac{h_{\min}}{\sqrt{R_{a.1}^2 + R_{a.2}^2}} \qquad (2.11)$$

where λ is a specific lubrication film thickness, h_{min} is the minimum film thickness (m), and R_{a1} and R_{a2} denote the average roughness for the interface materials. The corresponding minimum film thickness for isoviscious lubricant can be predicted by using the well-known Hamrock and Dowson formula as shown in Equation 3 (Hamrock & Dowson, 1981; Ren et al., 2015). This equation is widely applied in many tribo-pairs with varying contact geometries, including the point contact of hemisphere (ball) on a flat surface (plate) (Bart et al., 2012; Kabir et al., 2008). The minimum film thickness equation is expressed as follows:

$$h_{\min} = R_C \left[2.8 \left(\frac{V\eta_O}{ER_C} \right)^{0.6} \left(\frac{L}{ER_C^2} \right)^{-0.21} \right] \quad (2.12)$$

where R_C, V, η_0, L, and E denote the radius of curvature (Mistry et al., 2011), surface velocity (m/s), dynamic viscosity at atmospheric pressure of the lubricant (Pa s)—which can be obtained by multiplying the measured kinematic viscosity (m^2/s) by density (kg/m^3) normal load (N), and modules of elasticity (Pa), respectively. Therefore, we obtain the following:

$$\frac{1}{E} = \frac{1}{2} \left(\frac{1-\nu_1^2}{E_1} + \frac{1-\nu_2^2}{E_2} \right) \quad (2.13)$$

where ν and E denote the Poisson's ratio and young modulus of the interfaced materials, respectively.

2.8.4.2 Adsorption of lubricant on metal surface

In lubrication study, adsorption refers to the adherence of polar groups of lubricant molecules on the friction surface. I reduces the friction and wear by minimizing asperity contact between metal to metal interfaces. Adsorption ability of the lubricant onto friction surface can be quantified by free energy of adsorption (C. J. Reeves, 2013). The adsorption isotherm can be derived from the coefficient of friction. This isotherm shows the relationship between the concentration of additives in biodiesel and its coverage on the tribo-interface surfaces. The friction-derived adsorption isotherm can be obtained from the fractional surface coverage at a specific concentration as follows (Jahanmir & Beltzer, 1986a, 1986b):

$$\theta = \frac{\mu_{blend} - \mu_{ac}}{\mu_{blend} - \mu_{bc}} \quad (2.14)$$

where μ_{blend} is the coefficient of friction (COF) of biodiesel blend, μ_{ac} is the COF at a specific additive concentration, and μ_{bc} is the COF at the concentration above which the COF no longer increases or decreases. The Langmuir isotherm is the simplest adsorption model that provides useful insights into the concentration dependence surface adsorption (Adhvaryu et al., 2006). K_{eqi} is the equilibrium constant of the adsorption and is required to yield the ΔGads values of the additives on the rubbing surfaces. The equilibrium constant can be defined as follows in terms of surface coverage (θ) and additive concentration (C) (Adhvaryu et al., 2006):

$$K_{eqi} = \frac{\theta}{(1-\theta)C} \quad (2.15)$$

$$\frac{1}{\theta} = \left[\frac{1}{K_{eqi}} \times \frac{1}{C}\right] + 1 \quad (2.16)$$

The slope of the θ^{-1} versus C^{-1} isotherm line represents the equilibrium constant of the adsorption (K_{eqi}) (Adhvaryu et al., 2006). K_{eqi} is related to the Gibbs free energy for the adsorption process. The negative value of ΔG_{addi} indicates the spontaneous adsorption of the inhibitor on the sample surface (M. Deyab & Abd El-Rehim, 2013). The numerical value of ΔG_{addi} determines the type of adsorption as physical, chemical, or physicochemical (M. Deyab & Abd El-Rehim, 2013; Tebbji et al., 2007). The ΔG_{addi} of the inhibitor on the material surface can be calculated as follows (X. Li et al., 2012):

$$\Delta G_{addi} = -RT\ln(55.5 \times 10^{6} K_{eqi}) \quad (2.17)$$

where ΔG_{addi}, R, T, and K_{eqi} denote the adsorption energy of the inhibitor (kJ mol^{-1}), the universal gas constant (8.314472 J/mol.K), the operating temperature (K), and the equilibrium constant of the adsorption process, respectively.

2.9 Summary and conclusions

This chapter reveals that the oxidation stability of pure biodiesel depends on the degree of saturated fatty acids, which varies across different feedstocks. Coconut, palm, and tallow contain higher amounts of saturated fatty acids than those of *Jatropha*, soybean, sunflower, and rapeseed. As such, these commodities present a higher oxidation stability yet degrade with a longer storage time. The changes in the physical properties and chemical instability of biodiesel initiate the corrosion and tribological degradation of automotive materials, such as iron, iron-based alloy, steel, copper, copper-based alloy, aluminum, and aluminum-based alloy. Even when blended with diesel, biodiesel remains highly prone to corrosion and tribological degradation. Therefore, the degradation of the material and stability of biodiesel must be hampered by altering or modifying the fuel or metal surface. The use of antioxidants or corrosion inhibitors for fuel alteration is more feasible than material surface modification. Antioxidants delay auto-oxidation and retain the oxidation stability of biodiesel, whereas corrosion inhibitors form a protective oxide layer through the physical, chemical, or physicochemical adsorption processes. Such processes can be justified through different adsorption models and thermodynamic functions to quantify the effectiveness of corrosion inhibitors. Although many studies have investigated the corrosion inhibition of the fuel–metal interface by using different inhibitors, few studies have investigated the inhibition mechanism. Moreover, considering that palm biodiesel with different additive concentrations and elevated temperatures has never been investigated, the inhibition action and adsorption types of additives remain unknown. Therefore, future studies must investigate the inhibition mechanism of palm biodiesel against corrosion and the tribological degradation of its material. Improving the inhibition mechanism in any operating condition may allow the large-scale replacement of petrodiesel and the commercialization of biodiesel.

CHAPTER 3: EXPERIMENTAL

Corrosion inhibition and retardation of tribological degradation of automotive materials in both biodiesel and its blend were investigated by static immersion test and high frequency reciprocating rig (HFRR) respectively. This chapter presents the materials and methods used for achieving the objectives. It also includes a brief description of the instruments used along with their working principles.

3.1 Experimental

3.1.1 Materials

Among the metals used in automobile two major ferrous metals which are mostly exposed to fuel were chosen to inhibit their corrosion and tribological degradation. They are mostly gray cast iron and low carbon steel. Gray cast iron has a graphitic microstructure (Smith & Hashemi, 2011). The chemical composition of gray cast iron graphitic microstructure is 3% carbon and 1.84% silicon which is similar to the previous study (Fazal, M.A, et al., 2011). Silicon is a graphite stabilizing element in cast iron which helps to produce graphite instead of iron carbides; at 3% silicon almost no carbon is held in chemical form as iron carbide (Smith & Hashemi, 2011). Commercially available palm biodiesel and petroleum diesel was used as an immersion medium which was supplied by Weschem Technology, Malaysia and AZ One Global, Malaysia. The report of physical and chemical properties provided by the supplier is summarized in Table 3.1

Table 3.1: Physical and chemical properties of palm biodiesel

Properties	Units	Standard	Ranges	Values for present palm biodiesel
Density at 15˚C	g/cm^3	EN ISO 12185	0.86-0.9	0.875
Viscosity at 50˚C	mm^2/s	EN ISO 3104	3.5-5.0	4.3
Flash point	˚C	EN ISO 3679	Min 120	268
Cetane number	-	EN ISO 5165	Min 51	71.4
Moisture	ppm	EN ISO 12397	Max 500	443
Total ester content	% (m/m)	EN 14103	96.5	98.8
Methanol	% (m/m)	EN 14110	Max 0.20	<0.10
Mono-glyceride	% (m/m)	EN 14105	Max 0.80	0.18
Di-glyceride	% (m/m)	EN 14105	Max 0.20	<0.10
Tri-glyceride	% (m/m)	EN 14105	Max 0.20	<0.10
Total glycerol	% (m/m)	EN 14105	Max 0.25	0.10

In order to reduce corrosion of metals, inhibitors containing amine and hydroxyl group were used. They are tert-butyylamine (TBA), Benzotriazole (BTA), Butylate-dhydroxytoluene (BHT), Pyrogallol (PY). TBA is also used in retardation of tribological degradation along with two anti-oxidant such as Butylated hydroxyamisole (BHA) and Tert-butyl hydroxyl quinine (TBHQ). Anti-oxidant helps to suppress the auto-oxidation of biodiesel. All those additive were produced in R&M Chemical, UK and Sigma-Aldrich Chemistry, USA and supplied by Global Science Resource Sbn Bhd, Malaysia. List of different additives used in this study are shown in Table 3.2 with their details.

Table 3.2: Details of different additives

	Name	Abbreviation	Chemical formula	Structural formula	Molecular weight (g/mol)	Purity (%)
Corrosion inhibition study	Tert-butylamine	TBA	$C_4H_{11}N$	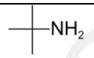	73.14	Min 99.0
	Benzotriazole	BTA	$C_6H_5N_3$	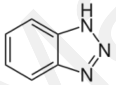	119.13	Min 99.0
	Butylate-dhydroxy-toluene	BHT	$C_{15}H_{24}O$	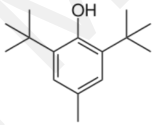	220.36	>99.0
	Pyrogallol	PY	$C_6H_6O_3$	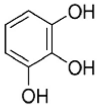	212.20	>98.0
Retardation of Tribological degradation study	Tert-butyylamine	TBA	$C_4H_{11}N$	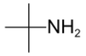	73.14	Min 99.0
	Benzotriazole	BTA	$C_6H_5N_3$	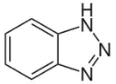	119.13	Min 99.0
	Butylated hydroxyamisole	BHA	$C_{11}H_{16}O_2$	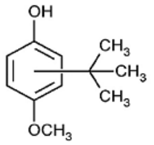	180.25	>98.0
	Tert-butyl hydroxyl quinine	TBHQ	$C_{10}H_{14}O_2$	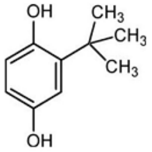	166.22	97.0

3.1.2 Experimental Design

There are three different phases in each section (Table 3.3). In both section, first phase of experiments was to find the better additive for ferrous metals exposed to biodiesel. Second phase of experiments for corrosion inhibition study was done with different concentrations of best additive in biodiesel (B100) for cast iron and low carbon steel at both 300 K and 353 K. Study at 300 K with different concentration is for identification of adsorption type while elevated temperature will provide information about thermodynamic parameters. Similar study was conducted for biodiesel blend (B20) in the third phase.

In order to investigate the effect of best additive concentration on lubricity of biodiesel, phase-2 was designed. It will also provide the film thickness of additive and roughness of metal surface which is needed for lubrication mechanism and adsorption analysis. Phase-3 was conducted with the same experimental condition as set-2 but for B20.

Table 3.3: Experimental Plan

Remedial study	Phase	Materials	Experimental condition	Experimental method
Corrosion	01	CI and LCS in TBA, BTA, PY, BHT doped B100	Duration-50days at 300 K	Static immersion test
	02	CI and LCS in doped B100 with different concentrations of best additive	Duration-50days at 300 K and 353 K Concentration-100/200/300/400/500	Static immersion test
	03	CI and LCS in doped B20 with different concentrations of best additive	Duration-50days at 300 K and 353 K Concentration- 100/200/300/400/500	Static immersion test
Tribological degradation	01	CI-440c ball in B100, B20 and B0 without additive and CI-440c ball in TBA, BHT, BHA, TBHQ doped B100	Duration- 3600 sec at 300 K Load-75 N, Frequency-33Hz, Stroke-2mm	High Frequency Reciprocating Rig (HFRR)
	02	CI-440c ball in doped B100 with different concentrations of best additive	Duration- 3600 sec at 300 K Load-75 N, Frequency-33Hz, Stroke-2mm Concentration- 300/400/500	HFRR
	03	CI-440c ball in doped B20 with different concentrations of best additive	Duration- 3600 sec at 300 K Load-75 N, Frequency-33Hz, Stroke-2mm Concentration- 300/400/500	HFRR

Figure 3.1 represents the flow chart of the experimental design which is segregated into two sections such as immersion and lubricity test.

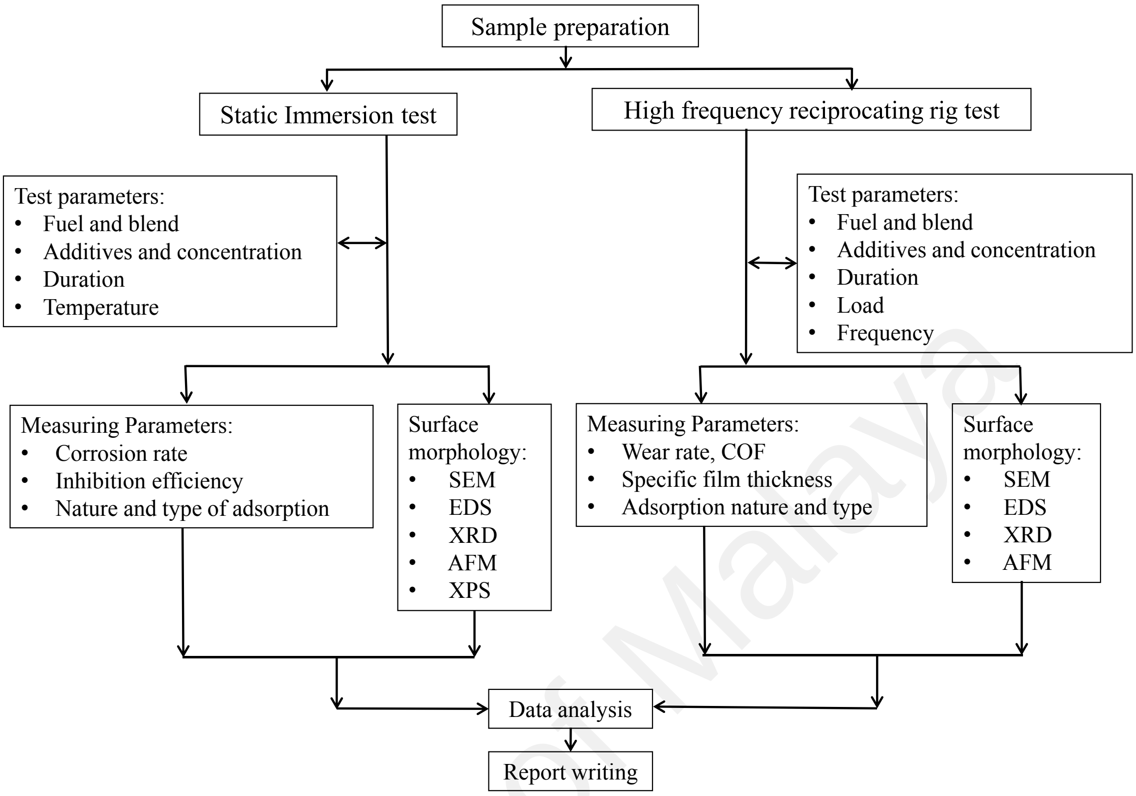

Figure 3.1: Flow chart of experimental design

3.1.3 Sample preparation

Sample preparation for immersion test was done according to the techniques used by Fazal et al., and Finšgar et al. (Fazal, M.A, et al., 2011; Finšgar & Jackson, 2014).Cast iron and low carbon steel round bar was used to make coupons by machining. Diameter of the coupons are 37 mm and 22.5 mm for cast iron and low carbon steel respectively with the same thickness of 2 mm. For static immersion test, a hole of 2mm diameter near the edge of the each coupon was made. Each coupon sample was mechanically abraded by SiC paper ranging from 800-1200 grade. Preparation of sample surface by grinding and polishing have negligible effect on corrosion behavior (Papavinasam et al., 2003). In order to do line scanning of sample cross-section, coupon was molded. To minimize edge effect of the sample, fine polishing is preferred instead of cutting which could alter of material properties due to heat generation (Barmatov et al., 2012).

Tribology was conducted on ball-on-plate tribo-test machine. The plate with dimensions of 15×15×3mm was made from same cast iron round bar. The counter part of tirbo-pair was a chromo alloy steel ball with a diameter of 10 mm, hardness of 62 HRc, and surface roughness of 0.040 μm. The samples were ground with abrasive SiC sand papers ranging from 800-1000 grade.

3.1.4 Sample cleaning

Prior to immersion and tribo test, samples were cleaned as per ASTM G1 standard (Standard, 2003). Samples were degreased with acetone followed by ultrasonic cleaning in the bath of absolute ethanol (Finšgar & Jackson, 2014). These were then dried and stored in desiccator before the immersion test to prevent atmospheric corrosion in the humid environment. After immersion tests for 50d, corrosion product was removed from corroded surface by rinsing with water, brushing with a fibre-bristle brush, and immersing in an ultrasound bath. Residual corrosion products on metal surface was removed by dipping for 5–10 s two times in 10–15% HCl with clarke solution inhibitor, rinsing, and brushing (Standard, 2003). While, after tribo test extruded product was cleaned from the scared surface by rinsing with water in an ultrasound bath. Finally, all samples were rinsed in acetone and then dried to immediately weigh. A high-precision digital mass balance (Denver Instrument) with a lowest count of 0.1 mg.

In this work, ball-on-plate tribological test was carried out by using (Ducom Reciprocating Friction Monitor – TR 282 Series) high frequency reciprocating rig (HFRR). Thereafter, samples were cleaned in an ultrasonic bath followed by rinsing in acetone and distilled water. After drying the sample mass measurement was carried out as an average of three measurements of high precision digital mass balance (Denver

Instrument) with a least count of 0.1 mg. Likewise, commercial biodiesel supplied by Weschem Technology used as state medium of blending.

3.2 Immersion test

Immersion tests were conducted at two different temperatures for 50days in the absence and presence of additives. Room temperature was observed 300 K while a hot plate (SMH-6 Daihan, Korea) was used to conduct the tests at elevated temperature (353 K). According to Sarvi et al.(Sarvi et al., 2009) fuel used in automotive experiences higher temperature (353 K) at inlet. A thermometer (G H Zeal) was used to confirm the required elevated temperature. Glass beakers (600 ml) made of Schott Duran, Germany and supplied by NovaScientific Resources Sbn. Bhd., Malaysia were used to immerse coupons into 500 ml fuel. Fuel was doped with different additive concentrations ranging from 100-500 ppm used as medium of immersion to investigate the corrosion inhibition. For storing the tested coupons, an electric dry cabinet (KD-122 Weifo) after the completion of immersion tests.

3.2.1 Measurement of weight loss, corrosion rate and inhibition efficiency

Weight of the dried sample was measured with five decimal accuracies. Average weight loss of duplicate immersed coupons in fuel was determined. The mean weight loss of duplicate coupons was recorded as a function of cumulative time and then converted into the corrosion rate by using Equation (3.1) (Fazal et al., 2013a).

$$\textit{Corrosion rate}\ \ (C_R) = 8.76\times10^{9}\,W \big/ D\,t\,A \qquad (3.1)$$

where C_R is the corrosion rate (micrometer per year, μm/year); and W, D, t, A, are the weight loss (kg), density of material (kg/m^3), immersion time (h), and exposed area (m^2), respectively.

In Equation (3.2), C_R and C_{Ri} represent the corrosion rate in B100 and TBA-doped B100, respectively. Inhibition efficiency (η) was determined from the weight loss measured after immersion test in palm biodiesel or its blend doped with different additive concentrations. Corrosion inhibition efficiency was calculated as follows (M. A. Deyab, 2014).

$$Inhibition\ \ efficiency\ \ (\eta) = \left[{C_R - C_{Ri}} \big/ {C_R} \right] \times 100\% \qquad (3.2)$$

3.2.2 Adsorption isotherms for the inhibition system

The performance of the additive was investigated using adsorption isotherms, which provide basic information on the interaction between the additive and the metal surface. The best-fitted experimental data for the isotherm model were determined and used to develop a suitable model for the study. The Langmuir model is the easiest and widely used isotherm (Ćurković et al., 2011). Langmuir hypothesized that a surface contains a certain number of sites, where species can adhere through physisorption or chemisorption. Surface coverage (θ) was determined to obtain the characteristic curve of the adsorption isotherm. For different concentrations of the additive, θ was calculated from the inhibition efficiency equation (θ = η/100). The calculated values were plotted in a graph and fitted to a suitable adsorption isotherm. The Langmuir mathematical relationships were used to fit the θ values (Foo & Hameed, 2010), as follows:

$$C_{Addi} \big/ \theta = 1 \big/ K_{eqi} + C_{Addi} \qquad (3.3)$$

where C_{Addi} is the concentration of the additive, and K_{eqi} is the equilibrium constant of the adsorption and is required to determine the energy of adsorption. K_{eqi} denotes the strength between the adsorbate (biodiesel) and the adsorbent (material surface).

3.2.3 Thermodynamic functions for corrosion inhibition process

Thermodynamic parameters are used to determine whether the adsorption process on a surface is spontaneous or not. The standard free energy (ΔG_{addi} = Gibbs energy) of the adsorption of the additive on the metal surface is the fundamental criterion of spontaneity. The magnitude and sign of ΔG_{ads} was calculated using the value of K_{eqi}, which was obtained from the reciprocal value of the intercept of the adsorption isotherm line. The negative value of ΔG_{addi} indicates the spontaneous adsorption of the inhibitor on the sample surface (M. Deyab & Abd El-Rehim, 2013). The numeric value of ΔG_{addi} confirms the type of the adsorption, either physical, chemical, or physicochemical (M. Deyab & Abd El-Rehim, 2013; Tebbji et al., 2007).

Effect of elevated temperature on corrosion inhibition can be identified by thermodynamic functions such as activation energy (E_a) and standard enthalpy (ΔH_{addi}) for adsorption processes. They facilitate to define the adsorption nature of different concentration of additive on sample surface exposed to fuel at elevated temperature. Equation as follow will provide the activation energy (E_a) of corrosion process in different additive concentrations (Connors, 1990):

$$E_a = \frac{2.303R \times \log \frac{C_{R@300K}}{C_{R@353K}}}{\left(\frac{1}{T_{353K}} - \frac{1}{T_{300K}} \right)} \qquad (3.4)$$

where, $C_{R@300K}$ and $C_{R@353K}$ are the inhibited corrosion rates at temperature 300K (T_{300K}) and 353 K (T_{353K}), respectively.

3.3 High Frequency Reciprocating test for lubricity

Friction and wear i.e. lubricity measurements were conducted using ball-on-plate high frequency reciprocating rig (TR-281-M8), Ducom Instruments (Bangalore, India). The evaluation of lubricity test of biodiesel and its blends were conducted as per ASTM D 6079, ISO 12156 standard (M. M. Maru et al., 2014; Standard, 2004). 440C ball was fixed into the reciprocating unit which is rubbing against the clamped metal plate (cast iron). 10 ml of testing fuel and fuel doped with additive was pour into the testing chamber. Temperature of this chamber was kept 300 K through the experiment. Simulated frequency of corresponding diesel engine running speed (2000 RPM) was selected which is 33 Hz under 75 N load. Frictional coefficient as a function of cumulative time (1h) was reported using Winducom software. Reciprocating unit of test rig has a stroke length of 2 mm to ensure minimum vibration owing to the lesser amplitude of displacement. The duration of one hour was used for each experimental trial. The mass of each sample was recorded before and after wear test to quantify mass loss and specific wear rate. The specific wear rate was calculated by using Archard equation (Onions & Archard, 1973), expressed as:

$$Specific wear rate(k) = \frac{m_{loss}}{\rho L s} \qquad (3.5)$$

Where, k, m_{loss}, ρ, L and s are Specific wear rate (m^3/N.m), mass loss of the sample (gm), density of the material (gm/m^3), load (N) and sliding distance (m) respectively. The commercially available palm biodiesel was weighted and mixed in 80 wt. % diesel fuel to produce B20 blend.

3.3.1 Determination of lubrication regime

Function of a lubricant is to introduce a medium of lower shear strength in between tribo interface by reducing number of asperity contacts (C. J. Reeves, 2013). In order to characterize the wear and friction mechanism between the ball and the plate surfaces, it is essential to determine the lubrication regime of individual biodiesel and its blends with or without additive. Lubricity regimes are naturally associated with dominant lubrication mechanism can be referred to as boundary lubrication, mixed/elastohydrodynamic lubrication, and hydrodynamic lubrication (Bartels et al., 2005). The value of specific film thickness (λ) identifies the Lubrication regime: (1) Boundary lubrication if $\lambda < 1$ (2) Mixed lubrication if $1< \lambda < 3$ (3) Elastohydrodynamic if $3< \lambda < 5$ and (4) Hydrodynamic if $\lambda > 5$. To determine lubrication regime or specific lubrication film thickness occurred contact point a calculation of minimum film thickness to surface roughness ratio is determined based on the following equation developed by Dowson and Higginson (Williams, 2005):

$$\lambda = \frac{h_{\min}}{\sqrt{R_{a.ball}^2 + R_{a.plate}^2}} \qquad (3.6)$$

where, λ is specific lubrication film thickness, $h_{\min}$ is minimum film thickness (m), $R_{a.ball}$ and $R_{a.plate}$ is average rms roughness for ball and plate respectively. Corresponding minimum film thickness can be predicted by means of well-known Hamrock and Dowson formula for isoviscous lubricant in equation. 3.7 (Hamrock & Dowson, 1981; Ren et al., 2015). This equation is widely applied in many tribo-pair for a variety of contact geometry including point contact of hemisphere (ball) on a flat surface (plate) (Bart et al., 2012; Kabir et al., 2008). The numerical form of minimum film thickness equation is expressed as:

$$h_{\min} = R_C \left[2.8 \left(\frac{V\eta_O}{ER_C} \right)^{0.6} \left(\frac{L}{ER_C^2} \right)^{-0.21} \right] \qquad (3.7)$$

where, R_C, V, η_0, L, E are radius of curvature of ball (m) (Mistry et al., 2011), surface velocity of the ball (m/s), dynamic viscosity at atmospheric pressure of the lubricant (Pa s); which can be obtained from measured kinematic viscosity (m^2/s) multiplied by density (kg/m^3), normal load (N), and modules of elasticity (Pa) respectively. Therein,

$$\frac{1}{E} = \frac{1}{2} \left(\frac{1-v_{ball}^2}{E_{ball}} + \frac{1-v_{plate}^2}{E_{plate}} \right) \qquad (3.8)$$

where ν and E is poisson ratio and young modulus of respective ball and plate specimen. In this study, ν_{ball} is 0.285, ν_{plate} is 0.211and E_{ball} is 200×10^9Pa, E_{plate} is 210×10^9Pa accordingly (Kabir et al., 2008; Lovell & Deng, 1999);

3.3.2 Adsorption of lubricant on metal surface

In lubrication study, adsorption refers to the adherence of polar groups of lubricant molecules on the friction surface. It reduces the friction and wear by minimizing asperity contact between metal to metal interfaces. Lubricant with long chain or tail molecules attaching itself to the solid surface and provide layer. Polar end (carboxyl group-COOH) of fatty acid is intermediate link to connect alkyl chain ($-CH_3$) with the surface. According to William Hardy, longer the hydrocarbon chain more effective the separation between solid surfaces (Adam, 1928; Brophy & Zisman, 1951). This lubrication also provides high degree of slip and low COF. Lubrication mechanism has two major categories; physical adsorption and chemical adsorption. Numeric value of Gibb's free energy requires to quantify the adsorption nature of lubricant layer on metal surface. Gibb's free energy is that energy which required to remove the lubricant layer from the surface. Above the critical temperature this energy decreases means less energy is needed to desorb the lubricant film.

This study derived adsorption isotherm from coefficient of friction. It shows the relationship between the concentrations of additive in biodiesel blend and its coverage on the tribo interface surfaces. Friction-derived adsorption isotherm can be obtained from following equation 3.9 of fractional surface coverage at the given concentration (Jahanmir & Beltzer, 1986a, 1986b).

$$\theta = \frac{\mu_{blend} - \mu_{ac}}{\mu_{blend} - \mu_{bc}} \quad (3.9)$$

where μ_{blend} is the COF of biodiesel blend; μ_{ac} is the COF at a given additive concentration; μ_{bc} is the COF at that concentration above which there is no further increase or decrease of COF. Among the adsorption models Langmuir isotherm is the simplest and a useful insight into the concentration dependence surface adsorption (Adhvaryu et al., 2006). Hence, Langmuir isotherm model is used in this work to analyze the adsorption isotherms of additives. A constant, K_{eqi}, which is equilibrium constant of the adsorption and is required to yield ΔG_{addi} values of the additives on the rubbing surfaces. K_{eqi} denotes the strength between the adsorbate (biodiesel) and the adsorbent (rubbing surfaces). Equilibrium constant can be defined as in terms of surface coverage (θ) and additive concentration (C) (Adhvaryu et al., 2006):

$$K_{eqi} = \frac{\theta}{(1-\theta)C}$$

$$\frac{1}{\theta} = \left[\frac{1}{K_{eqi}} \times \frac{1}{C}\right] + 1 \quad (3.10)$$

The slope (K_{eqi}^{-1}) of the θ^{-1} vs C^{-1} isotherm line represents the equilibrium constant of the adsorption (K_{eqi})(Adhvaryu et al., 2006). K_{eqi} is related to the Gibbs free energy for the adsorption process. The negative value of ΔG_{addi} indicates the spontaneous adsorption of the inhibitor on the sample surface (M. Deyab & Abd El-Rehim, 2013). The numeric value of ΔG_{addi} confirms the type of the adsorption, either physical, chemical, or physicochemical (M. Deyab & Abd El-Rehim, 2013; Tebbji et al., 2007). The ΔG_{addi} of the inhibitor on the material surface can be calculated using Equation 3.11 (X. Li et al., 2012).

$$\Delta G_{addi} = -RT\ln(55.5 \times 10^{6} K_{eqi}) \qquad (3.11)$$

where ΔG_{addi}, R, T, and K_{eqi} are the adsorption energy of the inhibitor (kJ mol^{-1}), universal gas constant (8.314472 J/mol·K), room temperature (300 K), and equilibrium constant of the adsorption process, respectively.

3.4 Surface morphology

After the immersion in biodiesel for 50 days, PANalytical EMPYREAN X-ray diffraction (XRD) machine was used to examine the corrosion compound formed on sample surface. In order to identify the bonding state of the compound, X-ray photoelectron spectroscopy (XPS: ULVAC-PHI Quantera II) is used. The image of surface texture after immersion test and tribo test was captured by QUANTA FEG 259 and PHNOM proX scanning electron microscopy (SEM). Alteration of elemental composition of exposed surface were characterized by energy dispersive X-ray spectroscopy (EDS). Line scanning of sample cross-section of sample after immersion was done by PHNOM proX scanning electron microscopy (SEM). Atomic force microscopy (AFM) is used to analyze the change in roughness of metal surface after the immersion and tribology test. In order to identify the type of wear, collated debris after filtering the tested fuel was analyzed through SEM/EDS.

3.4.1 Scanning Electron Microscope (SEM)/ Energy Dispersive Spectroscopy (EDS)

In order to examine the metal surface exposed to fuel in micro level, SEM micrographs were captured by QUANTA FEG 259 and PHNOM proX SEM machine. A high-energy beam of electrons scanning the tested sample surface in a roster scan pattern to make the image. The electrons interact with the atoms of sample metal and produces signals which provides information about the surface topography and composition.

SEM comprises with an electron gun and series of lenses in a vacuum chamber. The electron gun has three components, a tungsten wire as cathode, grid cap and the anode (Goldstein, 2012). The tungsten filament emits electron beam when heated to the operating temperature. This electron beam focusing is controlled by applying a negative voltage at grid cap. The series of lenses direct the electrons towards the specimen and more the electrons used, the more powerful the magnification.

The interaction between electron beam (incident beam) and the atoms that make up the specimen producing signals that contains information about the topography and composition. These signals lead to the emission of X-rays and three kinds of electrons: primary backscattered electrons, secondary electrons and Auger electrons. The SEM uses primary backscatter electrons and secondary electrons. Low energy secondary electrons emitted from the specimen surface make the topography and morphology. Electrons, bounced back out of the specimen after the elastic collision with the atoms underneath the sample surface know as backscatter electrons. These backscatter electrons are used to be pictured the image related to the material composition.

EDS typically integrated with SEM which identifies the constituent elements which are unknown. An EDS consists of a detector that contains a crystal to absorb the energy of incoming X-rays by ionizing. This energy of characteristics X-ray wavelength of the element is converted into the corresponding proportional electrical pulses (peaks). Energy peaks corresponding to X-ray generated from different energy shells (k, l and m) of different elements helps to do the elemental analysis of a particular material.

3.4.2 Atomic force microscopy (AFM)

Atomic force microscopy (AFM) were conducted on immersed sample in palm biodiesel for the purpose of investigating the 3D and 2D topography was to characterize the surface roughness. Operation condition was in contact mode under ambient conditions, at scan rate of 1.5Hz and scan angle 0 MFP-3d by an AFM instrument, Asylum Research, Inc.

In order to identify the aggressiveness of palm biodiesel on metal surface AFM is done by bringing a cantilever tip in contact with the rough surface to be imaged. A constant force is kept on tip while scanning across the tested surface. The cantilever is bended upward when an ionic repulsive force from the rough surface experienced by tip. The amount of deflection of the cantilever is measured by a laser spot reflected on to a split photo detector. The vertical movement of the tip follows the surface profile and is recorded as the surface topography by the AFM.

3.4.3 X-ray Diffraction (XRD)

X-ray Diffraction is a non-destructive analytical techniques which record the scattering intensity of an X-ray beam hitting a sample as a function of scattered angle, polarization and wavelength or energy. XRD reveals the information about the crystallographic structure, chemical composition, and physical properties of materials. X-rays can penetrate the sample, thus X-ray diffraction is generally recognized as a non-surface sensitive analysis tool.

X-ray are produced in an evacuated tube. An applied current heat up the tungsten filament which liberates electron beam and accelerated across a high voltage field and bombarded to a target (Cu or Mo). As electron collide with atoms in the target and slow down, a continuous spectrum of X-ray are emitted, which are termed Bremsstrahlung radiation. Cu and Mo is commonly used as target in X-ray tubes which emit 8 keV and 14 keV X-ray with corresponding wavelengths of 1.54 Å and 0.8 Å, respectively.

The radiation exits from the X-ray tube passes through a slit and incident on to the sample from which they are diffracted and recorded into a detector. The sample rotates at a constant angular velocity such that the angle of incident of the preliminary beam changes. The detector rotates at double angular velocity around the sample. Therefore, the diffraction angle (2θ) is always twice the glancing angle. The identification of an unknown sample can easily be achieved by comparing its X-ray diffractogram data with an internationally recognized database. X-rays wavelength of λ at angle θ are reflected form internal crystal plan separated by distance d. The diffraction results from the constructive wave interference can be quantify by Bragg's low (Equation 3.12 and Figure 3.2)

$$\lambda = 2d \sin\theta \qquad (3.12)$$

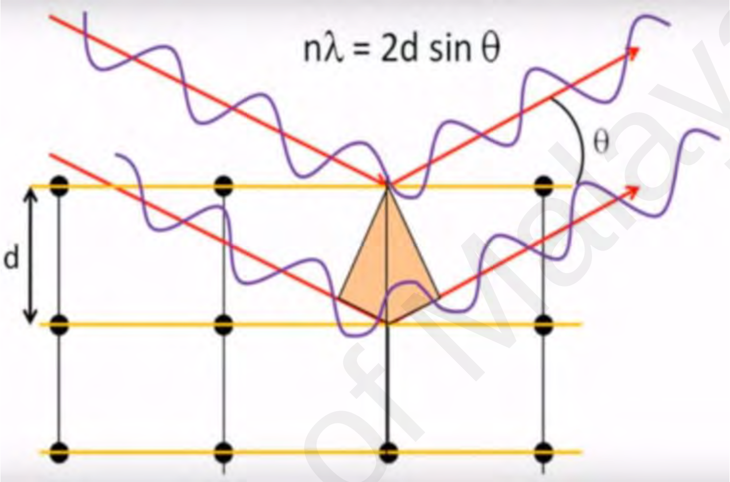

Figure 3.2: Bragg's low of diffraction

In present study, corroded surface was analyzed by X-ray diffractometer (PANalytical EMPYREAN) in the 2θ mode. It was operated at an accelerating voltage 40kV and an emission current of 40 mA using Cu K_α radiatin of wavelength, λ=1.54 Å. The samples were step-scanned in the 2θ range of 5° with a step size of 0.01 and a time of step of 3s.

3.4.4 X-ray Photoelectron Spectroscopy (XPS)

In order to identify the bonding state of the compound formed on metal surfaces after the immersion test, ULVAC-PHI Quantera II X-ray photoelectron spectroscopic machine is used in this study. Under vacuum pressure 3×10^{-7} Pa, a monochromatic AlKα radiation (1486.6 eV) was considered for the analysis. The diameter of the beam was 100 μm and the charge was neutralized by using electron flood gun and mono-atomic Ar ion gun. The wide and narrow scan analysis was performed using pass energy of 280 eV with 1 eV per step and 112 eV with 0.1 eV per step respectively. ESCA software was used to analysis the XPS data.

X-ray photoelectron spectroscopy (XPS) is a quantitative spectroscopic technique that measures the elemental composition, empirical formula, chemical sate and electronic state of the element that exist within the material. This can measure uniformity of elemental composition in three ways, viz., (a) across the top of the surface (or line profiling or mapping), (b) as a function of depth by ion beam etching (or depth profiling), (c) as a function of depth by tilting the sample (or angle resolved XPS). The main principle of XPS is the emission of electrons from the atoms by absorption of photons. The sample is irradiated with mono-energetic X-ray, usually Mg K_α (1253.6 eV) or Al K_α (1486.6 eV). Photoelectron are then transferred to the hemispherical analyzer using combined magnetic and electrostatic lens system (Vohrer et al., 2005). A spectrum is then generated by summing the signal form the channels as the analyzer/lens energies are scanned. This is how XPS spectra are obtained by irradiating a material with a beam of X-ray while simultaneously measuring the kinetic energy and number of electrons that escape from the top 1-20 nm of the material being analyzed. The kinetic energy, E_k of the photoelectrons emitted from the sample surface in given the following Equation (3.13)

$$E_k = h\nu - E_b - \phi_{sp} \qquad (3.13)$$

where, $h\nu$ is the energy of photon spectrometer; E_b is the binding energy of the atomic orbital; and Φ_{sp} is the work function.

The main advantage of the XPS technique lies on the chemical shift in the binding energy. These shifts are very important since they provide a tool to identify individual chemical states of the element. The elements are identified by the positions of the photoelectron peaks, while quantitative information is obtained from the peak intensities of peak areas. The identification of the chemical states is made from the exact measurement of peak positions and separations.

CHAPTER 4: RESULTS AND DISCUSSION

4.1 Introduction

This chapter presents the results obtained from immersion and tribological test of ferrous metals exposed to palm biodiesel, blends and additives doped biodiesel. Firstly, inhibition performance of inhibitors against corrosion and tribological degradation has been presented. Secondly, alteration of metal surface and compositional change after immersion and tribological test are reported. Thirdly, correlation between adsorption mechanism of inhibitor and thermodynamic functions for inhibition process has been established in corrosion study. On the other hand, study of tribology, assessment of lubrication regime and adsorption of additives are discussed.

4.1.1 Corrosion rate and Inhibitor efficiency

This study investigates the effect of tert-butyylamine (TBA), Benzotriazole (BTA), Butylate-dhydroxytoluene (BHT), Pyrogallol (PY) against corrosion of cast iron (CI) and low carbon steel (LCS) through immersion test in palm biodiesel (B100) at 300 K. The effects of each additive and the corresponding corrosion rates of CI and LCS immersed in B100 are examined. It has been suggested by the previous researchers that higher concentration of additive has better performance (Fazal, M.A, et al., 2011). Later on, Deyab (M. Deyab, 2016; M. Deyab & Abd El-Rehim, 2013; M. A. Deyab, 2014, 2016) has taken into account the higher concentrations (100-150 ppm) of additive and found better performance in corrosion inhibition. Therefore, 250 ppm concentration of additive was chosen for this study in order to get even better performance in reducing corrosion. **Error! Reference source not found.** differentiated the performances of each dditive with 250 ppm concentration. The corrosion rates of CI and LCS are 2.26 µm/y and 3.45 µm/y, respectively. Upon adding 250 ppm TBA in B100, the corrosion rates of CI and LCS are reduced to 0.46 µm/y and 0.3 µm/y, respectively. Compared with CI, LCS is more corrosion protective; in addition, its protective property further increases with the addition of TBA. However, the other additives, namely, BTA, BHT, and PY, are not significantly effective in reducing corrosion. LCS also exhibits better corrosion resistance than CI. The corrosion rate of LCS further decreases with the addition of TBA.

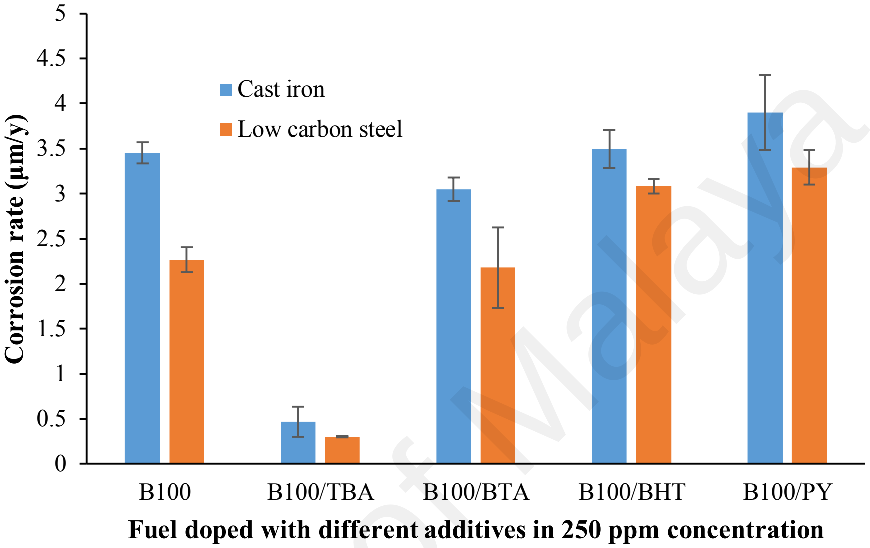

Figure 4.1: Corrosion rates of cast iron (CI) and low carbon steel (LCS) in B100 doped with various additives at 300 K

The inhibition efficiencies of TBA and BTA additives are illustrated in Figure 4.2. TBA performs nearly eight times better for CI and 20 times better for LCS than BTA in reducing corrosion rate. Fazal et al.(Fazal, M.A, et al., 2011) found maximum inhibition efficiency of 47% for 100 ppm TBA doped palm biodiesel. The present study found inhibition efficiency of 86.54% for 250 ppm TBA doped palm biodiesel compare to biodiesel and it performed significantly better than the other additives used in this study. The higher efficiency of TBA can be attributed to the presence of amine in its structure, which may form a protective layer against corrosion attack.

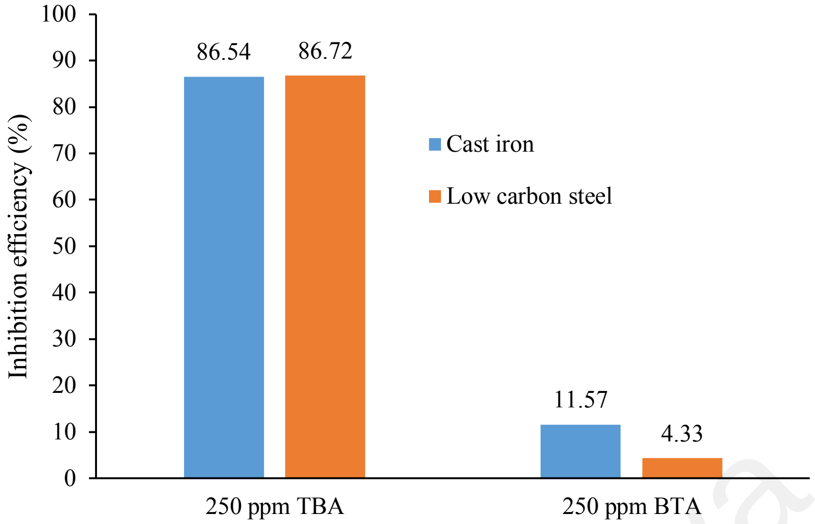

Figure 4.2: Inhibition efficiencies of TBA and BTA doped B100 toward cast iron (CI) and low carbon steel (LCS) corrosion at 300 K.

4.1.2 Morphology of corroded surface exposed to additive doped B100

Figure 4.3 presents the appearance of the corroded CI and LCS coupons exposed to B100 doped with different additives at 300 K. Both CI and LCS samples exposed to additive-doped B100 exhibit severe corrosion attack (Figure 4.3 b–d and Figure 4.3 f-h). However, the degree of corrosion attack is comparatively less in TBA-doped biodiesel (Figure 4.3 a and e). The remarkable improvement in preventing the surface degradation of CI and LCS exposed to TBA-doped biodiesel proves the significant effect in reducing corrosion attack.

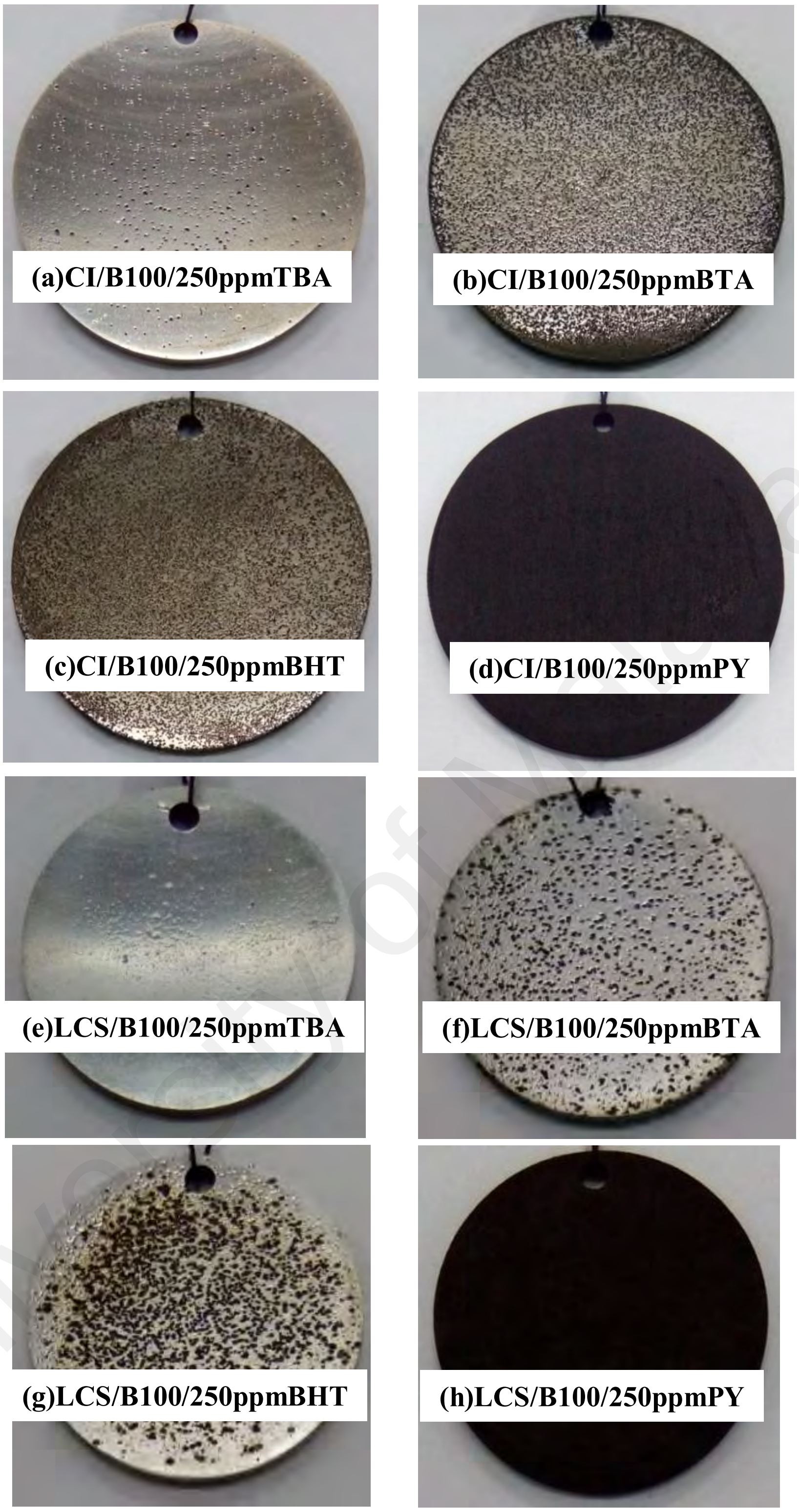

(a)CI/B100/250ppmTBA

(b)CI/B100/250ppmBTA

(c)CI/B100/250ppmBHT

(d)CI/B100/250ppmPY

(e)LCS/B100/250ppmTBA

(f)LCS/B100/250ppmBTA

(g)LCS/B100/250ppmBHT

(h)LCS/B100/250ppmPY

Figure 4.3: Appearances of cast iron (CI) and low carbon steel (LCS) coupons exposed to B100 with different additives at 300 K.

Figure 4.4 illustrates the SEM micrographs of CI and LCS surfaces exposed to B100 doped with TBA and PY additives. The CI and LCS surfaces immersed in biodiesel doped with PY are severely damaged by corrosion attack with large pits (Figure 4.4 b and d). The degradation of the metal surface can be attributed to chemical interaction between the metal surface and the biodiesel. PY is an organic compound consisting of three O atoms with an aromatic ring, which interact with the metal surface (Cook & Hackerman, 1951; Hackerman & Roebuck, 1954) and cannot prevent from corrosion in biodiesel. The SEM images (Figure 4.4) of CI and LCS immersed in TBA-doped B100 exhibit a remarkable reduction in corrosion attack. Small pits are observed on the CI surface (Figure 4.4 a), the amount of which is significantly less on the LCS surface (Figure 4.4 c). These results are consistent with previous findings on corrosion rate. The enhanced performance in corrosion inhibition of TBA-doped biodiesel could be attributed to the good adsorption of the additive, which creates a protective layer on the metal surface.

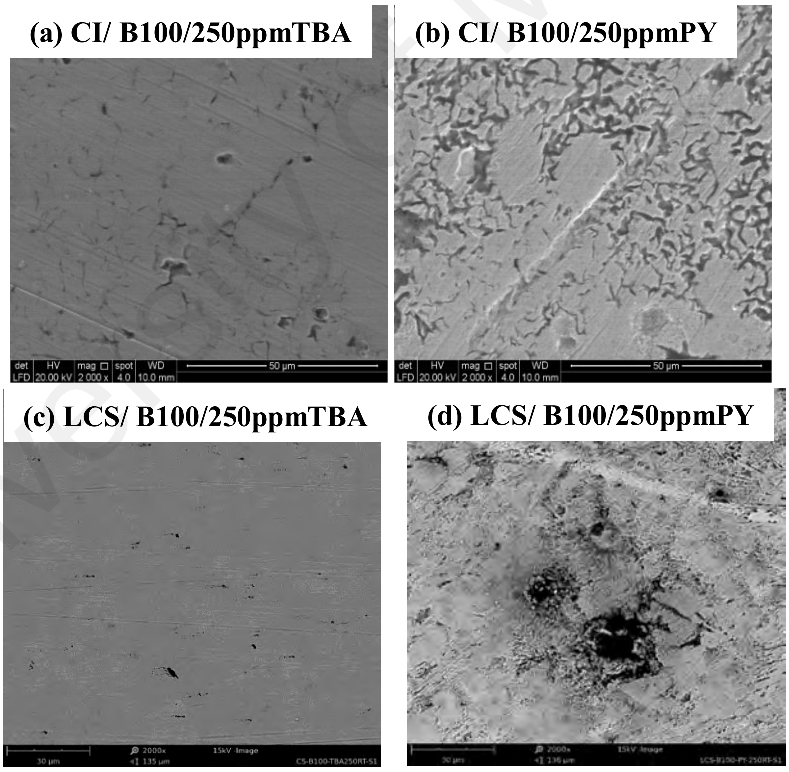

Figure 4.4: SEM images (2000× magnification) of cast iron (CI) and low carbon steel (LCS) surface after exposure to B100 in presence different additives at 300 K.

The EDS analysis of the CI surface exposed to TBA-doped B100 presents less concentrations of C and O than those of the PY-doped CI surface (4.5 a and b). Similar findings are also observed for the LCS surface. The peak of N is observed on both CI

(N: 1.6%) and LCS (N: 5.7%) surfaces, and might have been formed from TBA ($C_4H_{11}N$). The higher percentage of N found in the LCS surface makes it less prone to corrosion than the CI surface. The presence of N atom in TBA may enable it to form bond with the metal surface and improve the anticorrosion properties of the metal surface. Amine based TBA performed better than phenol based BTA because protonated amine present in TBA has the higher electrostatic attraction affinity to the charged metal surface (Fazal, M.A, et al., 2011; Li et al., 1997).

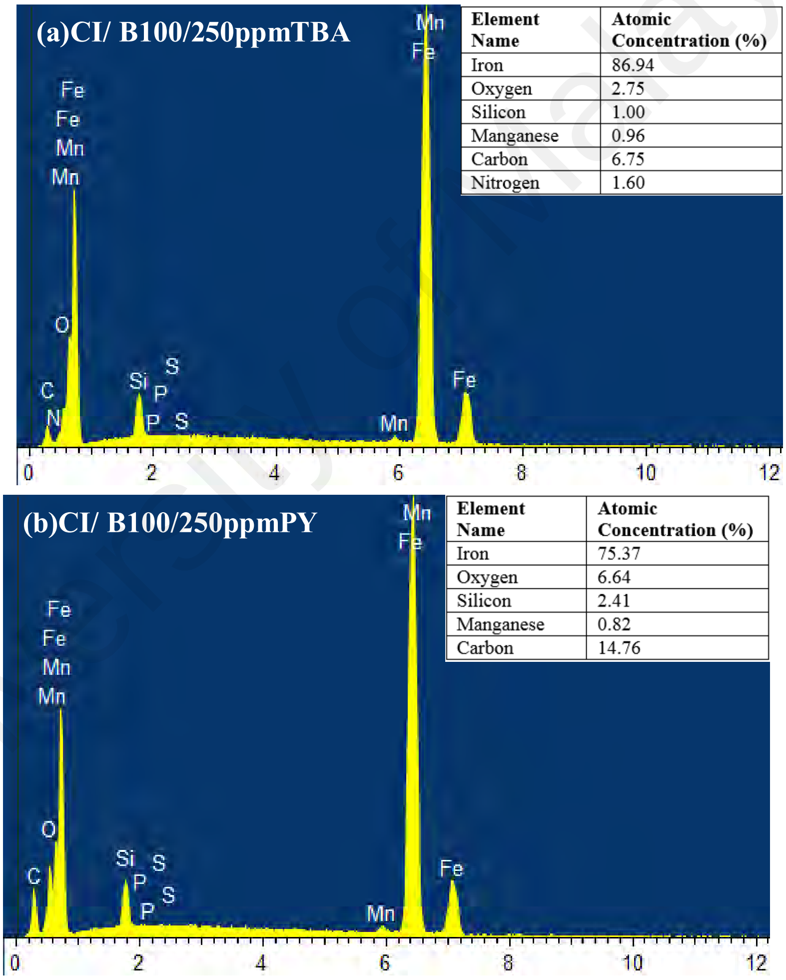

Element Name	Atomic Concentration (%)
Iron	86.94
Oxygen	2.75
Silicon	1.00
Manganese	0.96
Carbon	6.75
Nitrogen	1.60

Element Name	Atomic Concentration (%)
Iron	75.37
Oxygen	6.64
Silicon	2.41
Manganese	0.82
Carbon	14.76

4.5: EDS spectrum of cast iron (CI) and low carbon steel (LCS) surface after immersion in different additives doped biodiesel at 300 K

(c)LCS/ B100/250ppmTBA

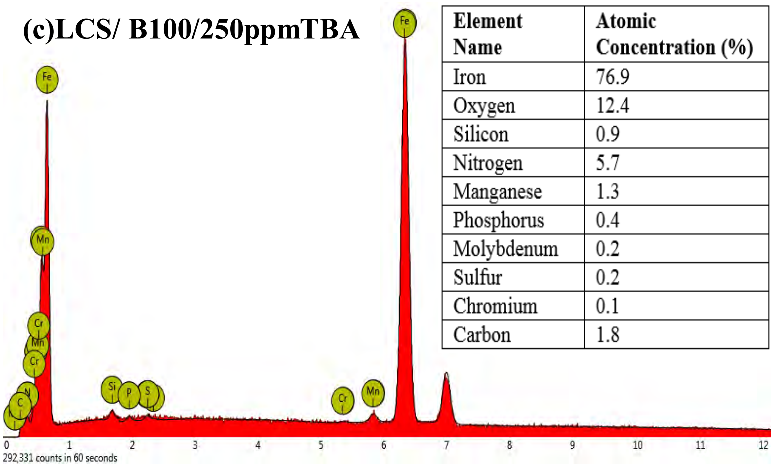

Element Name	Atomic Concentration (%)
Iron	76.9
Oxygen	12.4
Silicon	0.9
Nitrogen	5.7
Manganese	1.3
Phosphorus	0.4
Molybdenum	0.2
Sulfur	0.2
Chromium	0.1
Carbon	1.8

(d)LCS/ B100/250ppmPY

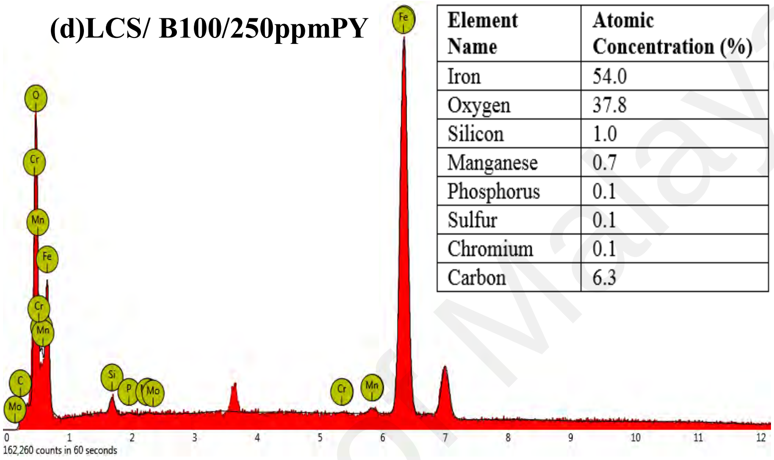

Element Name	Atomic Concentration (%)
Iron	54.0
Oxygen	37.8
Silicon	1.0
Manganese	0.7
Phosphorus	0.1
Sulfur	0.1
Chromium	0.1
Carbon	6.3

Figure 4.5, continued

The wide scan of XPS spectrum of CI and LCS surface exposed to 250 ppm TBA doped B100 is presented in Figure 4.6. It is found that the percentage of atomic concentration of C, O, N, Fe are 4.46, 10.23, 0.39, 84.92 for CI and 9.5, 10.28, 3.56, 76.67 for LCS respectively. Percentage of atomic concentration found from XPS is consistent with the result obtained in EDS (4.5 a and c) and previous studies (Fazal, M.A, et al., 2011; Hosseini et al., 2012). Peaks of Fe^{2+} ($2p^{3/2}$, 710 eV), Fe^{3+} ($2p^{1/2}$, 728 eV) along with C1s, O1s and N1s are observed in the XPS spectra which might indicate the existence of different compound in the adherent layer over the metal surface (Jin et al., 2015). Further analysis with XRD was done in the following for the confirmation of existing compound in a protective layer on metals surface.

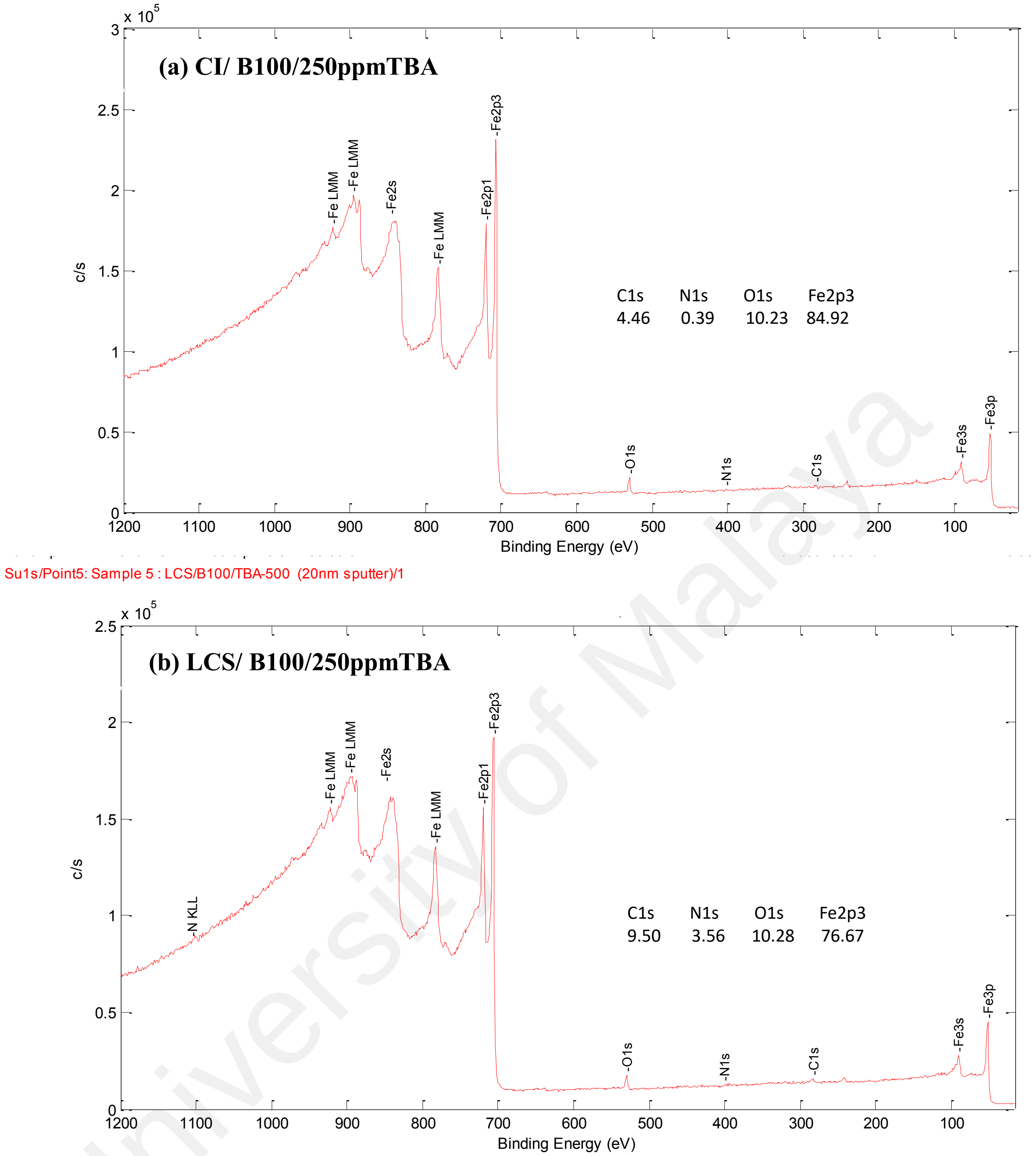

Figure 4.6: Wide scan of XPS spectrum of cast iron (CI) and low carbon steel (LCS) surface exposed to 250 ppm TBA doped B100.

Figure 4.7 provides the XRD patterns of the corrosion products on the corroded surface of CI and LCS after immersion in TBA- and PY-doped biodiesel. The analysis of the corrosion products on the metal surface detects mainly the oxide and hydroxide phases of Fe, particularly on that immersed in PY-doped biodiesel. This finding can be attributed to the failure of adsorption of PY molecules on the CI and LCS surfaces through the lone pair electron of the OH group (Martinez & Štern, 2001). It can also be attributed to the increased acidity and peroxide value of biodiesel (Karavalakis et al., 2011). The adherent products identified on the CI and LCS surfaces in PY-doped B100 are mostly Fe_2O_3, Fe_3O_4, FeO, and $Fe(OH)_2$ peaks (Figure 4.7 b and d). Among these products, the two diffraction peaks of $Fe(OH)_2$ and (Fe_2O_3) after the Fe peaks at around 19° and 20.50° are highly intense. This high corrosion attack is attributed to the lack of surface protection. These results clearly indicate that ferrous metals are prone to corrosion with palm biodiesel even after doping with BTA. The peak intensities of the aforementioned oxides and hydroxide are significantly reduced on the surfaces exposed to TBA-doped biodiesel (Figure 4.7 a and c). The reduction may be ascribed to the sufficient coverage of stable Fe nitrate hydrate protective layer over the CI and LCS surfaces, which blocks direct chemical attacks between the metal and the biodiesel (Fazal, M.A, et al., 2011; Li et al., 1997). A peak of the N-containing compound $Fe(NO_3)3.9H_2O$ at around 40° is formed on the metal surface exposed to TBA-doped biodiesel. The adsorption of TBA on a metal surface may help form an N-rich layer, which can contribute in reducing corrosion attack (Fazal, M.A, et al., 2011; Li et al., 1997). The adsorption of molecules on the metal surface via heterocyclic moiety N atoms (protonated amine) exhibits a stronger interaction compared with that via other heteroatoms (Yıldırım & Cetin, 2008).

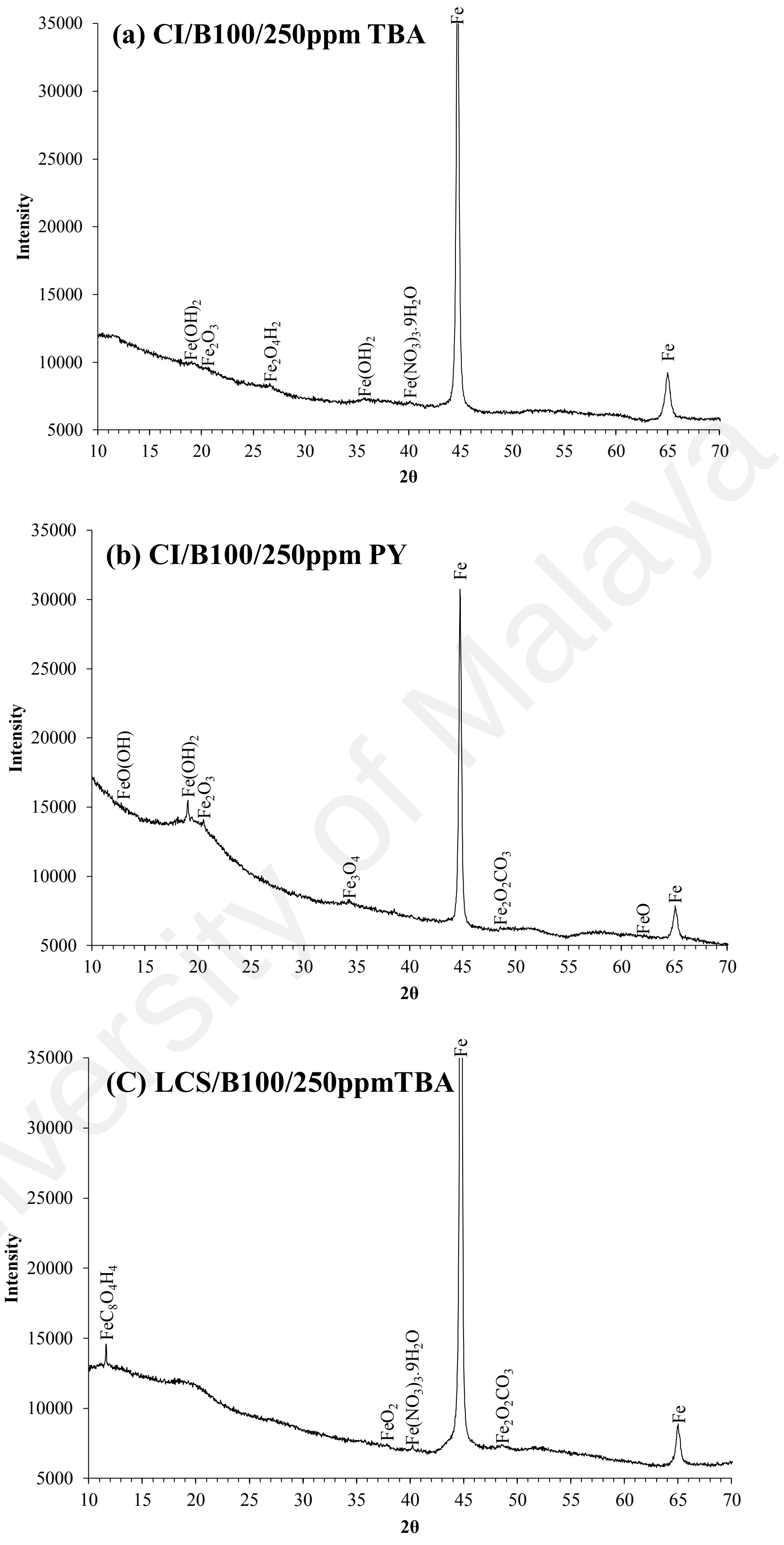

Figure 4.7: XRD pattern of cast iron (CI) and low carbon steel (LCS) surface after immersion in B100 with TBA and PY additives.

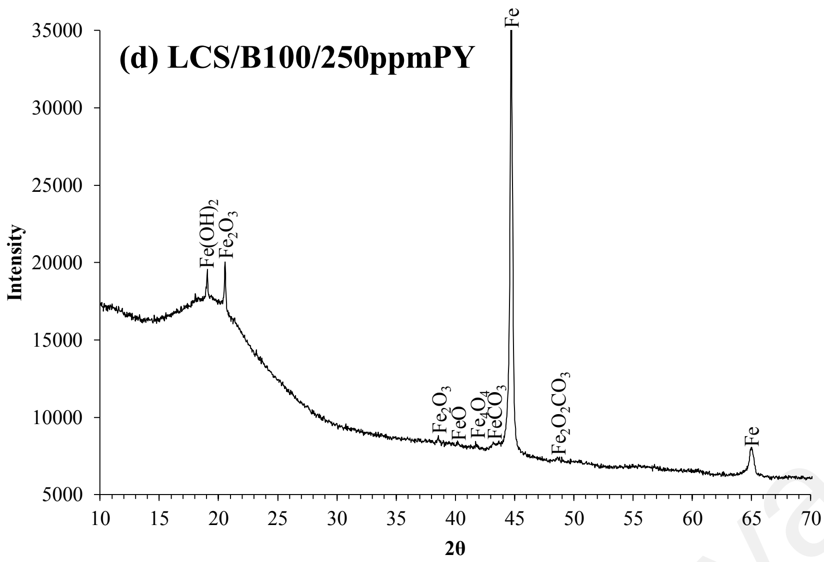

Figure 4.7, continued

Further evaluation of the corrosion inhibition effect of TBA was performed via AFM measurement with scan rate of 1.5Hz. Figure 4.8 presents the tapping-mode AFM photographs of the CI and LCS surfaces after immersion in biodiesel and TBA-doped biodiesel. Figure 4.8 a and c exhibit increased surface roughness due to corrosion attack on the metal surface immersed in B100 for 50 d. Abrupt surface irregularities are observed on the corroded surface of CI in B100 with an arithmetic mean roughness (R_a) of 30.012 nm, whereas that of LCS has less R_a (20.59 nm). Figure 4.8 b and d present a considerable reduction of surface roughness. This pattern can be attributed to the protection against corrosion attack provided by the protective layer formed on the metal surface in TBA-doped biodiesel (B. Zhang et al., 2015).

(a) CI / B100 **(b) CI / B100 / 250ppm TBA**

(c) LCS / B100 **(d) LCS / B100 / 250ppm TBA**

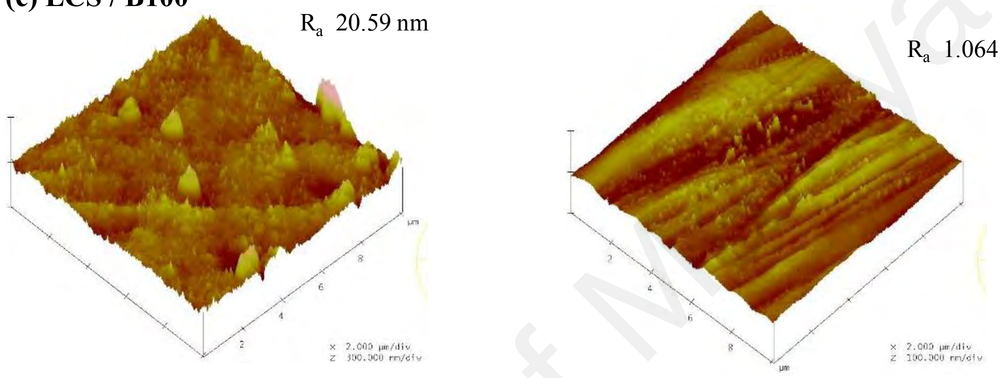

Figure 4.8: Tapping mode AFM photographs of cast iron (CI) and low carbon steel (LCS) surface after immersion in B100 and TBA doped biodiesel.

The cross section of the SEM images of CI and LCS are shown in Figure 4.9. This study found a layer structure with an average thickness of 19.97 µm (Figure 4.8a) and 7.78 µm (Figure 4.9 b) for CI and LCS, respectively. Further line analysis of the cross-section images is performed via EDX to reveal the corresponding elemental distribution. A nearly uniform region enriched with N and probably composed of $Fe(NO_3)_3.9H_2O$ is observed earlier via XRD (Fazal, M.A, et al., 2011). The main constituents within the layer are predominantly N, which proves the assumption of TBA adsorption on the LCS surface and forms a protective layer to prevent further interaction between the metal and the biodiesel. The finding indicates that the protective layer of the N-based compound is adsorbed on the bare metal surface with the formation of $Fe(NO_3)_3.9H_2O$.

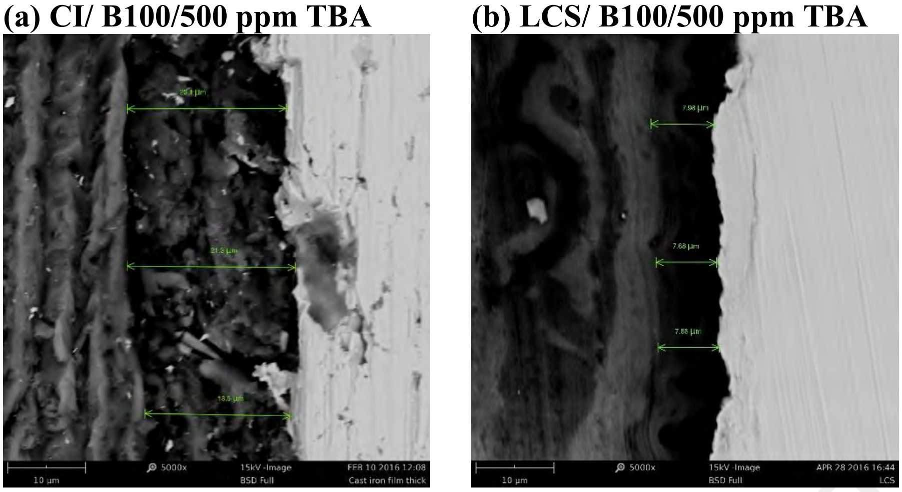
(a) CI/ B100/500 ppm TBA **(b) LCS/ B100/500 ppm TBA**

Figure 4.9: Scanning electron micrograph of cast iron (CI) and low carbon steel (LCS) cross-section after immersion in 500 ppm TBA doped biodiesel for 50 d

4.2 Corrosion inhibition using different concentrations of TBA additives in B100

In this section, inhibition performance, metal surface characterizations through SEM/EDS, XRD, XPS as well as adsorption isotherm model and type of adsorption have been explained in details.

4.2.1 Inhibition performance of different TBA concentrations

Effect of best additive (TBA) obtained in previous presented results in reducing the corrosiveness of biodiesel is investigated. Cast iron and low carbon steel immersion tests were conducted in palm biodiesel (B100) at room temperature (300 K) for 50 d. Figure 4.10 shows the relationship between inhibition efficiency and corrosion rate in palm biodiesel added with different concentrations of TBA at 300 K. It is seen in Figure 4.10 a that for CI the inhibition efficiencies are 46.86%, 81.17%, 92.72%, 96.53%, and 98.30% for biodiesel samples doped with 100, 200, 300, 400, and 500 ppm TBA, respectively. Maximum inhibition efficiency of 47% for cast iron was reported with 100 ppm TBA doped palm biodiesel (Fazal, M.A, et al., 2011). The corresponding corrosion rate of cast iron were 3.45 µm/y and 0.059 µm/y in B100 and 500 ppm doped B100 respectively (Figure 4.10 a). Similar study was done for investigating the effect of tert-butylamine (TBA) on the corrosion inhibition of low carbon steel (LCS) in palm biodiesel (B100). In Figure 4.10 b, it is seen that the corrosion rates in B100 and 500 ppm TBA doped B100 are found to be 2.266 µm/y and 0.135 µm/y respectively. Corrosion inhibition efficiencies of TBA doped biodiesel at 300K are shown in Figure 4.10 b which varies from 85.87% to 97% for 100 to 500 ppm TBA concentrations. In both case, corrosion rate decreases and inhibition efficiency with the increase of TBA concentration in biodiesel. The inhibition efficiency increases and reached almost saturation point at 500 ppm TBA doped biodiesel. This finding could be attributed to the progressive formation of stable and adherent protective layers on the metal surface after the addition of high TBA concentrations (Robert O. Dunn, 2005).

(a) Cast iron

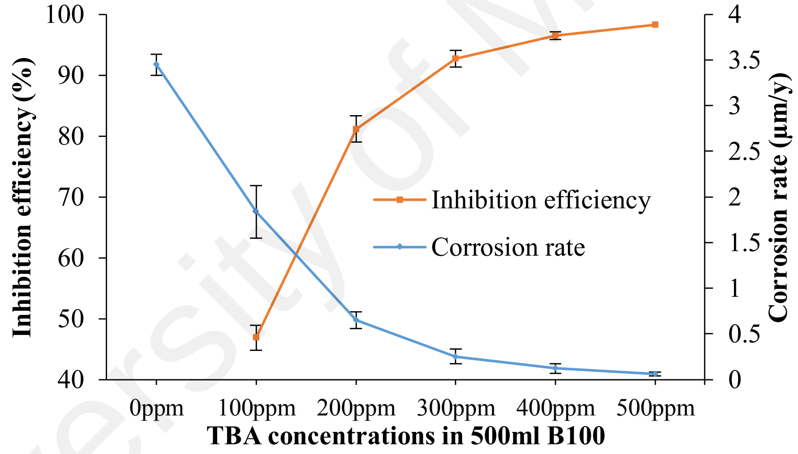

(b) Low carbon steel

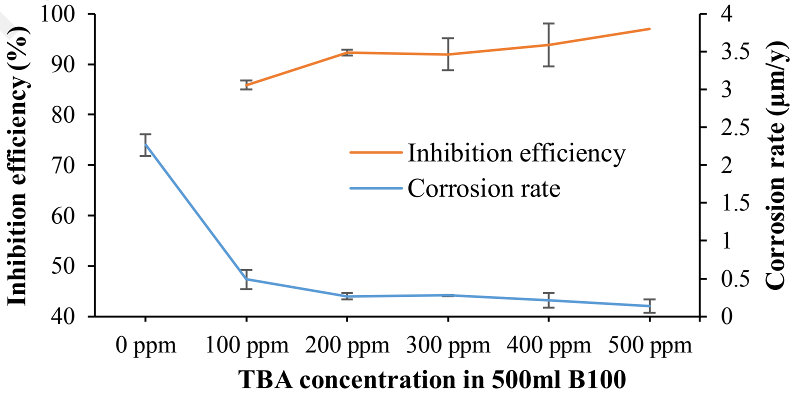

Figure 4.10: Relationship between inhibition efficiency and corrosion rate of cast iron (CI) and low carbon steel (LCS) with various TBA concentrations in B100 at 300 K

4.2.2 Surface Characteristics

Figure 4.11 presents the appearances of cast iron and low carbon steel coupons exposed to palm biodiesel added with different TBA concentrations at 300 K. Both CI and LCS samples exposed to B100 show severe uniform corrosion attack (Figure 4.11 b and i), whose corrosion degree is higher than that in TBA-doped biodiesel. The highly dense corrosion attack in B100 progressively decreases with increasing TBA concentration (Figure 4.11 c to g and Figure 4.11 j to n). B100 doped with 500 ppm TBA exhibits significantly less surface degradation for cast iron. Similar result was found for LCS in 300 to 500 ppm TBA doped B100. This phenomenon proves the remarkable inhibition of corrosion attack on biodiesel exposed metals surface.

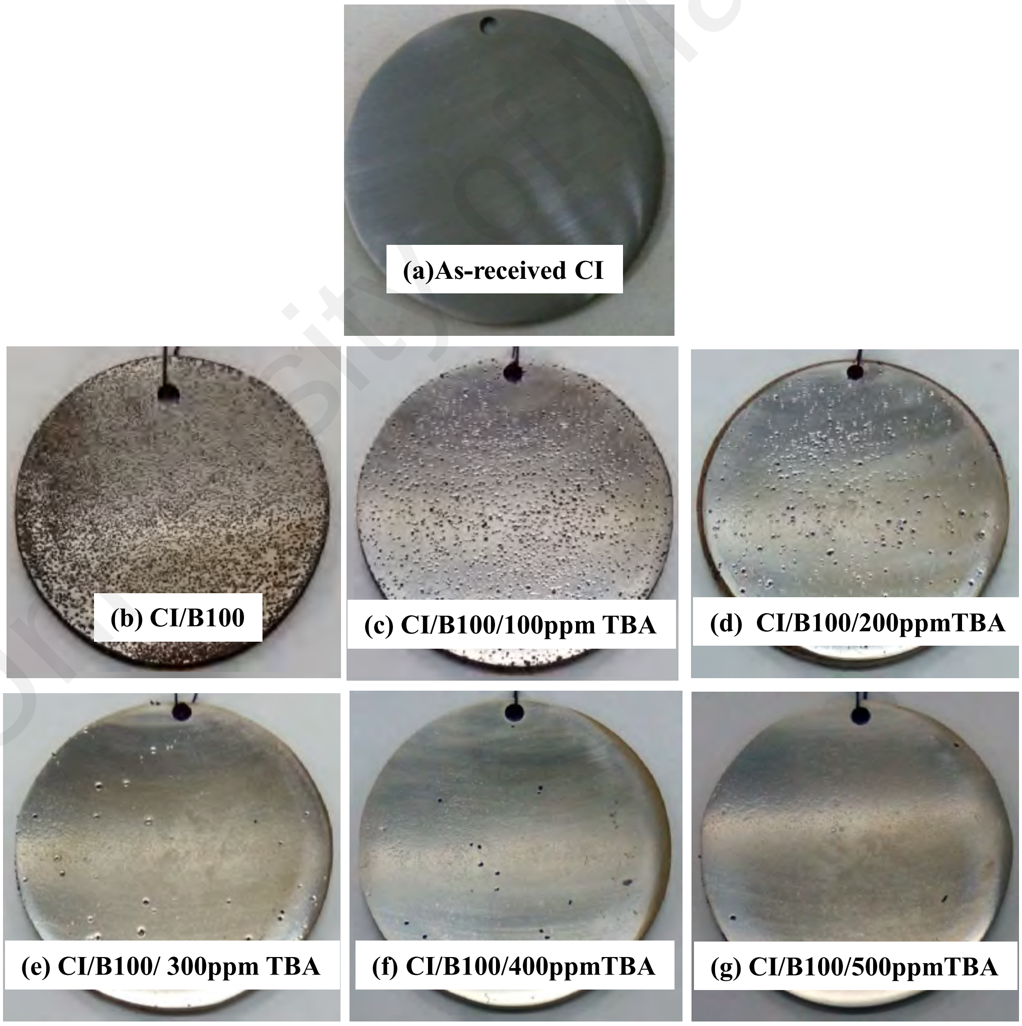

Figure 4.11: Appearance of cast iron (CI) and low carbon steel (LCS) surface before and after exposure to B100 in the absence and presence of TBA additive at 300K

(h) As received LCS

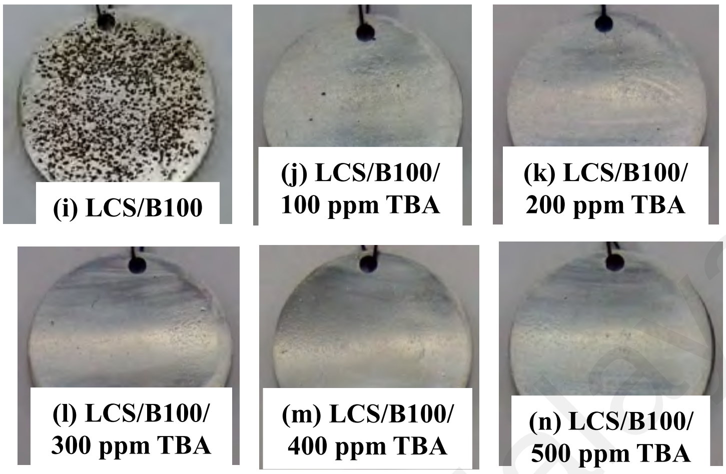

(i) LCS/B100

(j) LCS/B100/ 100 ppm TBA

(k) LCS/B100/ 200 ppm TBA

(l) LCS/B100/ 300 ppm TBA

(m) LCS/B100/ 400 ppm TBA

(n) LCS/B100/ 500 ppm TBA

Figure 4.11, continued

Figure 4.12 represents three-dimensional atomic force microscopic (AFM) images. It shows the changes in surface roughness upon exposure to the biodiesel and 500 ppm TBA doped biodiesel. Phase images of CI and LCS surface immersed in biodiesel are seen in Figure 4.12 a and c which are degraded with average roughness of 30.012 nm and 20.59 nm respectively compared to that of immersed in 500 ppm TBA doped biodiesel. Biodiesel doped with 500 ppm TBA shows very less average surface roughness of 1.985 and 1.6 nm for CI and LCS which are the indications of remarkable improvement against surface degradation.

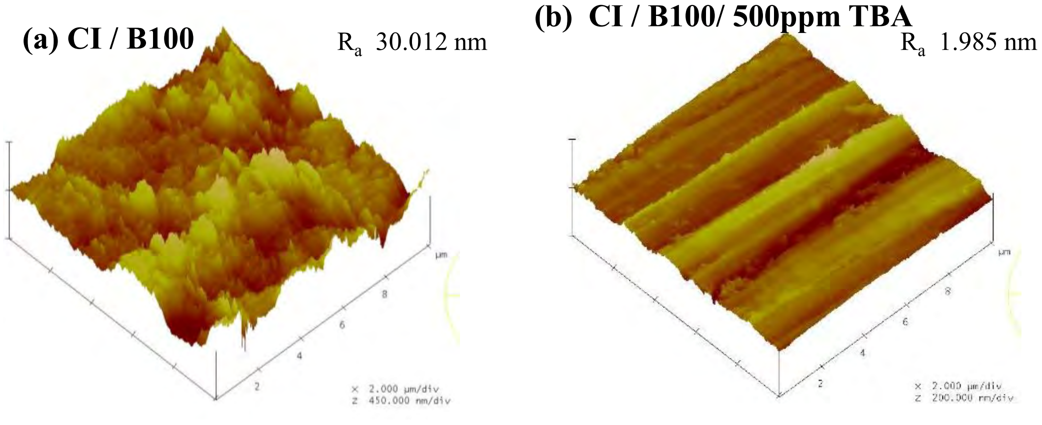
(a) CI / B100

(b) CI / B100/ 500ppm TBA

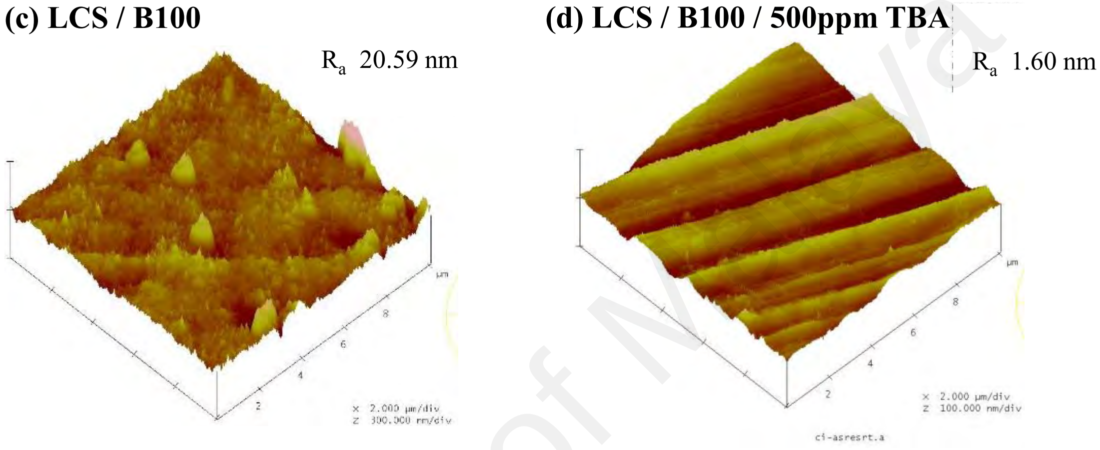
(c) LCS / B100

(d) LCS / B100 / 500ppm TBA

Figure 4.12: Tapping mode AFM photographs of the cast iron (CI) and low carbon steel (LCS) surface exposed to B100 and TBA doped B100

Changes in the surface morphology of the CI and LCS sample immersed in biodiesel and TBA-doped biodiesel at 300 K were further investigated through SEM analysis (Figure 4.13). Figure 4.13 a and e show the as-received CI and LCS surface which exhibit severe degradation when exposed to B100 (Figure 4.13 b and f). The degradation of the CI and LCS surface could be due to chemical interaction between metal surface and biodiesel molecules. In contrast, SEM image of samples immersed into TBA doped biodiesel revealed significantly reduced corrosion attack. However, some pits are observed in Figure 4.13 c and g for 100 ppm TBA doped biodiesel. These pits are remarkably decreased at 500 ppm TBA doped biodiesel (Figure 4.13 d and h). This finding is consistent with the results reported by Deyab et al. (M. Deyab & Abd El-Rehim, 2013; M. A. Deyab, 2014). Improvement of corrosion inhibition could be attributed to the moderate surface coverage of protective layer. In addition, with increased TBA concentration, the formation of protective coverage of TBA could be promoted and its thickness could be gradually increased (Chengjun He et al., 2015; B. Zhang et al., 2015). In the following sections, the metal surfaces are investigated through EDS and XRD analyses.

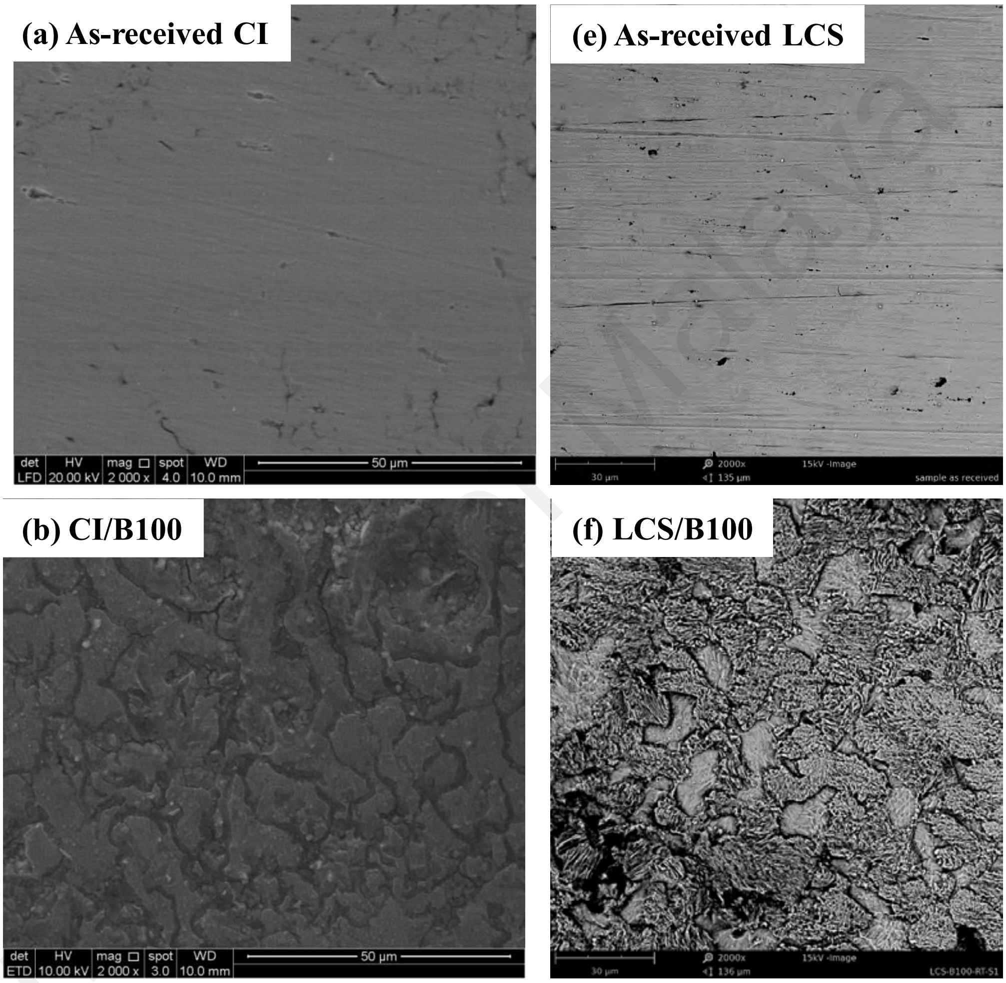

Figure 4.13: SEM images (2000× magnification) of the cast iron (CI) and low carbon steel (LCS) surface before and after exposure to biodiesel in the absence and presence of TBA additive at 300 K.

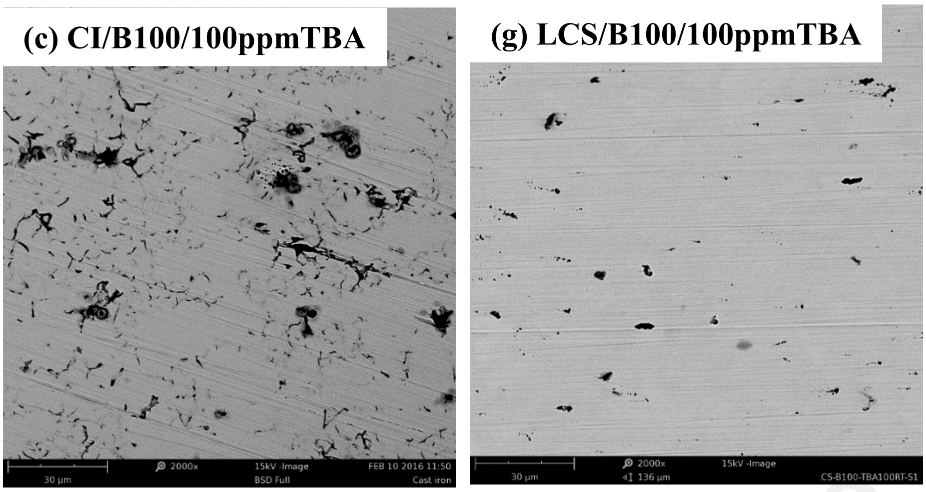

(c) CI/B100/100ppmTBA **(g) LCS/B100/100ppmTBA**

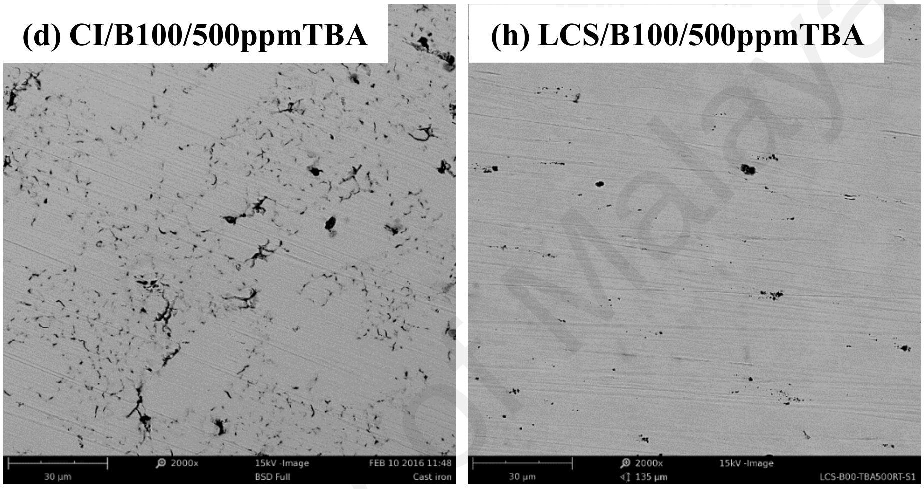

(d) CI/B100/500ppmTBA **(h) LCS/B100/500ppmTBA**

Figure 4.13, continued

The EDS analysis of the CI surface exposed to B100 shows increased concentrations of carbon (C) and oxygen (O) as compared to those in the as-received metal surface (Figure 4.14 a and b). Furthermore, the C and O contents decrease in biodiesel doped with TBA. In particular, the O content in TBA-doped B100 decreases by 60%–70% (Figure 4.14 c). On the other hand, elemental analysis of LCS exposed to B100 mostly shows higher concentration of oxygen than that in as-received metal surface (Figure 4.14 d and e). It was seen in Figure 4.14 e that enriched oxygen content (27.1 %) has a great effect on the morphological change of the LCS surface. Variation of oxygen content on metal surface could be the evident of metal oxidation formation and consequent corrosion attack.

In both CI and LCS, additional oxygen content is observed to be reduced significantly in TBA doped biodiesel as revealed by Figure 4.14 c and f. It is worthy to note in Figure 4.14 c and f that, the peaks of nitrogen with considerable concentration are detected which may originated from TBA ($C_4H_{11}N$). The existence of nitrogen atom in TBA may enable it to make bond with CI and LCS surfaces and thus, improving the anticorrosion properties of the metal surface.

(a) As-received CI **(d) As-received LCS**

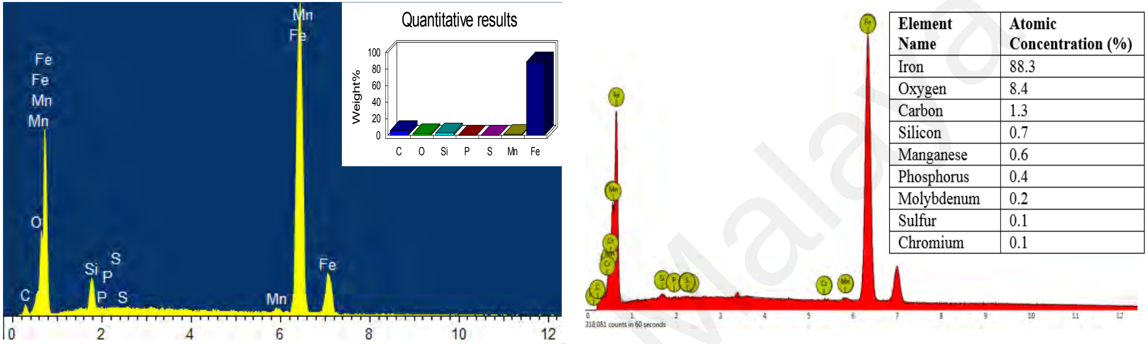

Element Name	Atomic Concentration (%)
Iron	88.3
Oxygen	8.4
Carbon	1.3
Silicon	0.7
Manganese	0.6
Phosphorus	0.4
Molybdenum	0.2
Sulfur	0.1
Chromium	0.1

(b) CI / B100 **(e) LCS / B100**

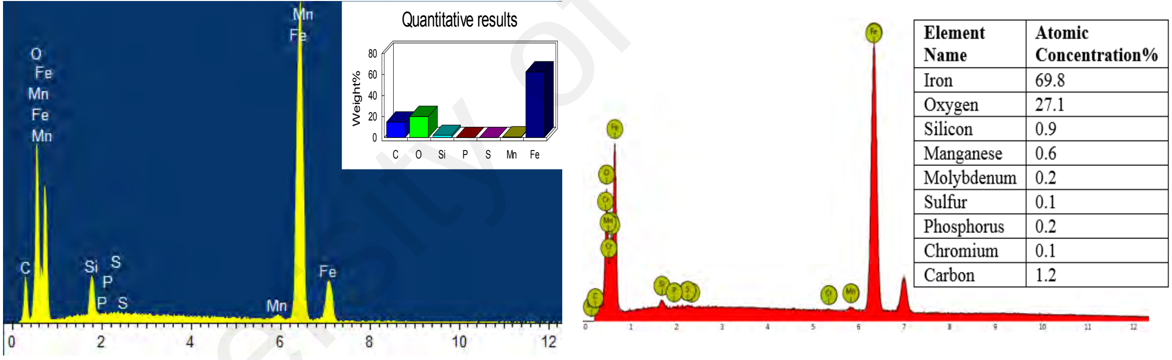

Element Name	Atomic Concentration%
Iron	69.8
Oxygen	27.1
Silicon	0.9
Manganese	0.6
Molybdenum	0.2
Sulfur	0.1
Phosphorus	0.2
Chromium	0.1
Carbon	1.2

(c) CI / B100 / 500ppm TBA **(f) LCS / B100 / 500ppm TBA**

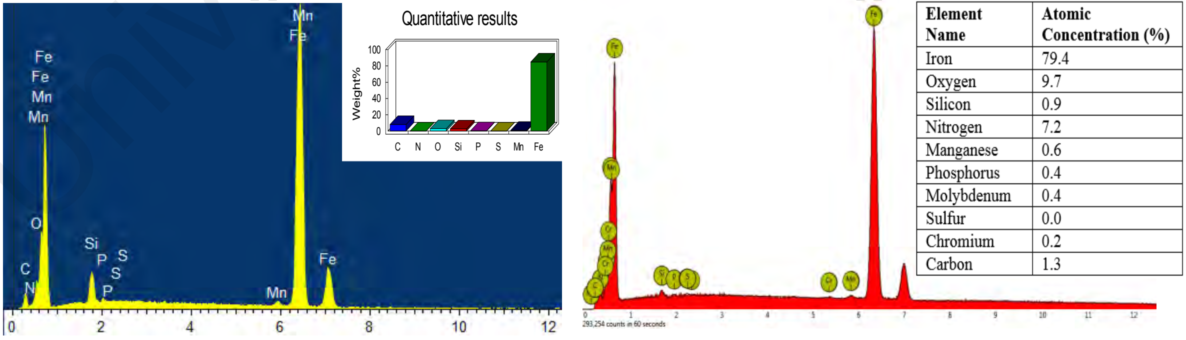

Element Name	Atomic Concentration (%)
Iron	79.4
Oxygen	9.7
Silicon	0.9
Nitrogen	7.2
Manganese	0.6
Phosphorus	0.4
Molybdenum	0.4
Sulfur	0.0
Chromium	0.2
Carbon	1.3

Figure 4.14: EDS spectrum on cast iron (CI) and low carbon steel (LCS) surface before and after exposures in biodiesel in absence and presence of TBA additive at 300K

XRD pattern of the corrosion products formed on the corroded surface of cast iron and low carbon steel after immersion in biodiesel for 50 d in Figure 4.15, shows metal mineral phases (Cui et al., 2015) which can reveal reclaimed oxygen quality influences in corrosion. The results of the XRD analysis suggests from Figure 4.15 a and c that the majority of the phases present on the biodiesel-exposed metal surface are oxides and oxide hydrides of iron. These adherent corrosion products includes hematite (Fe_2O_3), magnetite (Fe_3O_4), ferrous oxide (FeO) and $Fe(OH)_2$. Based on observations throughout the CI and LCS surface, three signature diffraction peaks of Fe, $Fe(OH)_2$ and (Fe_2O_3) around 2θ values of 45°, 19°and 20.50° show the strongest intensity. These deposited oxides and hydroxide phases may be the result of chemical reaction between metal surface and peroxides or acids present in biodiesel (Karavalakis et al., 2011). The peak intensity of these oxides and hydroxide are significantly reduced on the surfaces exposed in TBA doped biodiesel (Figure 4.15 b and d). A nitrogen containing compound $Fe(NO_3)_3.9H_2O$ is found to be formed with higher intensity on metal surface exposed in 500 ppm TBA doped biodiesel. Similar findings were obtained by Fazal et al.(Fazal, M.A, et al., 2011) and Li et al.(Li et al., 1997) where they reported that the formation of iron nitrate hydrate ($Fe(NO_3)_3.9H_2O$) could be the result of following chemical reaction among fuel, metal surface and amine based TBA ($R\text{-}NH_2$) additive.

$$
\begin{aligned}
&R-NH_2 \rightarrow R-\ddot{N}+2H^+\\
&R-\ddot{N}+O_2+H_2O \rightarrow R-OH+NO_2\\
&NO_2+H_2O \rightarrow NO_3+H_2\\
&Fe+O_2+H_2O \rightarrow Fe(OH)_2\\
&3Fe(OH)_2+3NO_3+7H_2O \rightarrow Fe(NO_3)_3.9H_2O+Fe_2O_4H_2 \qquad (4.1)
\end{aligned}
$$

According to Hosseini (Hosseini et al., 2012) electron pair on oxygen atoms of the nitro group are the preferred site for adsorption of amine based inhibitor on metal surface. This nitrogen content seems to contribute immensely in corrosion inhibition which may be attributed to the adsorption of TBA on metal surface and formation of a protective layer against subsequent corrosion.

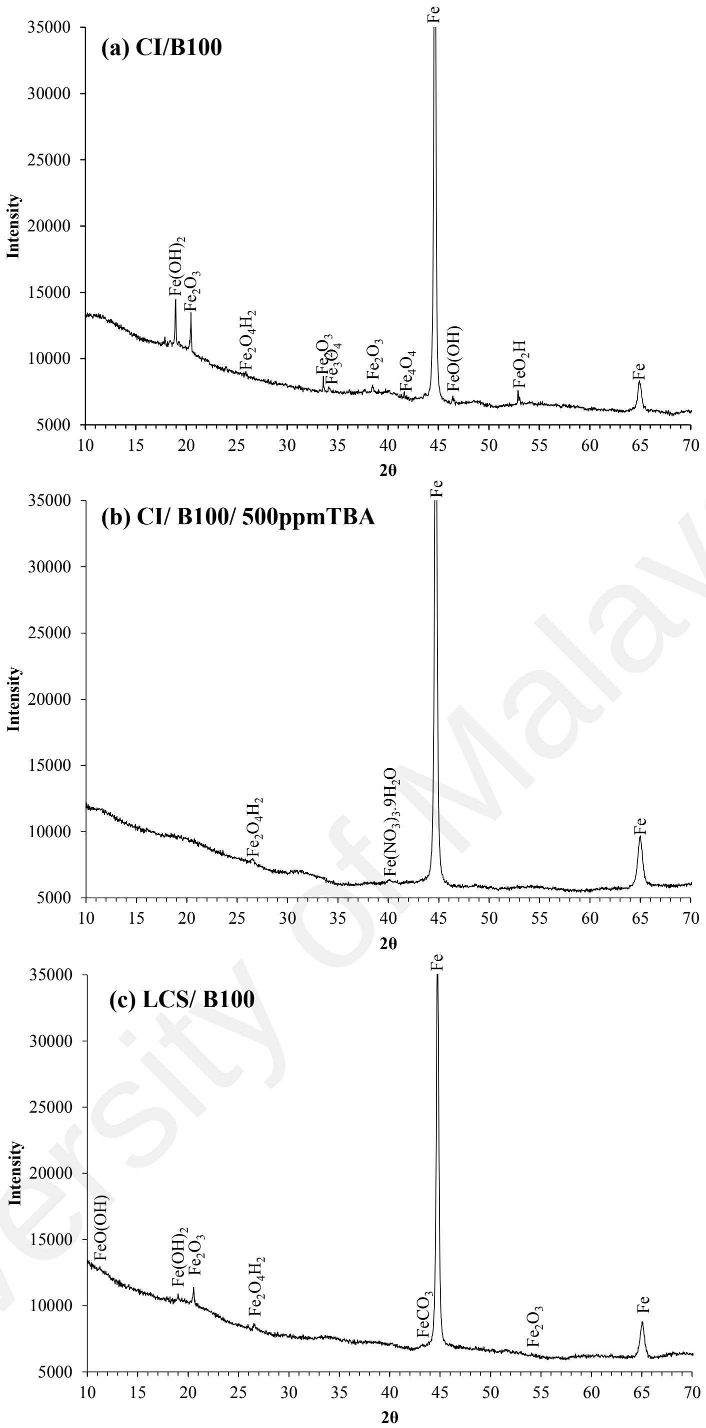

Figure 4.15: XRD pattern of the cast iron (CI) and low carbon steel (LCS) surface before and after exposure to biodiesel in the absence and presence of TBA additive at 300 K

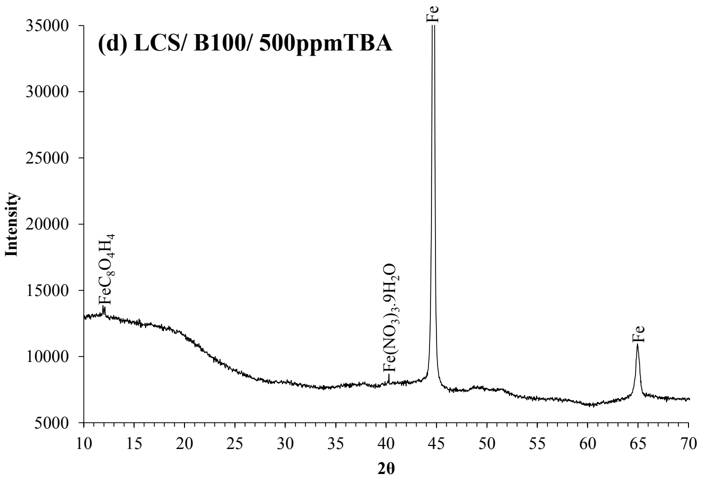

Figure 4.15, continued

The chemical bonding nature of the corrosion product on tested cast iron and low carbon steel surface can be revealed by the X-ray photoelectron spectroscopy (XPS). Under vacuum pressure 3x10^{-7} Pa, a monochromatic AlKα radiation (1486.6 eV) was considered for the analysis. The diameter of the beam was 100 μm and the charge was neutralized by using electron flood gun and mono-atomic Ar ion gun. The wide and narrow scan analysis was performed using pass energy of 280 eV with 1 eV per step and 112 eV with 0.1 eV per step respectively. ESCA software was used to analysis the XPS data.

Distinct peaks in wide scan were analyzed by multiple peaks deconvolution. Figure 4.16 illustrate the high resolution narrow scanned XPS peaks of C1s and Fe 2p in corroded samples (CI and LCS) after the immersion in B100. Figure 4.16 a and c represent the C1s spectra. It is seen in Figure 4.16 a that spectra consists of two major peaks corresponding to the binding energy of 284.60 eV (C-C or C-H) and 286.16 eV (C-O-H or C-O-C) for cast iron. These peaks are remarkably less in Figure 4.16 c for low carbon steel and the corresponding to the binding energy of 283.87 eV (C-C or C-H) and 287.89 (C=O or C-O-C) (Fazal, MA, et al., 2011b; Jin et al., 2015).

The Fe 2s XPS spectra of corrosion product on cast iron and low carbon steel immersed in B100 are shown in Figure 4.16 b and d. Two clear peaks in XPS spectrum of cast iron indicate that the major corrosion products consist of Fe^{2+} ($2p^{3/2}$; 708.95 eV) and Fe^{3+} ($2p^{3/2}$; 721.67 eV) (Jin et al., 2015). Similar findings were observed for the low carbon steel where the corresponding binding energy is 706.63 eV (Fe^{2+} ; $2p^{3/2}$) and 719.16 eV (Fe^{3+} ; $2p^{3/2}$). On the basis of relative area ratio under the fitted curve, it can be concluded that in the corrosion product the quantity of Fe^{2+} ($2p^{3/2}$) is dominant. This finding is in consistent with the result observed in XRD where peaks of hematite (Fe_2O_3) is noticeable.

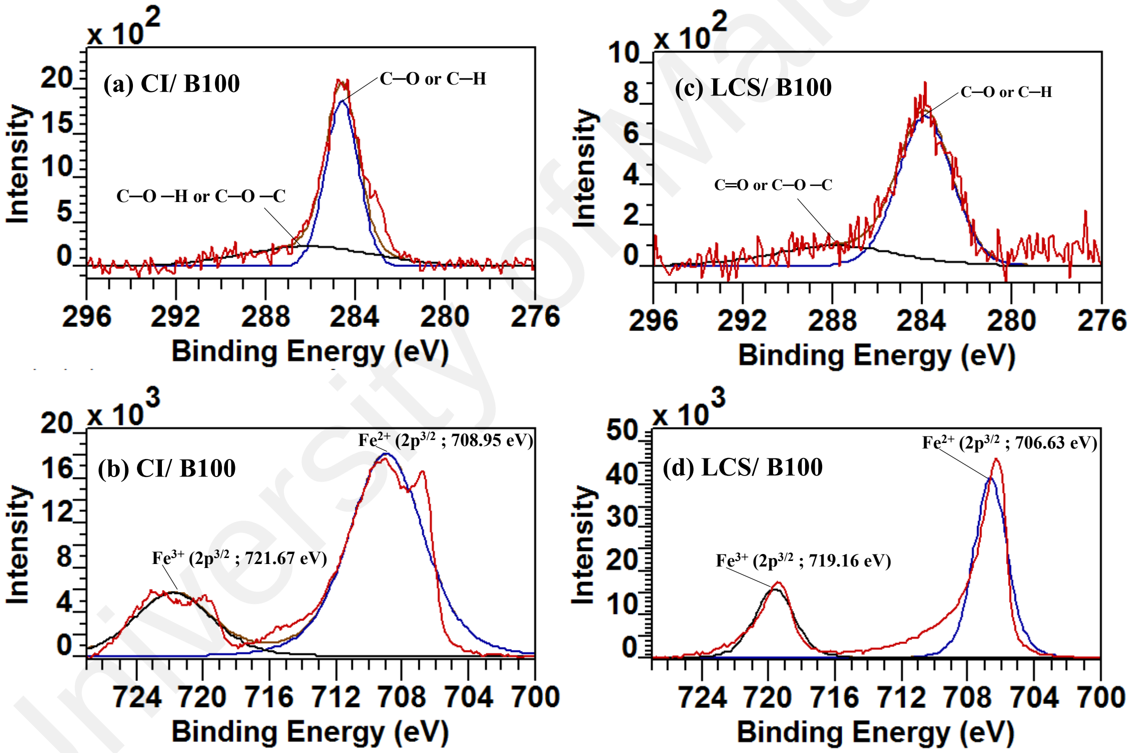

Figure 4.16: Narrow scanned XPS spectrum of corrosion product on cast iron (CI) and low carbon steel (LCS) after immersion in B100

Figure 4.17 illustrates the peaks of TBA treated cast iron and low carbon steel. There is a little shifting of center peaks Cs1 and Fe2p. Samples immersed in B100 (Figure 4.16) contains no nitrogen peaks except base nitrogen which is due to environment (Lopez, Schreiner, De Sánchez, & Simison, 2003). However, samples immersed in TBA doped biodiesel show presence of nitrogen peaks at 397.02 eV (cast iron) and 407.08 eV (low carbon steel) which could be the evident of nitrogen containing compound ($Fe(NO_3)_3.9H_2O$) on metal surfaces as protective layer. Binding energy of the peaks agree the literature study reported for the organic compound containing nitrogen (Hashemi & Hogarth, 1988). Therefore, it is assumed that the nitrogen which came from TBA ($C_4H_{11}N$) is associated with the formation of $Fe(NO_3)_3.9H_2O$. Similar nitrogen containing compound $Fe(NO_3)_3.9H_2O$ was reported by Fazal et al.(Fazal, M.A, et al., 2011) and (Hosseini et al., 2012).

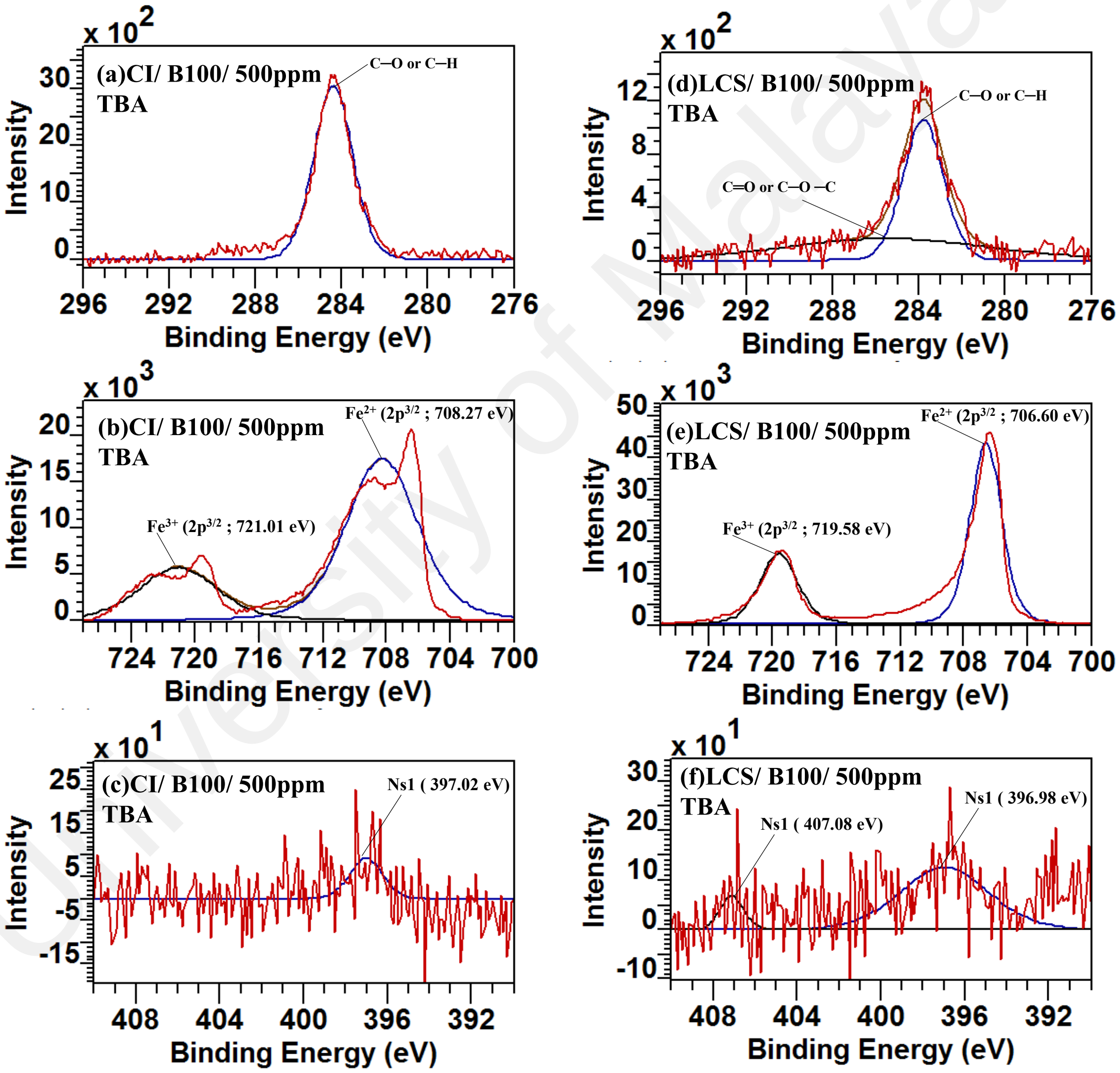

Figure 4.17: Narrow scanned XPS spectrum of corrosion product on cast iron (CI) and low carbon steel (LCS) after immersion in TBA doped B100

4.2.3 Analysis of adsorption isotherm model and type of adsorption

The adsorption isotherms were used to determine the inhibitor performance of TBA and identify the adsorption type on the metal surface. As shown in Figure 4.18, the corresponding line of C_{addi}/θ_{avg} versus C_{addi} represents the characteristic isotherm curve of the adsorption for different TBA concentrations added to palm biodiesel at 300 K. The regression coefficient (R^2) obtained from Figure 4.18 a and b are close to the unity, indicating that the adsorption of TBA on the cast iron and low carbon steel surface follows the Langmuir adsorption isotherm model (M. A. Deyab, 2014).

(a) Cast iron

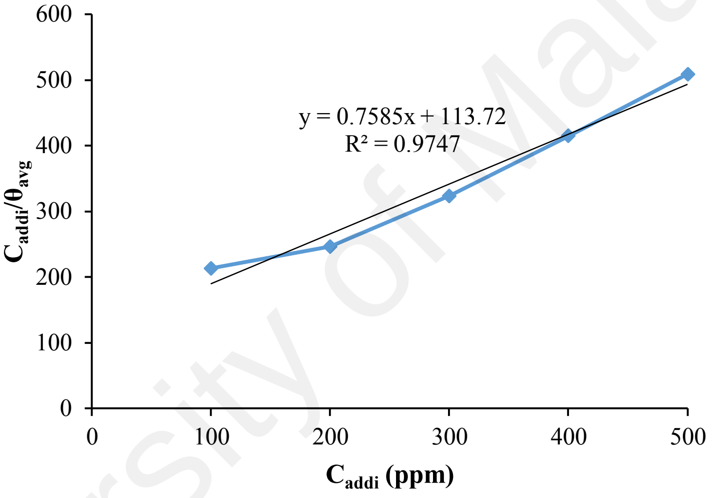

(b) Low carbon steel

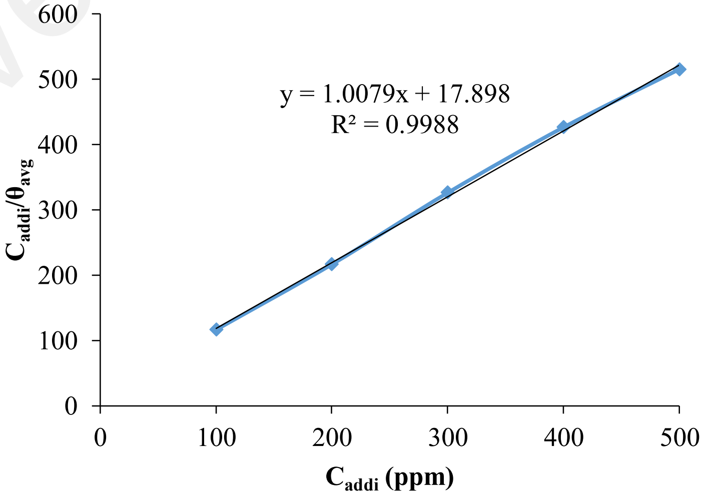

Figure 4.18: Plot of C_{addi}/θ_{avg} versus C_{addi} for the isotherm line for different TBA concentrations added to palm biodiesel at 300 K.

The reciprocal of the intercept of the isotherm line represents the equilibrium constant of the adsorption (K_{eqi}). High values of $\mathrm{K_{eqi}}$ indicate stronger adsorption of the inhibitor (M. Deyab & Abd El-Rehim, 2013). The K_{eqi} value is employed to determine the separation factor ($\mathrm{K_L}$) by using Equation (4.1) (Mall et al., 2005):

$$K_L = \left[1 + K_{eqi} C_{Addi}\right]^{-1} \qquad (4.1)$$

This equation identifies the type of the isotherm under the following conditions: (i) Favorable adsorption if $0 < K_{\mathrm{L}} < 1$ and (ii) Unfavorable adsorption if $K_{\mathrm{L}} > 1$. The obtained K_{eqi} values from the isotherm line are 0.0088 $\mathrm{ppm^{-1}}$ and 0.0559 $\mathrm{ppm^{-1}}$ for cast iron and low carbon steel respectively. The corresponding values of the separation factor ($\mathrm{K_L}$) for both the metals are within the range of $0 < \mathrm{K_L} < 1$ (Table 4.1). This finding indicates the favorable adsorption of the TBA inhibitor (Mall et al., 2005).

Table 4.1: Values of separation factor ($\mathrm{K_L}$) for various concentrations of TBA at 300 K

TBA concentration (ppm)	$\mathrm{K_L}$ (cast iron)	$\mathrm{K_L}$ (low carbon steel)
100	0.532	0.152
200	0.362	0.082
300	0.274	0.056
400	0.221	0.043
500	0.185	0.035

The free energy of adsorption ($\Delta \mathrm{G_{addi}}$) is necessary to find the spontaneity of the favorable adsorption process. The free energy of adsorption was calculated using Equation. 4.2 (X. Li et al., 2012).

$$\Delta G_{addi} = -RT \ln(55.5 \times 10^{6} K_{eqi}) \qquad (4.2)$$

where ΔG_{addi}, R, T, and K_{eqi} are the adsorption energy of the inhibitor (kJ $\mathrm{mol^{-1}}$), universal gas constant (8.314472 J/mol·K), room temperature (300 K), and equilibrium constant of the adsorption process respectively. Depending on the value of $\Delta \mathrm{G_{addi}}$, the adsorption process could be (i) chemical adsorption (if ΔG_{addi}<-40 KJmol^{-1}), (ii) physicochemical adsorption (if -40≤ ΔG_{addi}≤-20 KJmol^{-1}), or (iii) physical adsorption (if ΔG_{addi}>-20 KJmol^{-1}).

In the present study, the obtained free energy value of adsorption on cast iron and low carbon steel according to the Equation. 4.2 are−32.47 kJ·mol^{-1} and −37.05 kJ·mol^{-1} respectively. The negative value indicates that the interaction between the inhibitor molecules and the metal surface occurs spontaneously (M. Deyab & Abd El-Rehim, 2013). The magnitude of ΔG_{addi} confirms the occurrence of physicochemical adsorption; this process ensures the combination of electrostatic interaction and sharing of electrons between the charged additive molecules and the charged metal surface (M. Deyab & Abd El-Rehim, 2013; Tebbji et al., 2007). Hence, the adsorption of TBA on the cast iron and low carbon steel surface in biodiesel blend at 300 K are mainly physicochemical adsorption, which forms a protective layer and prevents further interaction between metal and biodiesel and thereby reduces metal corrosion.

4.3 Corrosion inhibition using different concentrations of TBA additives in B20

Currently, B20diesel-biodiesel blend is widely investigated by different researchers for automobile application. In this section, effect of 100, 200, 300, 400 and 500 ppm TBA on the corrosion of CI and LCS have been investigated.

4.3.1 Inhibition efficiency

This section discusses the adsorption kinetics of corrosion inhibitor on cast iron and low carbon steel immersed in biodiesel blend (B20) for 50 days at 300 K. Figure 4.19 and Figure 4.20 illustrated a comparative study of cast iron and low carbon steel corrosion rate, inhibition efficiency of B20 and TBA doped B20 at 300 K. In each study, TBA doped B20 shows remarkable reduction of corrosion rate and with the increase of TBA concentration corrosion rate decreases. It proves the effectiveness of TBA additives against corrosion of tested metals. Corresponding corrosion inhibition efficiencies of TBA doped B20 at 300K shows remarkable improvement which vary from 31.15% to 81.92% (cast iron) for 100-500 ppm TBA concentrations. Meanwhile, in the study for low carbon steel, inhibition efficiencies vary from 38.02% to 69.88%.

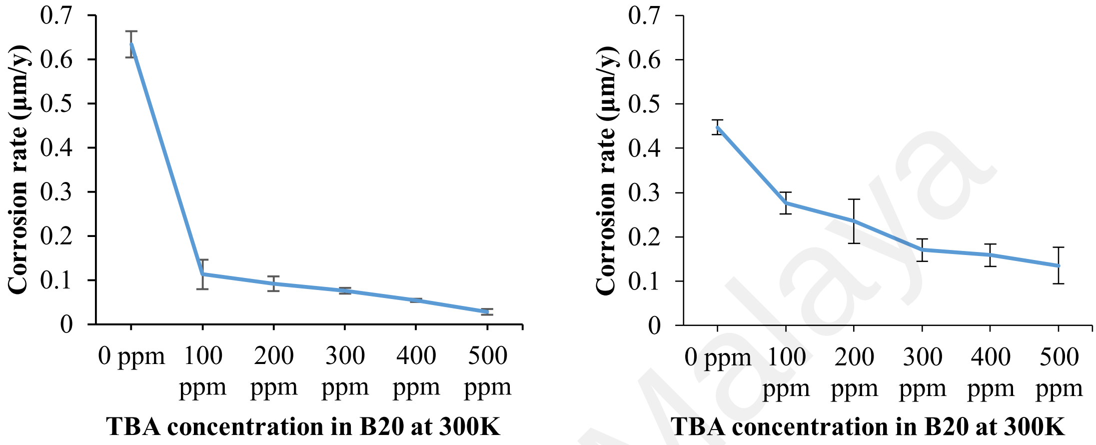
(a) Cast ion **(b) Low carbon steel**

Figure 4.19: Corrosion rate of cast iron (CI) and low carbon steel (LCS) exposed to B20 in presence and absence of TBA with various concentrations at 300 K

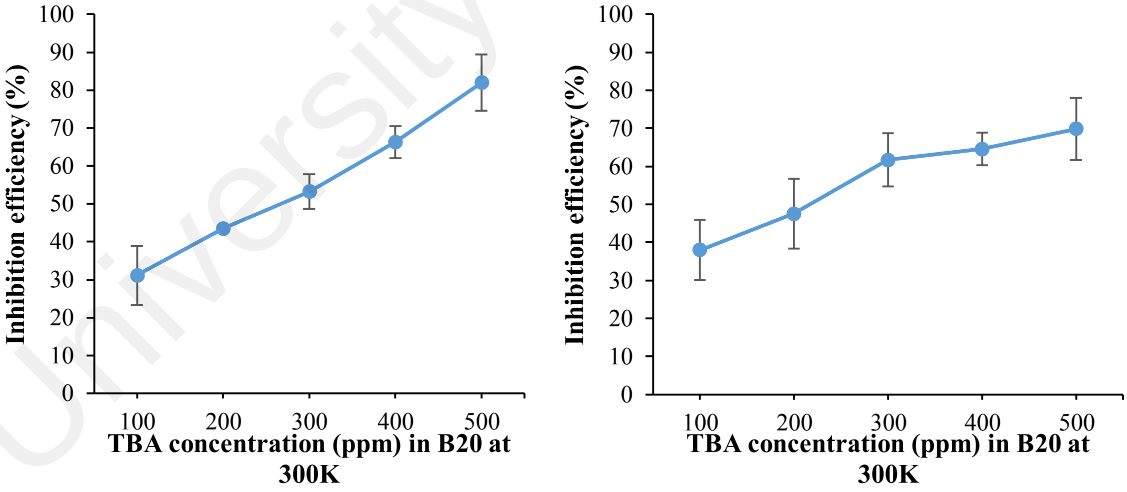
(a) Cast ion **(b) Low carbon steel**

Figure 4.20: Inhibition efficiency of TBA doped B20 with various concentrations at 300 K

4.3.2 Surface Characteristics

Figure 4.21 illustrates the effect of B20 and TBA doped B20 on cast iron and low carbon steel surfaces at 300 K. Densely uniform corrosion is observed in Figure 4.21a for cast iron while less uniform corrosion is seen for low carbon steel Figure 4.21 c. This occurrence of corrosion on metal surface remarkably minimized with TBA doped B20 especially at 500 ppm.

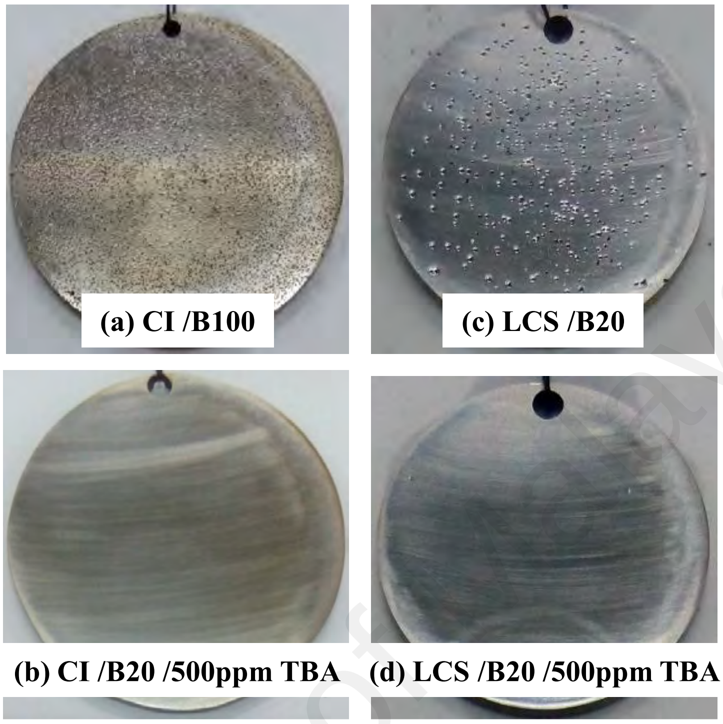

(a) CI /B100

(c) LCS /B20

(b) CI /B20 /500ppm TBA

(d) LCS /B20 /500ppm TBA

Figure 4.21: Appearance of the cast iron (CI) and low carbon steel (LCS) surface after immersion test in B20 and 500ppm TBA doped B20 at 300 K

Discontinuous and scattered pits were seen over the cast iron surface exposed in B20 (Figure 4. 22). Conversely, TBA doped B20 shows significant reduction of corrosion attack. Pits observed in Figure 4. 22 a significantly decreased in TBA doped B20 particularly with 500 ppm which is in consistent with the results studied by other researchers (M. Deyab & Abd El-Rehim, 2013; M. A. Deyab, 2014). It is clear from Figure 4. 22 c that compared to cast iron low carbon steel is less prone to corrosion and almost no corrosion observed on low carbon steel after the exposure to B20 in presence of 500 ppm TBA (Figure 4. 22 d).

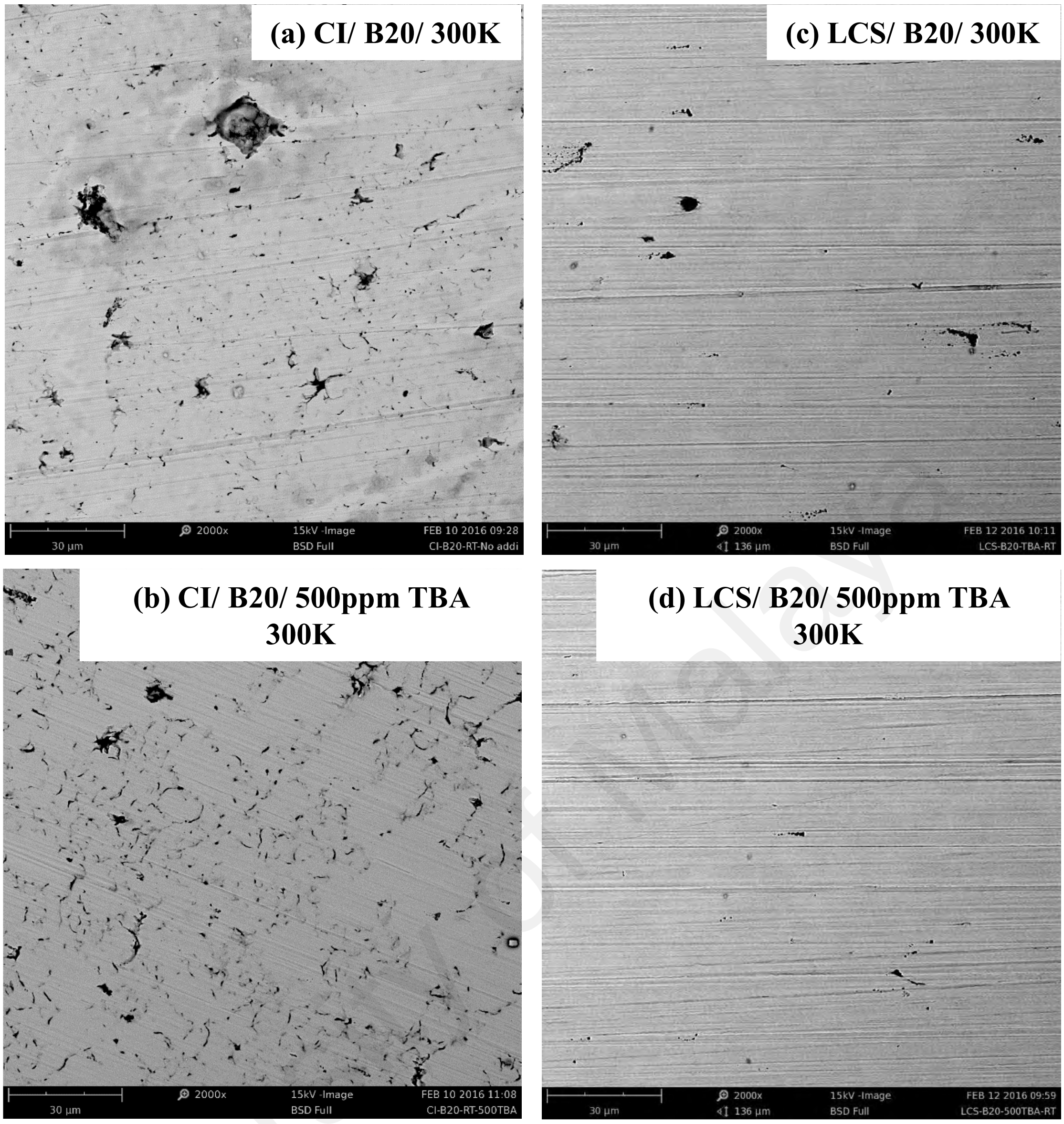

Figure 4. 22 SEM images (2000× magnification) of the cast iron (CI) and low carbon steel (LCS) surface after exposure to B20 and 500ppm TBA doped B20 at 300 K

Elemental analysis of post-corrosion surface in Figure 4.23 a, c show high concentration of oxygen. This enriched concentration of oxygen along with Fe could be the result of corroded compound formed on metal surface. However, CI and LCS immersed in TBA doped B20 reveals noticeable reduction of oxygen 6.8% and 6.6% at 300 K respectively (Figure 4.23 b, d). This less percentage of oxygen content on metal surface could be the evident of reduction of metal oxidation. Furthermore, moderate intense peak of nitrogen (N) were observed on metal surface exposed to TBA doped B20. This peaks of N may come from amine based TBA ($C_4H_{11}N$) additive which could help to attach TBA on metal surface to form intermediate layer and prevent direct exposer of metal to corrosion prone area.

(a) CI/ B20

Element Name	Atomic Concentration (%)
Iron	48.6
Oxygen	42.9
Carbon	5.7
Silicon	2.2
Manganese	0.3
Phosphorus	0.2
Sulfur	0.1

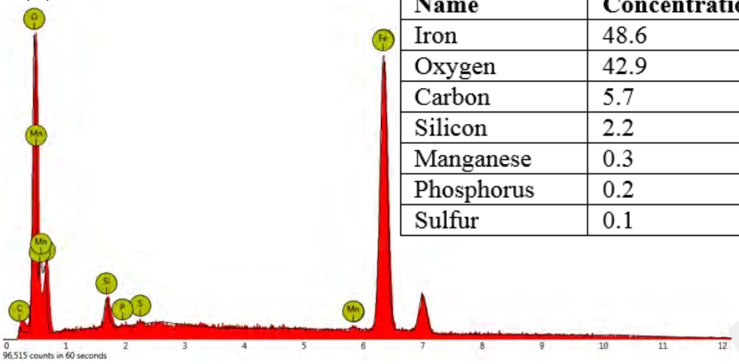

(b) CI/ B20/ 500ppm TBA

Element Name	Atomic Concentration (%)
Iron	67.3
Oxygen	6.8
Carbon	12.3
Nitrogen	9.2
Silicon	3.7
Manganese	0.2
Phosphorus	0.3
Sulfur	0.2

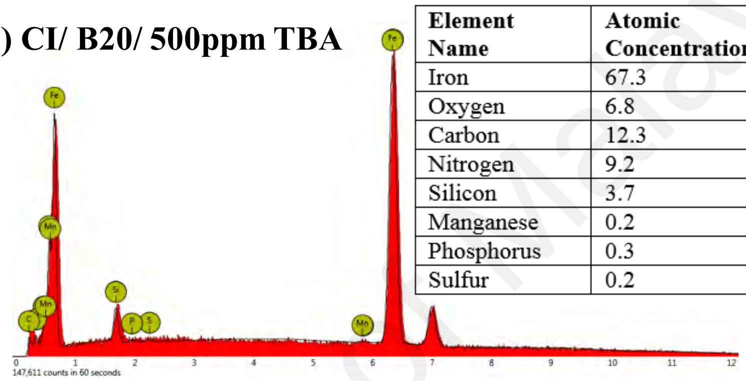

(c) LCS/ B20

Element Name	Atomic Concentration%
Iron	68.8
Oxygen	25.1
Silicon	0.1
Manganese	0.9
Chromium	0.5
Carbon	4.7

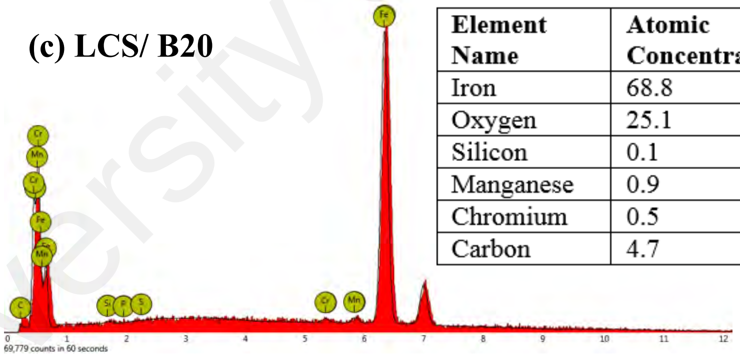

(d) LCS/ B20 / 500ppm TBA

Element Name	Atomic Concentration%
Iron	60.0
Oxygen	6.6
Nitrogen	10.1
Silicon	0.4
Manganese	0.3
Chromium	0.2
Phosphorus	0.2
Carbon	22.2

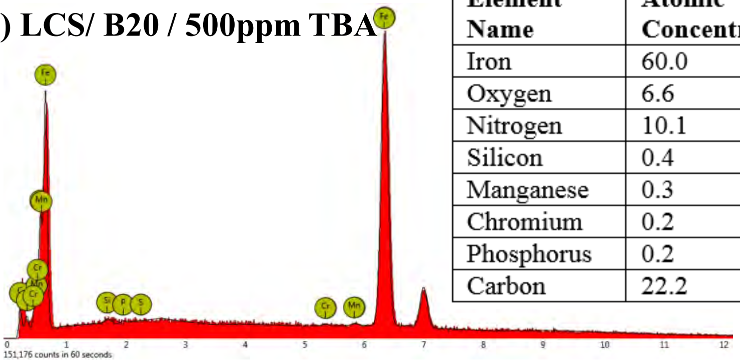

Figure 4.23: EDS spectrum on cast iron (CI) and low carbon steel (LCS) surface after immersion test in B20 in absence and presence of TBA additive at 300K

XRD patterns of cast iron and low carbon steel immersed in B20 and TBA doped B20 at 300K are shown in Figure 4.23. In Figure 4.23 a, Fe along with hematite (Fe_2O_3) and $Fe(OH)_2$ of the corrosion products appeared with intense peaks. These oxides phases formation may be the result of interaction between ferrous metal and corrosive molecules of B20 (Karavalakis et al., 2011). However, higher corrosion attacks owing to insufficient surface coverage are significantly reduced in TBA doped B20 (Figure 4.23 b, d). Almost no and very low intense of ferrous oxides were observed for 500ppm TBA doped B20 at 300 K. Peak of $Fe(NO_3)_3.9H_2O$ which is found to be formed as protective layer over the metal surface could be the cause of reduced corrosion attack. Sufficient coverage of this protective layer may provide blockage of active surfaces (Fazal, M.A, et al., 2011; Li et al., 1997).

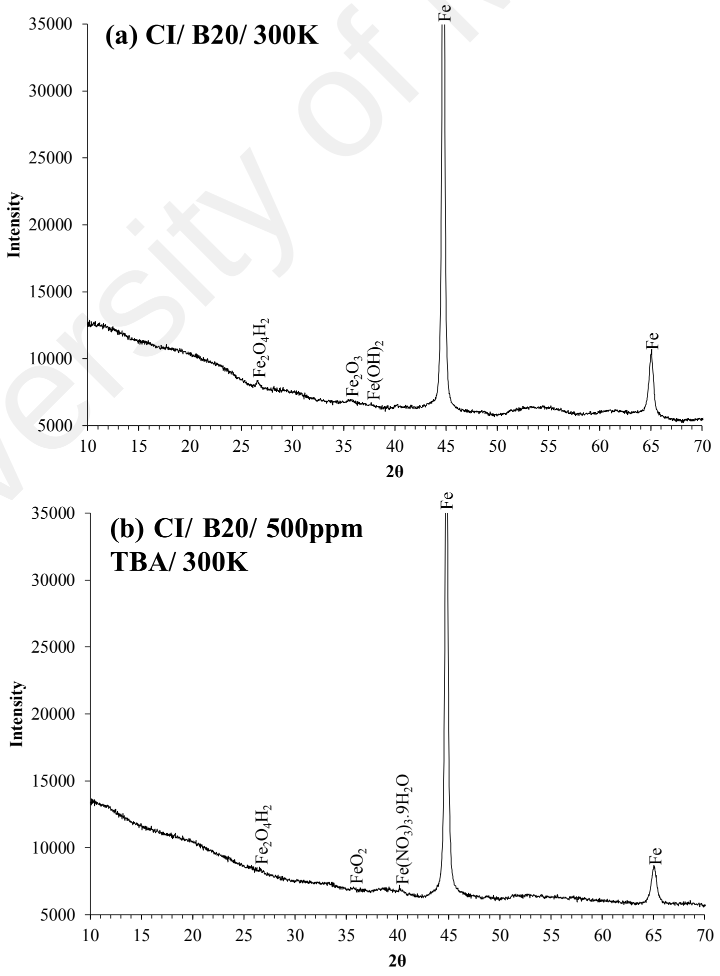

Figure 4.24: XRD pattern of cast iron (CI) and low carbon steel (LCS) surface after immersion in B20 and TBA doped B20 at 300K

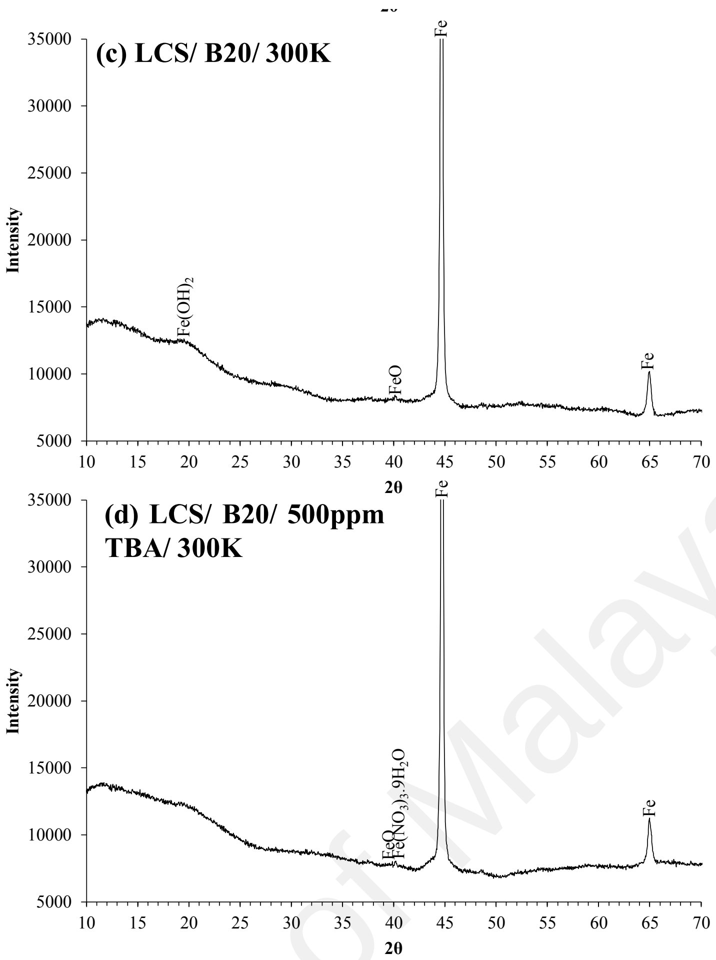

Figure 4.24, continued

4.3.3 Analysis of adsorption isotherm and type of adsorption process

Figure 4.25 represents the isotherm line of TBA for cast iron and low carbon steel. Regression coefficient (R^2) indicating that adsorption of TBA on both cast iron and low carbon steel surface obeys Langmuir adsorption isotherm (M. A. Deyab, 2014). Value of K_{eqi}, yields form the Figure 4.25 a and b is essential for quantification of free Gibbs energy (ΔG_{addi}). Calculated values of ΔG_{addi} are -30.292 kJ/mol (CI) and -31.47 kJ/mol (LCS). The negative values of ΔG_{addi} confirm the feasibility of the spontaneous adsorption and the numeric values are in consistent with physicochemical adsorption (M. Deyab & Abd El-Rehim, 2013).

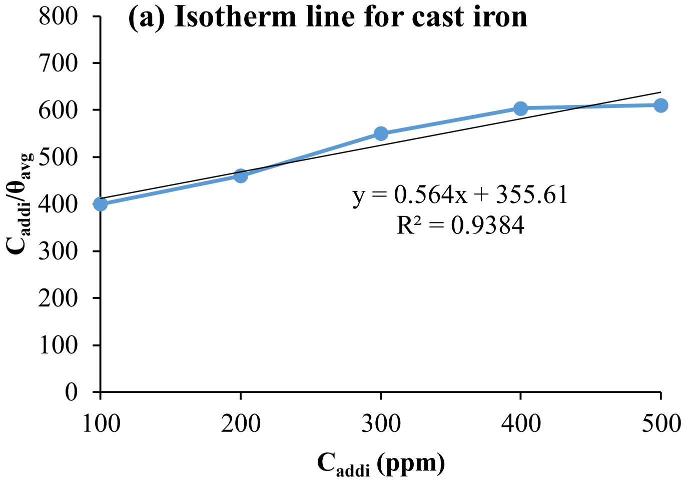

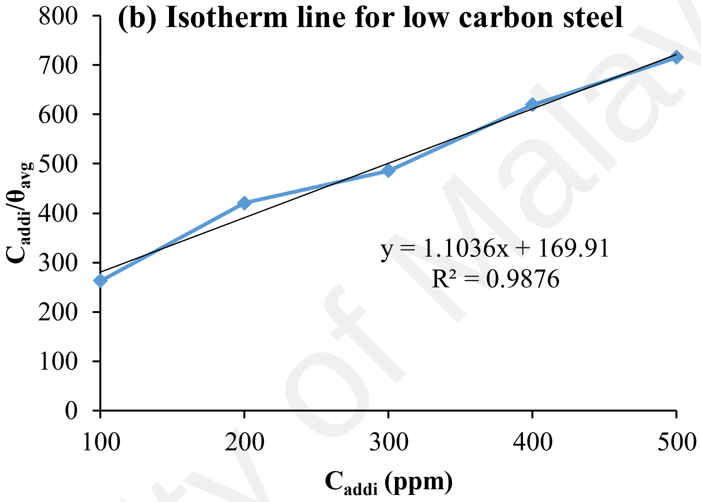

Figure 4.25: Plot of C_{addi}/θ_{avg} versus C_{addi} for isotherm line of TBA with different concentrations in B20 at 300K

4.4 Corrosion inhibition in B100 at elevated temperature (353 K)

This section aims to investigate the effect of elevated temperature on the inhibition performance of TBA. It also presents the adsorption of TBA additive on low carbon steel surface by means of adsorption isotherm and thermodynamic parameters.

4.4.1 Corrosion rate and inhibitor efficiency

It is seen in Figure 4.26 a that compared to cast iron, low carbon steel is less prone to corrosion at elevated temperature. Corrosion rate decrease with the increase of TBA additive concentration at high temperature. It is seen in Figure 4.26 b that inhibition efficiency increases in the presence of TBA in biodiesel and gradually increases with the increase of TBA concentration. This could be attributed to the higher concentration of amine based additive in palm biodiesel which could be responsible for the accelerated corrosion inhibition at elevated temperature.

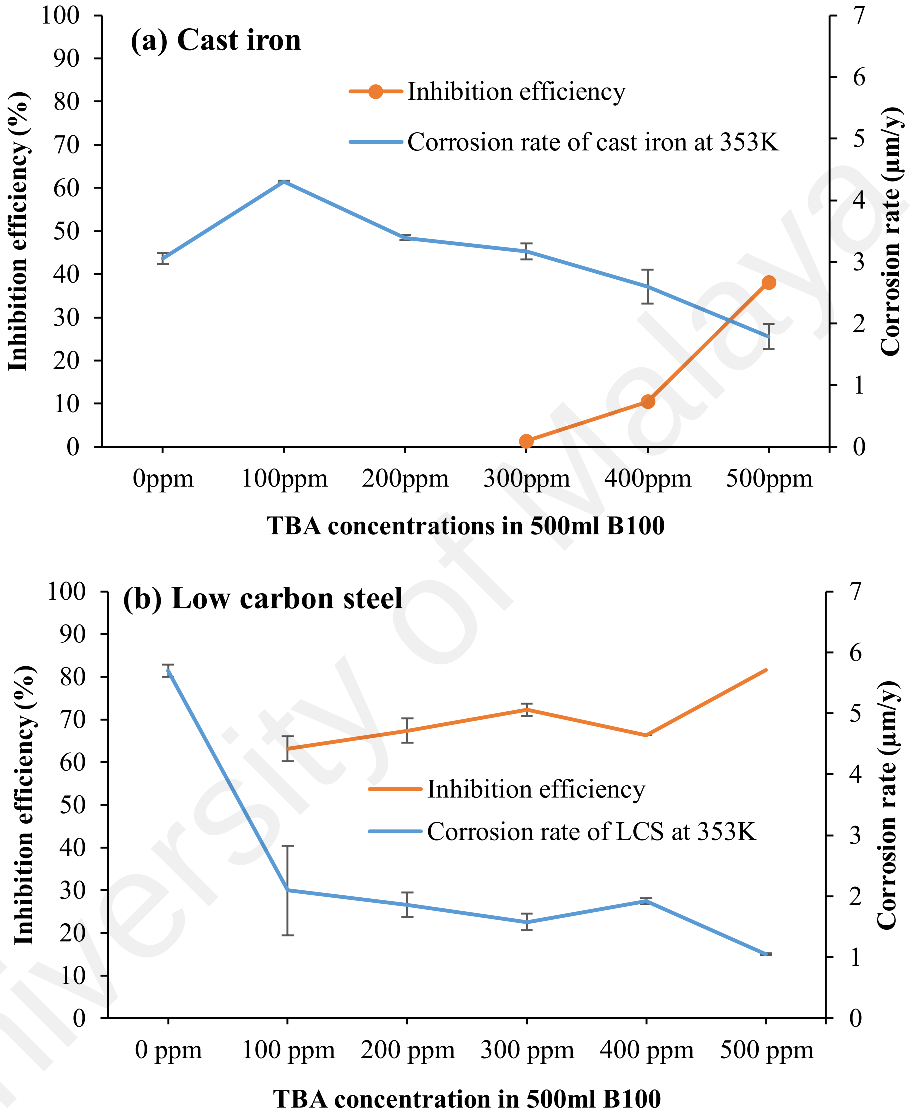

Figure 4.26: Comparison of inhibition efficiency and corrosion rate and of (a) cast iron and (b) low carbon steel in TBA doped biodiesel with different concentrations at 353K

4.4.2 Exposed metal surface morphology

Figure 4.27 represents the appearances of cast iron and low carbon steel coupons after the immersion tests in biodiesel and 500 ppm TBA doped biodiesel at 353 K. As received CI and LCS sample exposed to B100 shows severe corrosion attack (Figure

4.27 a and c). At elevated temperature the intensity of corrosion attack is significantly higher than that of ambient temperature. The highly dense uniform corrosion attack shown by Figure 4.27 a and c seems to be decreased upon addition of TBA in biodiesel. 500 ppm TBA doped biodiesel performed fairly well in reducing corrosion attack.

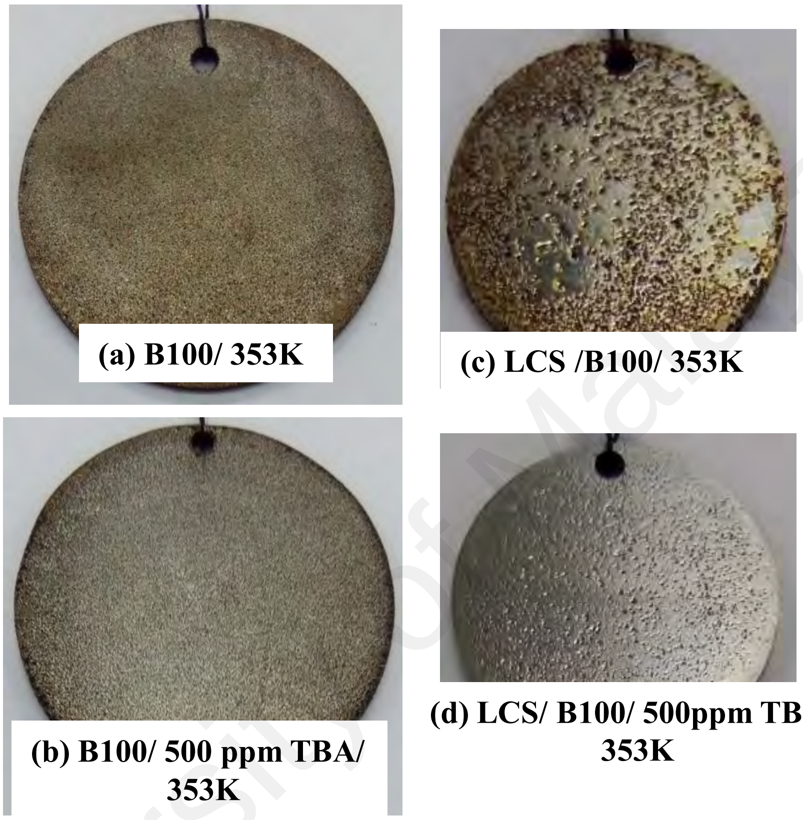
(a) B100/ 353K

(c) LCS /B100/ 353K

(b) B100/ 500 ppm TBA/ 353K

(d) LCS/ B100/ 500ppm TBA/ 353K

Figure 4.27: Appearances of cast iron (CI) and low carbon steel (LCS) coupons exposed to B100 and TBA doped B100 at elevated (353 K) temperature.

Change in morphology of metal surface is seen in SEM micrographs (Figure 4.28). It is seen in the Figure 4.28 that corrosion attack on surface are discontinuous in nature and scattered all over the surface. Corrosion attack on metal surface at elevated temperature is more severe with bigger pits than that of room temperature which means with increase of temperature corrosion rate increases (Fazal, MA, et al., 2011b). Furthermore, elemental analysis found higher element O on coupon surface which is due to formation of oxides inside corrosion products by metal surface and oxygenated biodiesel interaction. At elevated temperature, biodiesel could be highly oxidized and could form complex corroded compound (Karavalakis et al., 2011). However, addition of TBA additive in biodiesel makes it significantly less corrosive against cast iron and low carbon steel.

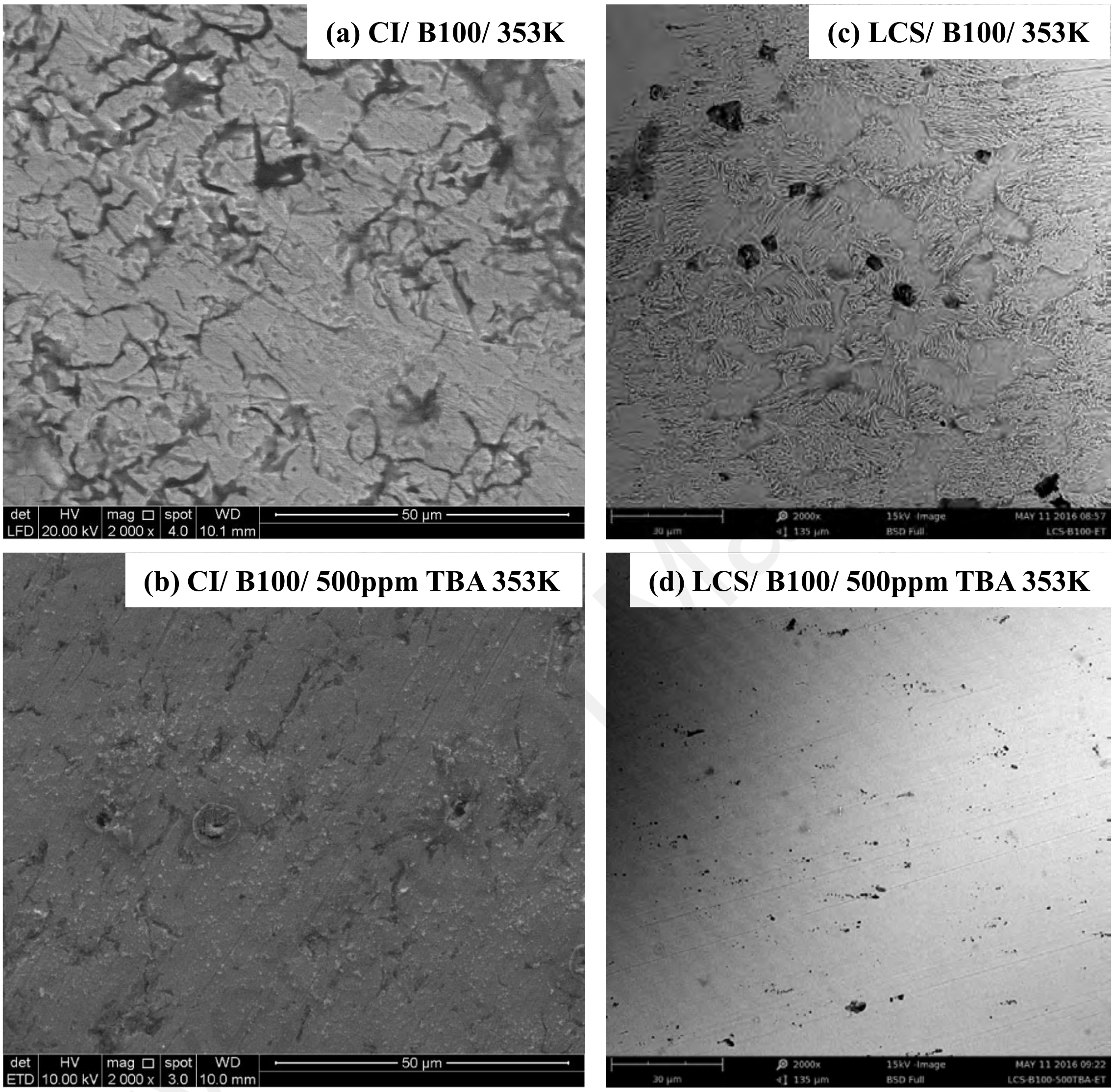

Figure 4.28: SEM images of cast iron (CI) and low carbon steel (LCS) surface after immersion in biodiesel and 500ppm TBA doped biodiesel at 353 K

XRD patterns post-corrosion surface of CI and LCS in B100 and TBA doped B100 at 353K are shown in Figure 4.29. XRD analysis of CI and LCS surface after immersion test in B100 found metal surface enriched with corroded compound, such as hematite (Fe_2O_3), magnetite (Fe_3O_4), $FeCO_3$ and FeO and $Fe(OH)_2$. Intense interference peak of Fe_2O_3 , $Fe(OH)_2$ were found around 2θ value of 21˚ and 19˚ for cast iron. Meanwhile, $Fe(OH)_2$ found to be intense around 21˚for low carbon steel. These oxides and hydroxides phases of corrosion products adsorb/adhere to the coupon surface may be the result of interaction between metal surface and unsaturated fatty acids which could be oxidized at elevated temperature (Karavalakis et al., 2011). According to Monyem and Gerpen (Monyem & Van Gerpen, 2001), oxidized biodiesel results higher acid and peroxide value which is the major cause of enhanced corrosion.

However, at higher concentration of TBA in B100 the intensity of ferrous oxides was minimized. It shows a good agreement with the results obtain earlier at room temperature. Samples immersed in 500 ppm TBA doped B100 show signature diffraction peaks of $Fe(NO_3)_3.9H_2O$. It could be attributed to the formation of nitrogen based intermediate layer which may come from amine based TBA ($C_4H_{11}N$) additive and prevent direct exposer of metal to corrosion prone area (Fazal, M.A, et al., 2011; Li et al., 1997).

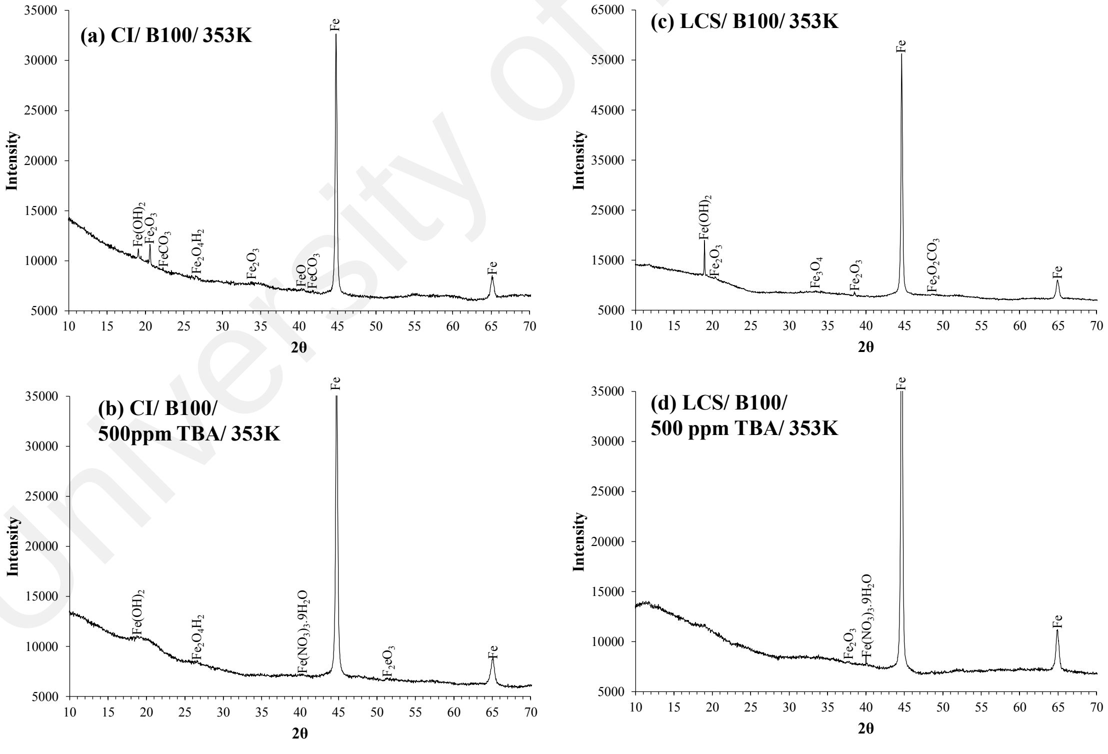

Figure 4.29: XRD pattern of cast iron (CI) and low carbon steel (LCS) surface before and after exposures in biodiesel in absence and presence of TBA additive at 353K

4.4.3 Adsorption isotherm model and thermodynamic parameters

Figure 4.30 illustrated the isotherm line of TBA additive with five different concentrations in biodiesel. It is seen in Figure 4.30 that regression coefficient (R^2) of isotherm line is close to unity which indicates that adsorption of TBA on LCS follows Langmuir adsorption isotherm (M. A. Deyab, 2014). Gibbs free energy (ΔG_{addi}) at 353K needs to be reconfirmed for the certainty of TBA adsorption. Therefore, value of equilibrium constant of adsorption process (K_{eqi}) is required which is reciprocal of the intercept of the isotherm line (Figure 4.30). The obtained K_{eqi} value from the isotherm line is 0.0189 ppm^{-1}. Equilibrium constant of adsorption process (K_{eqi}) helps to yield the value of separation factor (K_L) which is needed for identification the type of the isotherm whether it is favorable adsorption ($0 < K_L < 1$) or unfavorable adsorption ($K_L > 1$). It is seen in Figure 4.33 that the value of the separation factor (K_L) for all TBA concentrations (100-500 ppm) are within the range of $0 < K_L < 1$ which demonstrates favorable adsorption (Mall et al., 2005).

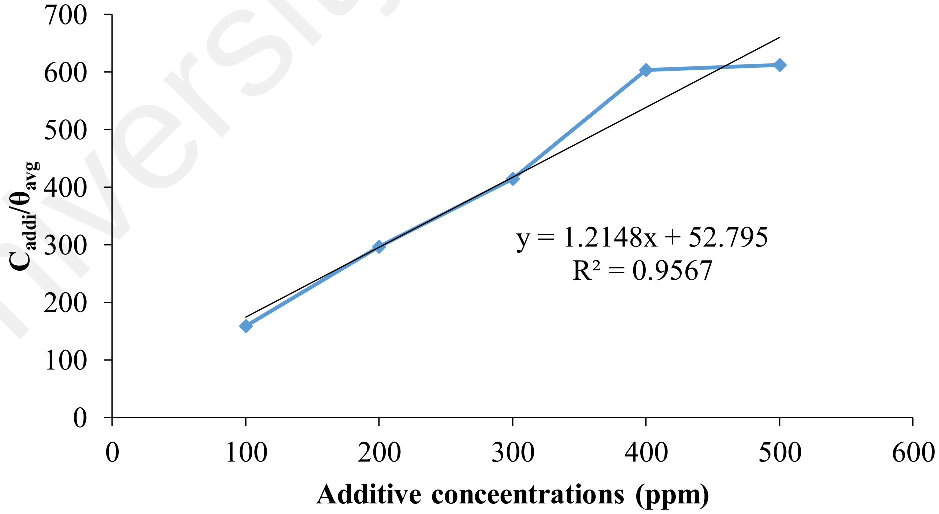

Figure 4.30: Isotherm line of TBA with different concentrations in B100 at 353K.

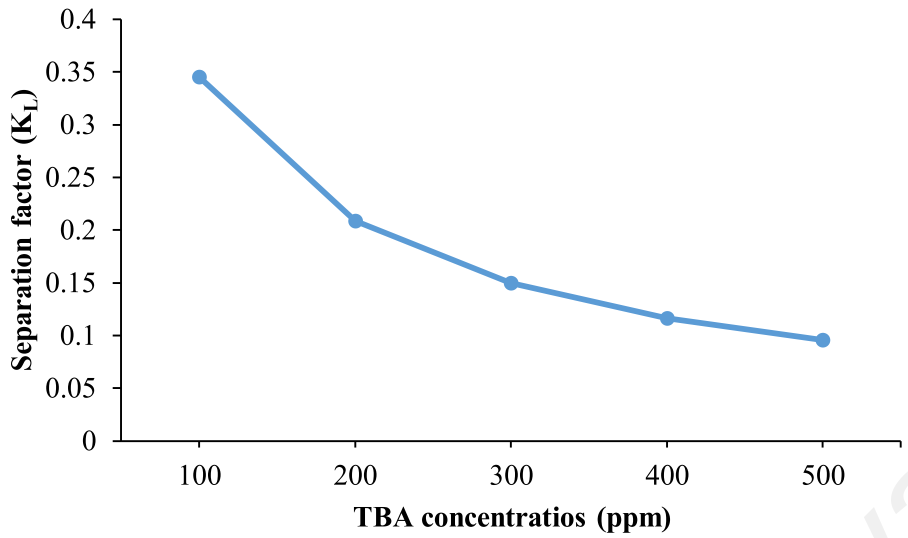

Figure 4.31: Separation factor for various concentrations of TBA at 353 K

Equation of Gibbs energy (ΔG_{addi}) identifies the spontaneity and type adsorption (X. Li et al., 2012). Calculated values of ΔG_{addi} is -40.69 kJ/mol at 353K. Negative value of ΔG_{addi} confirms the feasibility of spontaneous adsorption. This value complies the range of physicochemical adsorption (if $-40 \leq \Delta G_{addi} \leq -20$ KJmol^{-1}) (M. Deyab & Abd El-Rehim, 2013). In adsorption whether it is endothermic or exothermic process can be quantify by standard enthalpy of adsorption (ΔH_{addi}) (Musa et al., 2009). Gibbs–Helmholtz equation is used to find the value of enthalpy of adsorption (Atkins, 1978). ΔH_{addi} is the slope of $\Delta G_{addi} / T$ versus $1/T$ line (Figure 4.32). Absolute value of ΔH_{addi} is found to be current study is -18.79 kJ/mol. Negative sign of ΔH_{addi} indicates that the adsorption of TBA molecule on the low carbon steel surface is an exothermic process (Herrag et al., 2010).

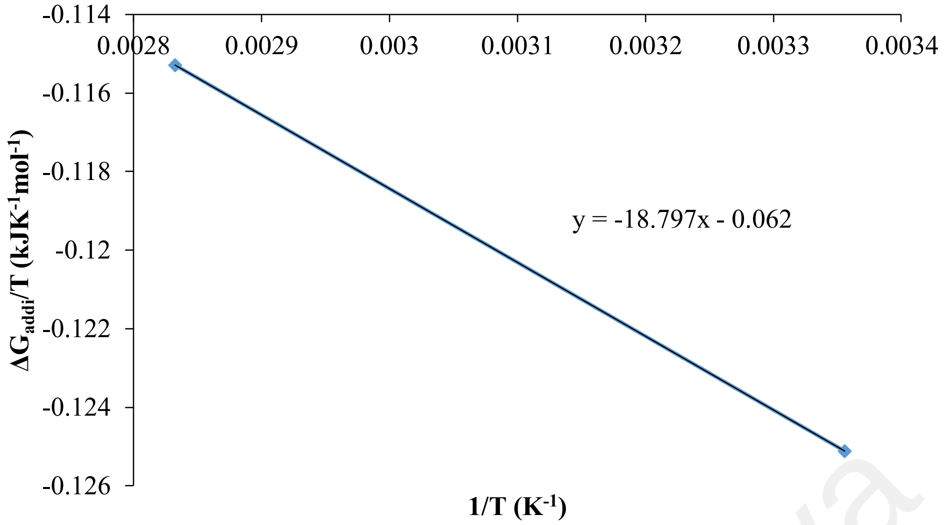

Figure 4.32: Plot of $\Delta G_{addi}/T$ versus 1/T for adsorption of TBA additive on low carbon steel surface exposed to B100

It is seen from Table 4.2, activation energy (E_a) increased with increasing concentration of TBA. The increase in the E_a may be interpreted as the formation of an adsorption film (M. A. Deyab, 2014). According to Gapi et al. (Gopi, Bhuvaneswaran, Rajeswarai, & Ramadas, 2000) rise of E_a with respect of concentration is the indication of a stronger adherence of TBA on low carbon steel surface at elevated temperature which is inconsistence with the current findings. It is further confirmed by the value of heat adsorption (Q) for TBA (Table 4.2).

Table 4.2: Calculated values of the degree of surface coverage, activation energy and heat of adsorption for TBA

TBA concentration (ppm)	θ_{300K}	θ_{353K}	E_a (kJ/mol)	Q (kJ/mol)
100	0.858	0.631	15.319	-21.071
200	0.923	0.673	24.194	-29.276
300	0.919	0.722	32.386	-24.545
400	0.937	0.663	28.926	-33.833
500	0.970	0.816	36.611	-33.036

4.5 Corrosion inhibition in B20 at elevated temperature (353 K)

Unstable fuel properties of higher biodiesel blends B5 and B10 were found to have made it corrosive when it comes in contact with the metal. This section will discuss the adsorption kinetics of corrosion inhibitor on cast iron immersed in biodiesel blend (B20) for 50 days at 353 K. It also extended its investigation on thermodynamic functions for corrosion inhibition process at elevated temperature.

4.5.1 Corrosion rate and inhibitor efficiency

Figure 4.33 and Figure 4.34 illustrated cast iron corrosion rate and inhibition efficiency of TBA doped B20 at 353 K. It is seen in Figure 4.33 that corrosion rate is high at elevated temperature as compared to that of room temperature. It could be attributed to partial desorption of additive from cast iron surface at increased temperature (A. Singh, Singh, & Quraishi, 2010). Nevertheless, TBA doped B20 shows remarkable reduction of corrosion rate and with the increase of TBA concentration corrosion rate decreases. It proves the effectiveness of TBA additives against corrosion of cast iron coupons even at elevated temperature. Inhibition efficiencies vary only from 86.46% to 92.00% at elevated temperature (353 K). Still it demonstrates higher inhibition efficiency compared to room temperature. Literally, TBA doped B20 proves its better inhibition efficiency which could be due to the successive formation of protective layer adhered on sample surface (Robert O. Dunn, 2005). Further analysis of thermodynamic parameters is needed to find the adsorption nature of additive at 353 K.

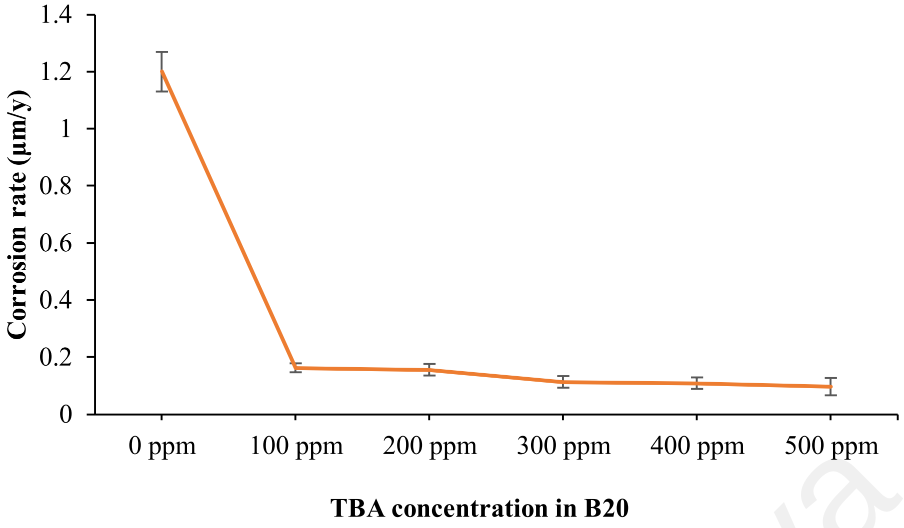

Figure 4.33: Corrosion rate of cast iron exposed to B20 in presence and absence of TBA with various concentrations at 353 K.

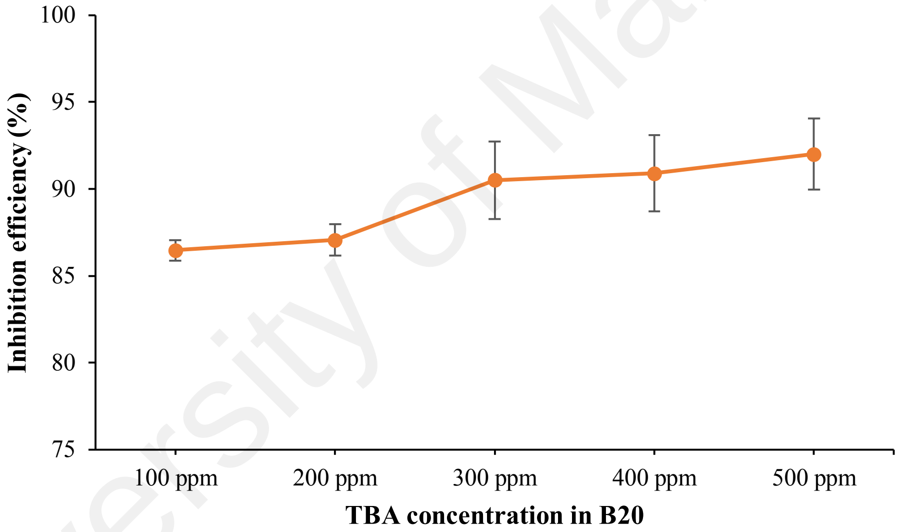

Figure 4.34: Inhibition efficiency of TBA doped B20 with various concentrations at 353 K.

4.5.2 Surface Characteristics

The effect of elevated temperature (353 K) on the performance of TBA additive concentrations is illustrated in Figure 4.35. Severe damage by corrosion attack was observed at 353 K in Figure 4.35 a. Conversely, TBA doped B20 particularly with 500 ppm shows significant reduction of corrosion attack. It is exhibited in Figure 4.35 b that damage observed in Figure 4.35 a significantly decreased which is in consistent with previous studies (M. Deyab & Abd El-Rehim, 2013; M. A. Deyab, 2014).

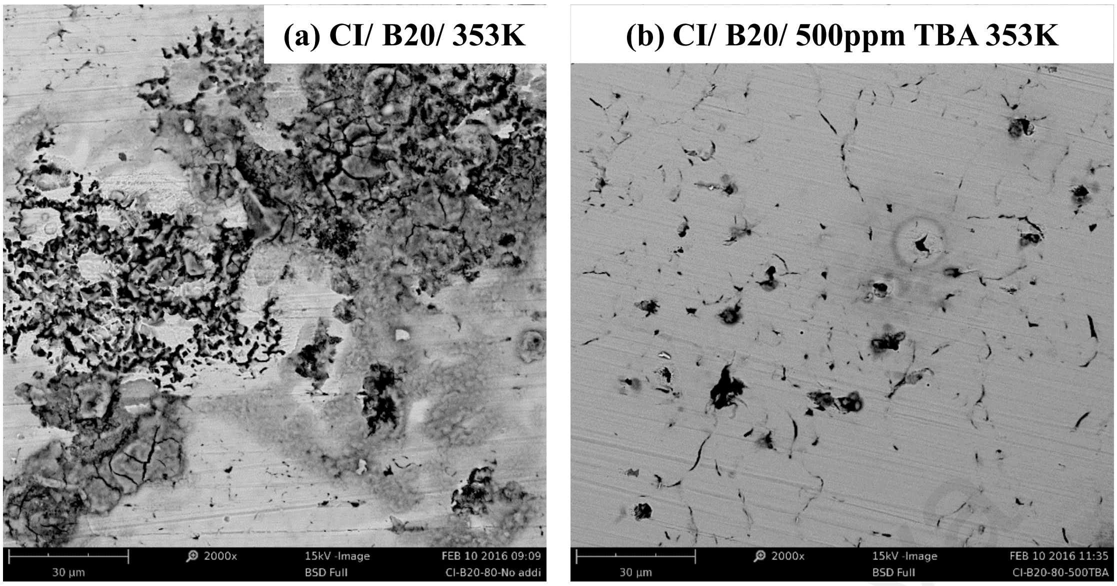

Figure 4.35: SEM images (2000× magnification) of the cast iron (CI) surface after exposure to B20 in the absence and presence of TBA additive at 353 K.

Elemental analysis of B20 exposed surface in Figure 4.36 a shows high concentration of oxygen at 353 K. This enriched concentration of oxygen along with Fe could be the result of corroded compound formed on CI surface. It could be due to the oxidation of B20 at increased temperature. However, CI immersed in TBA doped B20 reveals noticeable reduction of oxygen 7.5% (Figure 4.36 b). This less percentage of oxygen content on cast iron surface could be the evident of reduction of metal oxidation. Furthermore, moderate intense peak of nitrogen (N) were observed on metal surface exposed to TBA doped B20. This peaks of N may come from amine based TBA ($C_4H_{11}N$) additive which could adhere on metal surface to form intermediate layer and prevent direct exposer of metal to corrosion prone area.

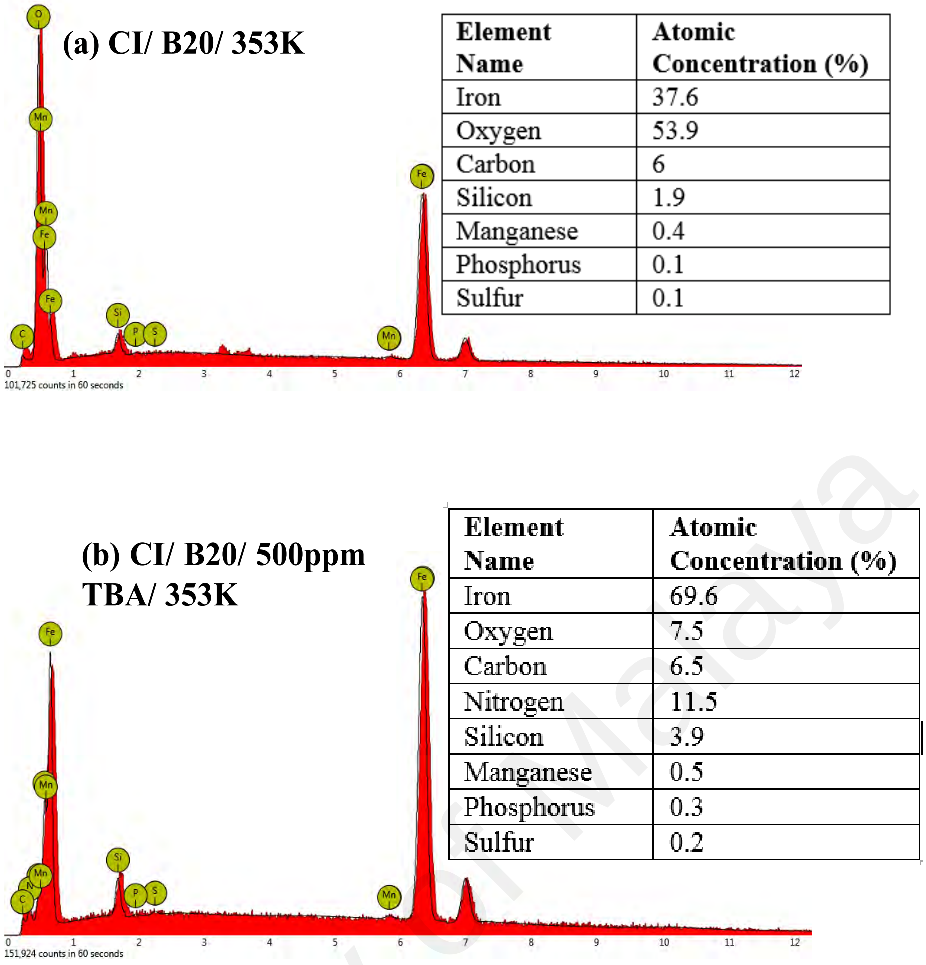

(a) CI/ B20/ 353K

Element Name	Atomic Concentration (%)
Iron	37.6
Oxygen	53.9
Carbon	6
Silicon	1.9
Manganese	0.4
Phosphorus	0.1
Sulfur	0.1

(b) CI/ B20/ 500ppm TBA/ 353K

Element Name	Atomic Concentration (%)
Iron	69.6
Oxygen	7.5
Carbon	6.5
Nitrogen	11.5
Silicon	3.9
Manganese	0.5
Phosphorus	0.3
Sulfur	0.2

Figure 4.36: EDS spectrum on cast iron (CI) surface after immersion test in B20 in (a) absence and (b) presence of TBA additive at 353 K

XRD patterns of cast iron immersed in B20 and TBA doped B20 at 353 K are shown in Figure 4.37. In Figure 4.37 a, Fe along with hematite (Fe_2O_3), ferrous oxide (FeO) and $Fe(OH)_2$ of corrosion products appeared with intense peaks at elevated temperature. Similar results was found at room temperature with less intense peaks. These oxides phases formation may be the result of interaction between cast iron and oxidized biodiesel at elevated temperature (Karavalakis et al., 2011). Oxidized biodiesel increases the acidity and peroxide value which caused enhanced corrosion (Monyem & Van Gerpen, 2001). Higher corrosion attacks owing to insufficient surface coverage are significantly reduced in TBA doped B20 (Figure 4.37 b). Peak of $Fe(NO_3)_3.9H_2O$ which is found to be formed as protective layer over the surface of CI. It could be the cause sufficient coverage and may provide blockage over the active areas of the metal surface (Fazal, M.A, et al., 2011; Li et al., 1997).

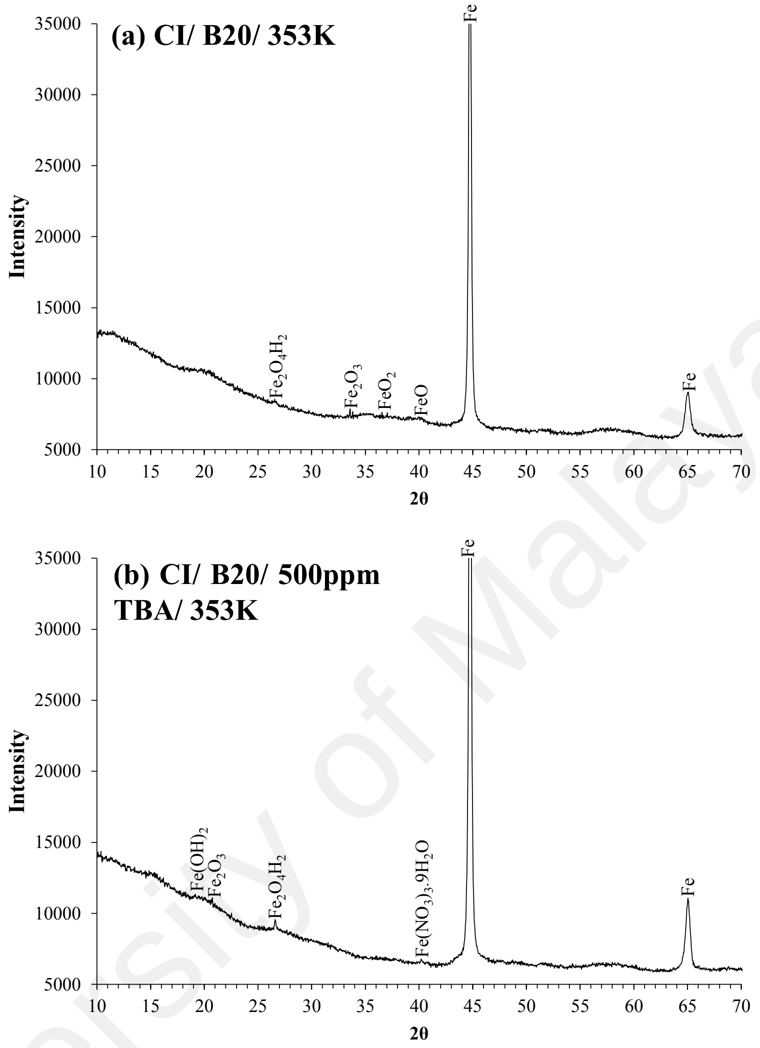

Figure 4.37: XRD pattern of cast iron surface after immersion in (a) B20 and (b) TBA doped B20 at 353 K

4.5.3 Thermodynamic function of adsorption of corrosion inhibition process

Effect of elevated temperature on activation energy (Equation 3.4) of different concentration of TBA additive demonstrated in Table 4.3. The increasing value of E_a with the increase of additive concentrations indicate requirement of higher energy value for the occurrence of reaction. It is seen in Table 4.3 that surface coverage increase with increase of TBA concentration at 353 K. Analogous increase in activation energy with the increase of TBA additive concentrations is the indication of physical adsorption (electrostatic) of TBA on cast iron surface (Elayyachy, Hammouti, El Idrissi, & Aouniti, 2011).

Table 4.3: Activation energy in different additive concentrations

Additive concentrations (ppm)	θ_{300K}	θ_{353K}	E_a kJ/mol
100	0.312	0.865	6.030
200	0.435	0.871	8.742
300	0.532	0.905	6.737
400	0.663	0.909	11.517
500	0.819	0.920	20.416

Further study on free Gibbs energy (ΔG_{addi}) at 353K needed to reconfirm the certainty of adsorption nature. K_{eqi}, yields form the Figure 4.38 is essential for quantification of ΔG_{addi}. Regression coefficient (R^2) indicating that adsorption of TBA on cast iron surface perfectly obeys Langmuir adsorption isotherm (M. A. Deyab, 2014).

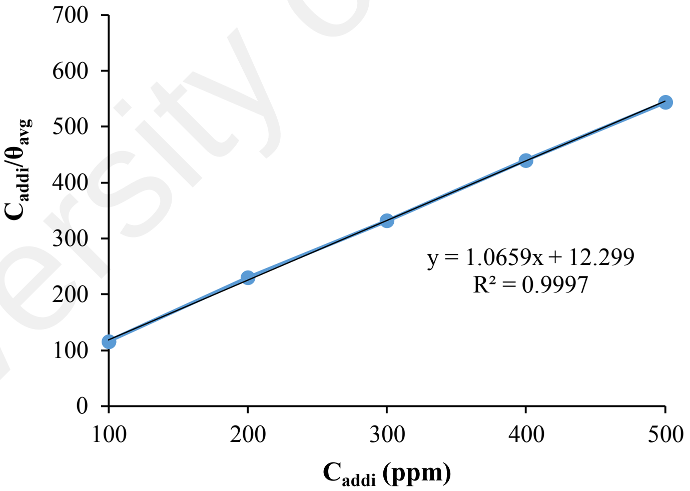

Figure 4.38: Plot of C_{addi}/θ_{avg} versus C_{addi} for isotherm line of TBA with different concentrations in B20 at 353K.

Negative values of free Gibbs energy (ΔG_{addi}) confirm the feasibility of the spontaneous adsorption. Calculated values of ΔG_{addi} is -44.971 kJ/mol at 353K. Value of ΔG_{addi} within -40 kJ/mol and -20 kJ/mol is consistent with physicochemical adsorption (M. Deyab & Abd El-Rehim, 2013). While more negative value than -40 kJ/mol confirm the occurrence of chemical adsorption by sharing or transferring electrons form inhibitor molecules to the metal surface to form co-ordinate bond (M. Deyab & Abd El-Rehim, 2013). According to Musa et al. chemical adsorption is attributable undoubtedly to endothermic process (Musa et al., 2009). In chemical adsorption whether it is endothermic or exothermic process can be distinguished by considering another thermodynamic parameter which is standard enthalpy of adsorption (ΔH_{addi}). ΔH_{addi} can be calculated by linear regression between $\Delta G_{adddi}/T$ and $1/T$ of following Gibbs–Helmholtz equation (Atkins, 1978).

$$\frac{\Delta G_{addi}}{T} = \frac{\Delta H_{addi}}{T} + C \qquad (4.3)$$

Figure 4.39 shows the line of $\Delta G_{addi}/T$ versus $1/T$ where slope of is equal to the value of ΔH_{addi}. It is suggested that in exothermic process the absolute value of ΔH_{addi} lower than 40 kJ/mol. Whereas, chemical adsorption by endothermic process absolute value of ΔH_{addi} approaches to 100kJ/mol or above (Herrag et al., 2010). Absolute value of ΔH_{addi} found in current study is 188.59 kJ/mol which is quite larger than common value of chemical adsorption heat. It implies that adsorption of TBA additive on cast iron surface expose to B20 at 353K is mostly chemical adsorption by endothermic process.

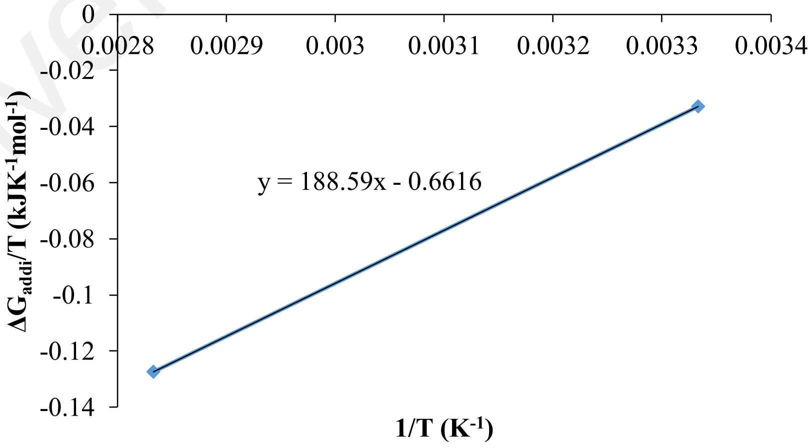

Figure 4.39: Plot of $\Delta G_{addi}/T$ versus 1/T for adsorption of TBA additive on cast iron surface exposed to B20

4.6 Retardation of tribological degradation using different additives

The purpose of this section is to study the lubrication characteristics of additive doped palm biodiesel by using ball on plate high frequency reciprocating rig (HFRR). Tert-butyylamine (TBA), Benzotriazole (BTA), Butylated hydroxyamisole (BHA) and Tert-butyl hydroxyl quinine (TBHQ) were used to enhance lubricity. Experiment was conducted for 3600 sec with a frequency of 33 Hz at 300 K under 75 N load. The worn surface of the cast iron plate was examine by SEM and XRD analysis. Results exhibit that 250 ppm TBHQ doped B100 shows 7.35% reduction in COF compared to pure B100. It can be attributed to the formation of thin layer which suppresses higher coefficient of friction and wear. It also confirms the boundary lubrication regime on the metal surface.

4.6.1 Friction coefficient and wear analysis

Figure 4.40 a shows the coefficient of friction (COF) was high and unstable during run-in-period which became steady after 450 sec. It may be ascribed to the presence of scratchy surface at the initiation of rubbing and after a while became smoother by removing asperities (M. Habibullah et al., 2015). It is seen in Figure 4.40 a and b that COF and weight loss of cast iron plate is high for both B0 and B20 compared to B100 This result can be attributed to the fact that the layer of lubricant between the contact surfaces thins as a consequence of fuel and material degradation (Agarwal, 1999). Average COF for B0, B20 and B100 are 0.0931, 0.0888 and 0.0679 respectively. Better performance of B100 can be attributed to the adsorption of ester molecules of B100 on cast iron surface which may provide scuffing protection (Fazal et al., 2013b). This finding can also be explained by the adsorption of biodiesel on the metal surface because of the functionalities of the ester, along with the long hydrocarbon chains of fatty acid residue (M. Habibullah et al., 2015; Mosarof et al., 2016). Hence, a monolayer film is formed on the metal surface and improves lubricating performance (B. K. Sharma, Doll, & Erhan, 2008).

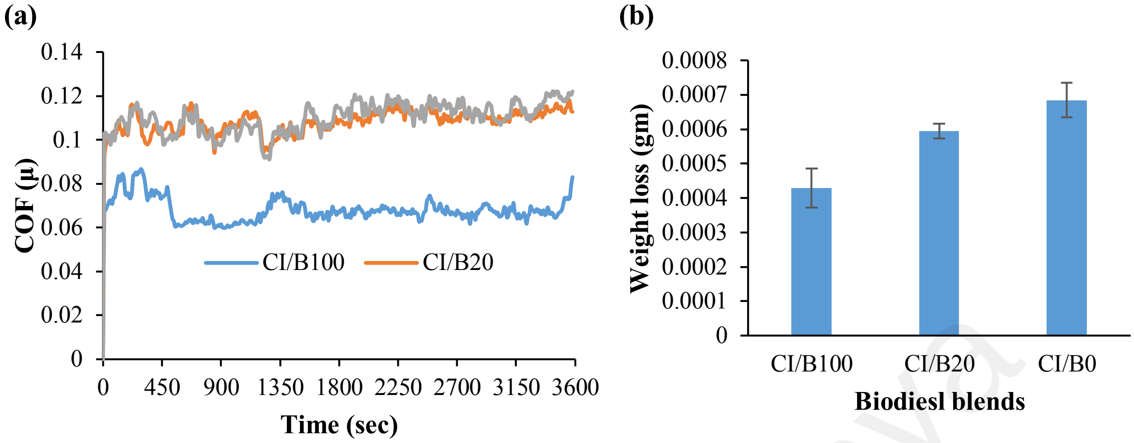

Figure 4.40: Friction coefficient and weight loss of cast iron in B100, B20 and B0

It is observed form the Figure 4.41 (a,b) that except TBHQ doped B100 all doped biodiesel showing higher COF ever compared to B100 itself. It may due the failure of lubrication film formation (Zulkifli et al., 2013) or degradation of fuel by oxidation (Agarwal, 1999). TBHQ doped palm biodiesel shows 7.35% reduction in COF compared to pure B100. It may be due to the active antioxidant (TBHQ) which can make a faster complex bond with free radical of palm biodiesel to reduce oxidation and thus increase biodiesel lubricity (Albuquerque et al., 2012).

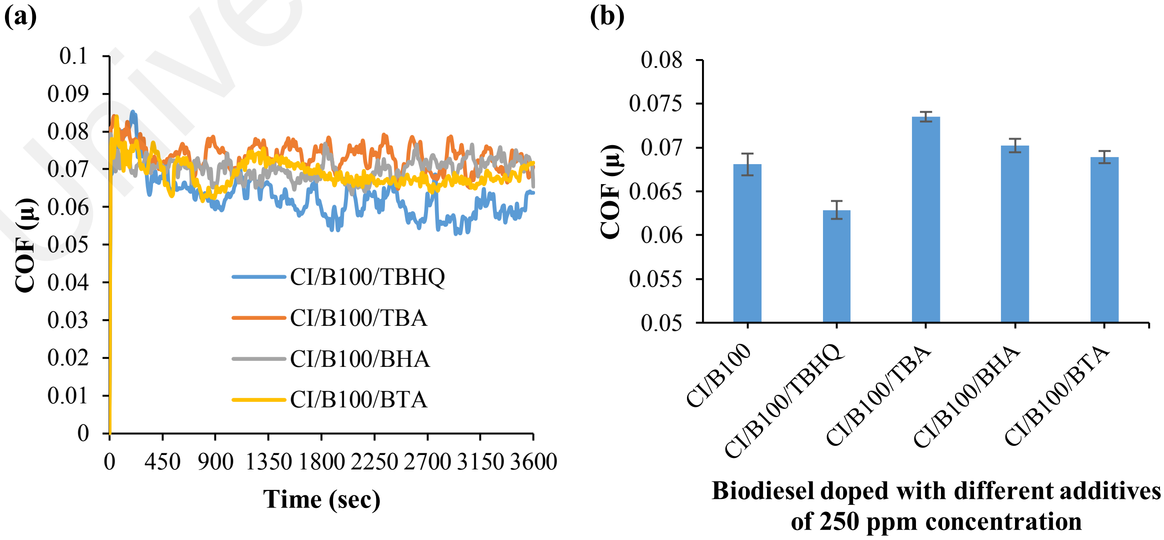

Figure 4.41: Coefficient of friction in various additives doped B100

Figure 4.42 shows variation of the wear scar width (WSW) and specific wear rate for various fuels at the completion of the HFRR tests. Doped B100 shows less wear scar width than B100 (Figure 4.42 a). Figure 4.42 b shows that specific wear rate of cast iron at B0 and B20 are 1.6 and 1.4 times higher than B100. Except TBHQ doped biodiesel, all doped B100 show higher specific wear rate. TBHQ doped B100 show 9.25% reduction of specific wear rate. This finding can be explained by the procrastination of fuel deterioration in terms of fatty acid. This fatty acid enhances lubrication properties by film formation (M. Habibullah et al., 2015; Mosarof et al., 2016). Furthermore, lubricity increases with increase of fatty acid chain length which thicken the film and thereby increase protected surface (Havet, Blouet, Valloire, Brasseur, & Slomka, 2001).

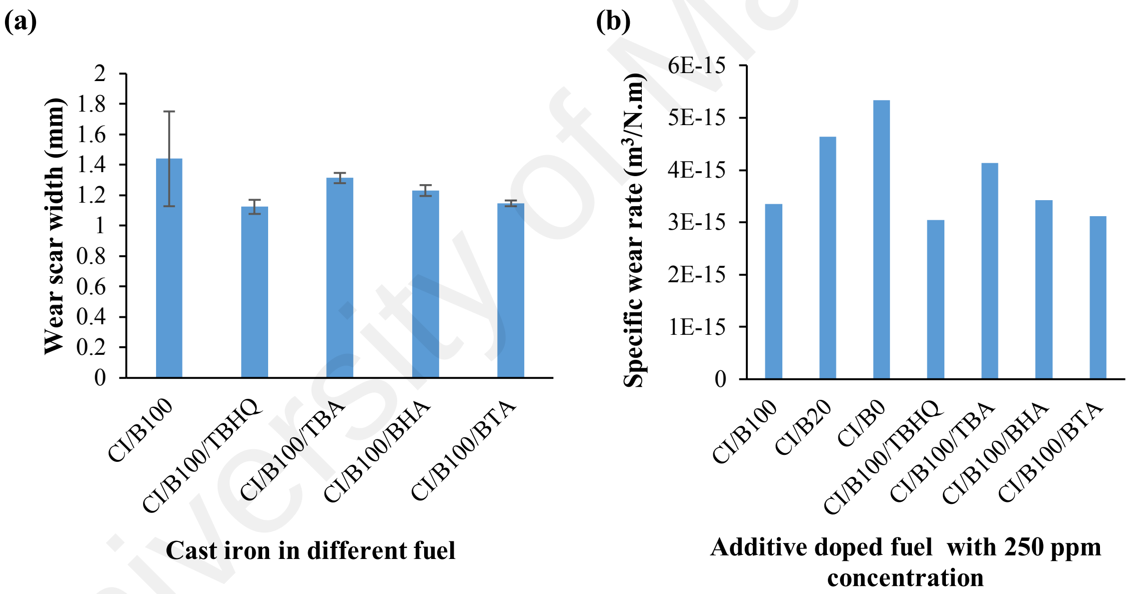

Figure 4.42: Wear scar width and specific wear rate of cast iron plate in different fuels

4.6.2 Worn surface

The roughness test of rubbed surface of cast iron was carried out by means of a profilometer (Mitutoyo SJ-201) after SEM. An average (R_a) and quadratic mean (R_q) of the profile deviation along the sliding direction was determined. Figure 4.43 shows SEM image of cast iron surface before and after the HFRR test. HFRR test in TBHQ doped B100 shows the smoother surface after as received sample. Figure 4.44 shows the value of roughness after HFRR test. It appears that 250 ppm content of TBHQ in B100 considerably reduces surface roughness of cast iron. Lower roughness corresponds to the higher concentration of lubrication film (Sulek et al., 2010).

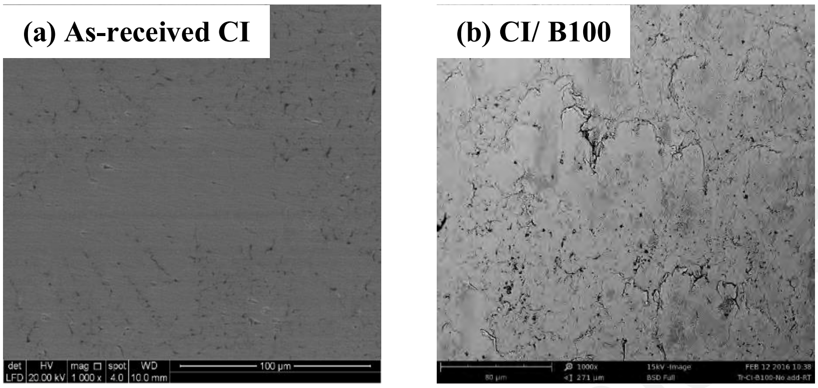
(a) As-received CI

(b) CI/ B100

(c) CI/ B100/ 250 ppm TBHQ

(d) CI/ B100/ 250 ppm TBA

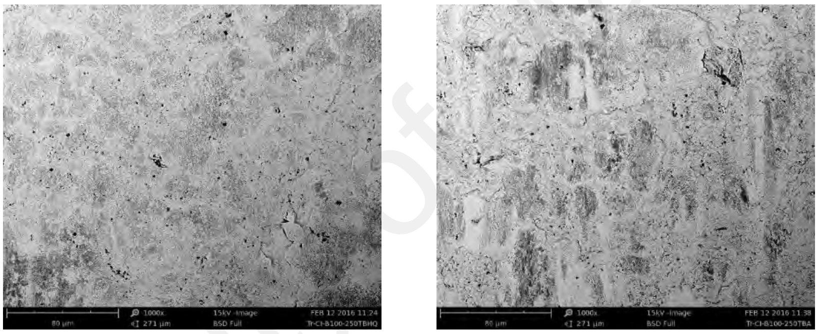

(e) CI/ B100/ 250 ppm BHA

(f) CI/ B100/ 250 ppm BTA

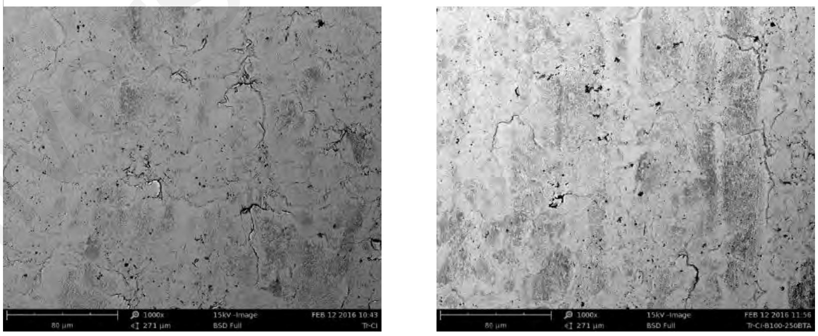

Figure 4.43: Appearances of cast iron wear surface after HFRR test

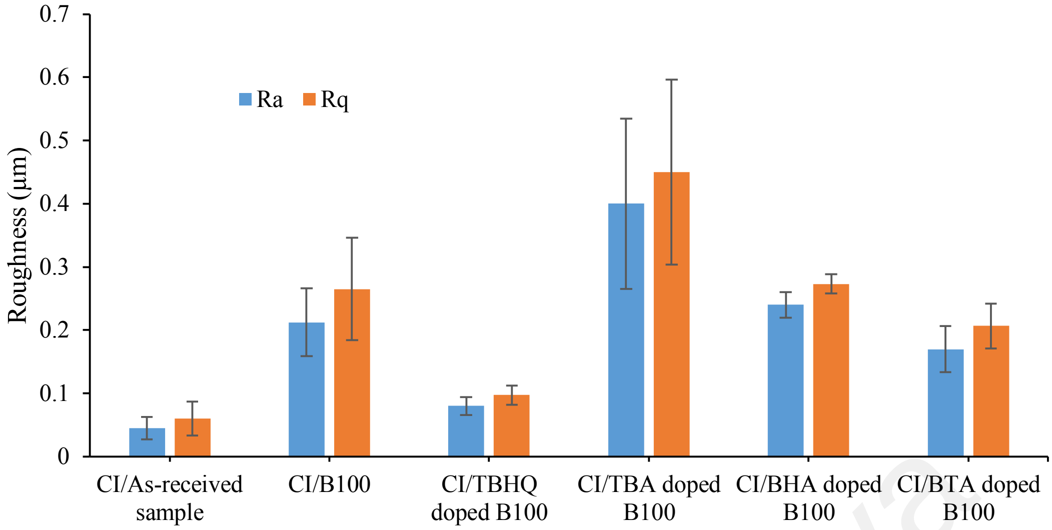

Figure 4.44: Roughness or cast iron surface before and after the HFRR test.

XRD patterns of cast iron after HFRR test in B0, B20, B100 and 250ppm TBHQ doped B100 are shown in Figure 4.45. In Figure 4.45 a and b, peaks of iron along with carbide (Fe_3C) and ferrous oxide (FeO) products appeared. Fe_2O_3 was found in Figure 4.45 c around 2θ value of 32˚. These oxides phases formation may be the result of interaction between cast iron and B100 which could be oxidized during HFRR test (Karavalakis et al., 2011). It could be the cause of high contact resistance of friction pair and insufficient lubricant film. However, higher COF owing to insufficient lubricant film is significantly reduced in TBHQ doped B100 in Figure 4.45 b (M. Habibullah et al., 2015). OH^- found in FeO(OH) may come from existing OH group found in structural formula of TBHQ ($C_{10}H_{14}O_2$). Sufficient coverage of this compound may provide blockage in direct contact of metal and biodiesel blend (Fazal, M.A, et al., 2011; Li et al., 1997).

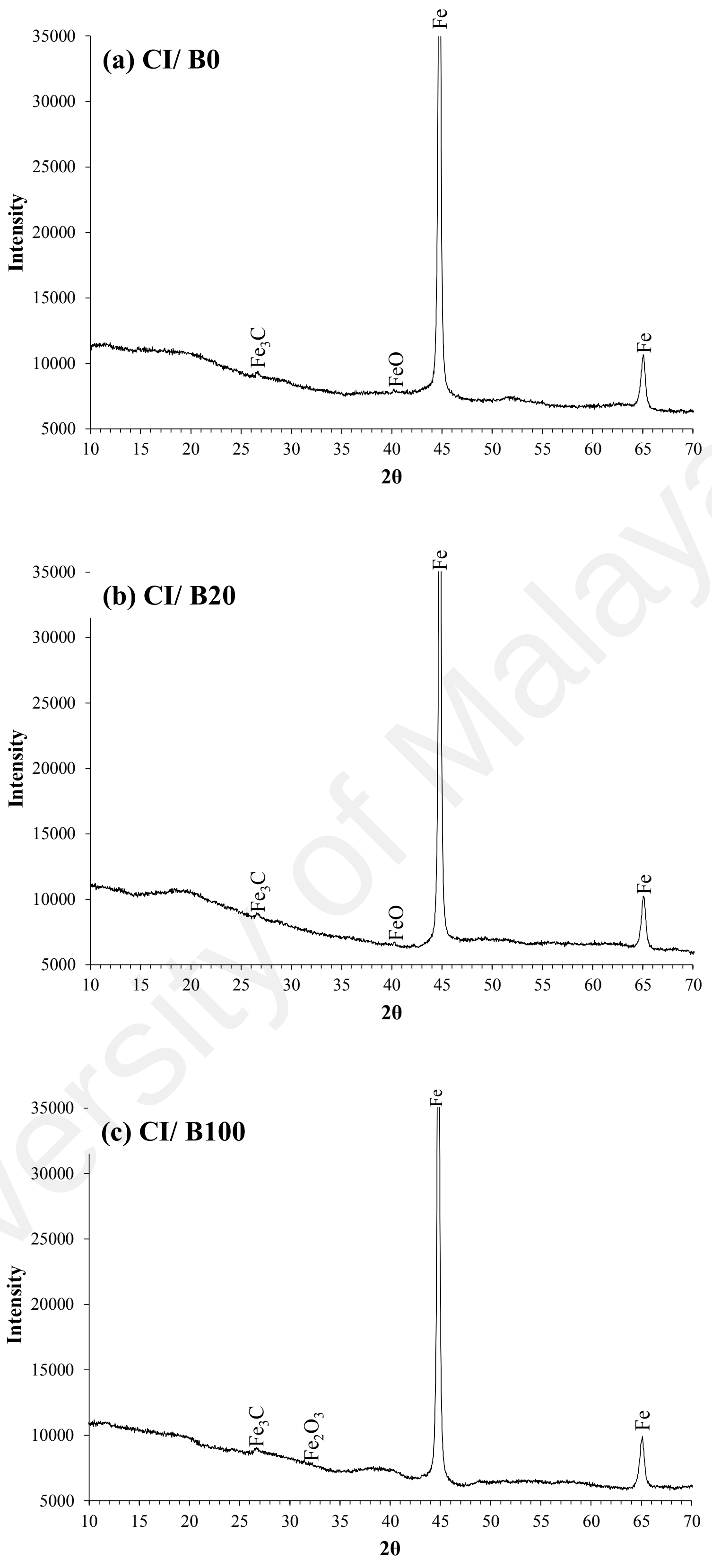

Figure 4.45: XRD pattern of cast iron surface after wear test in presence of B0, B20, B100 and 250ppm TBHQ doped B100.

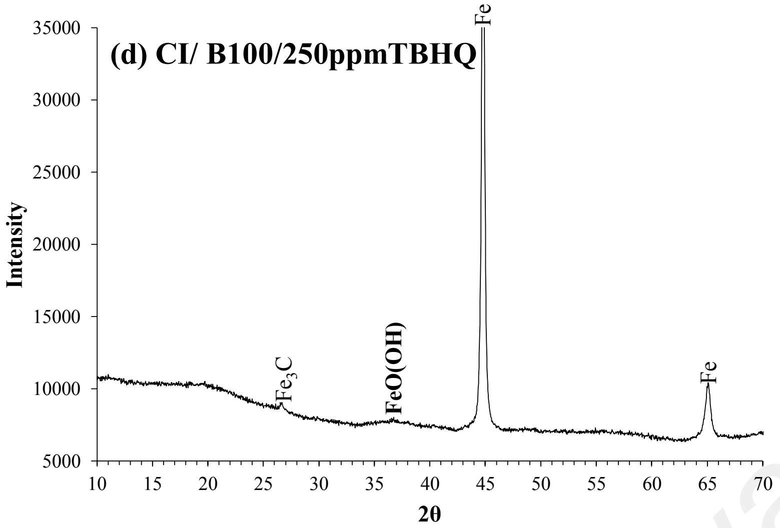

Figure 4.45, continued

4.6.3 Lubrication regime

Table 4.4 and Figure 4.46 illustrated the specific film thickness (λ) for B100 in presence and absence of additives. The numeric values of λ is in between 0.015 and 0.031for all tests which confirm boundary lubrication or boundary friction is the lubrication regime due the presence of a thin fluid film (Ren et al., 2015). Among them TBHQ doped B100 offers highest value of λ. It could be attributed to formation of a thin molecular layer through adsorption mechanism (Bhushan, 2013a, 2013b). It is also reported that additive containing polar carboxyl group (RCOOH) of biodiesel can react with the contacting surface through an adsorption and form a film which reduces number of asperity contact as well as reduces friction and wear by having low interfacial shear stress (Stachowiak & Batchelor, 2013).

Table 4.4 Specific film thickness in absence and presence of additives

Fuel	Rms roughness	Specific film thickness
B100	0.291	0.022
TBHQ doped B100	0.215	0.031
TBA doped B100	0.447	0.014
BHA doped B100	0.312	0.021
BTA doped B100	0.262	0.025

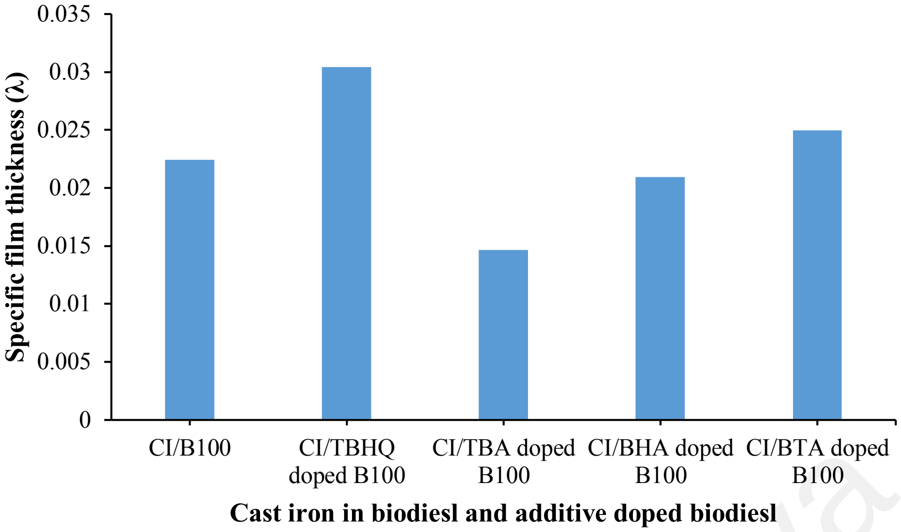

Figure 4.46: Lubrication regime of biodiesel in presence and absence of different additives

4.7 Retardation of tribological degradation using different concentration of TBHQ

In this section, doped B100 and B20 with various TBHQ additive concentrations are differentiated according to their lubrication properties. Experiment was conducted for 3600 sec with a frequency of 33 Hz at 300 K under 75 N load by using ball (440C) on plate (cast iron) high frequency reciprocating rig (HFRR). Results exhibit that friction coefficient and wear scar decrease with the increase of TBHQ concentration in both B100 and B20. This study also confirms adsorption type of TBHQ on cast iron surface along with the isotherm principle.

4.7.1 Comparison of COF and specific wear rate

The variation of coefficient of friction (μ) with time at are shown in Figure 4.47. It is seen in Figure 4.47 a that with the increase of TBHQ concentration in B100, coefficient of friction decreases. Analogous result also found for B20 (Figure 4.47 b). It can also be seen in Figure 4.47 that at the very beginning of the test coefficient of frictions showed unsteady but after a while all it followed a steady trend. Initially higher friction coefficient, can be attributed to high stress concentration generated as a result of low contact area and higher number of sharp asperities (M. Habibullah et al., 2015). These asperities were disappeared with time by making the surface smoother and thereby caused the steady state friction co efficient.

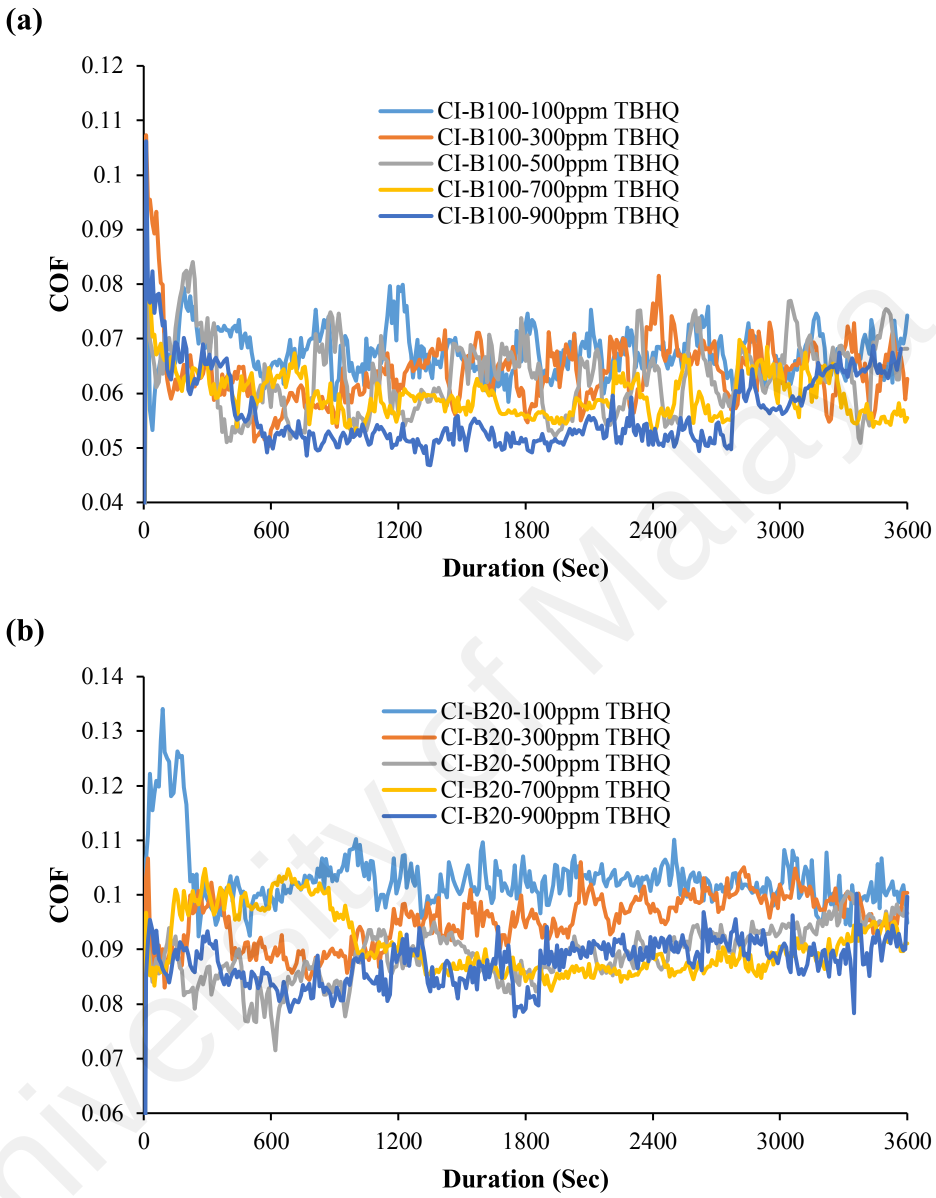

Figure 4.47: Coefficient of friction in various TBHQ doped (a) B100 and (b) B20

Figure 4.48 shows the average coefficient of friction at various concentrations of TBHQ in B100 and B20. Figure 4.48 reveals that the friction coefficients are gradually decreasing with the increase of concentration at 300K. Remarkable reduction of COF is exhibited in Figure 4.48 b for TBHQ doped B1000 compared to TBHQ doped B20. It could be due to the active antioxidant (TBHQ) which can make a faster complex bond with free radical of B100 to reduce oxidation and thus increase biodiesel lubricity (Albuquerque et al., 2012).

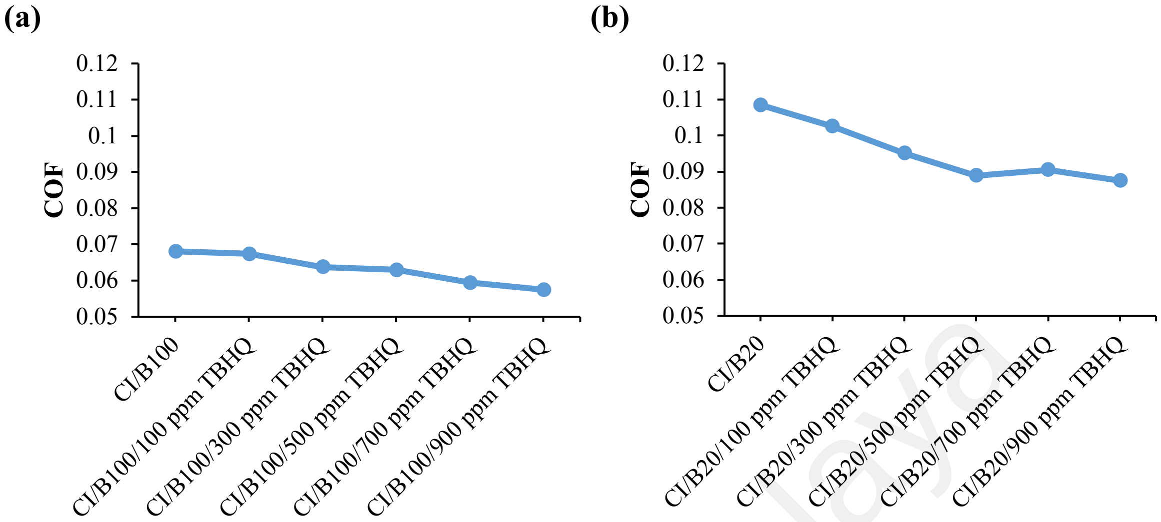

Figure 4.48: Average coefficient of friction in various TBHQ doped (a) B100 and (b) B20

Figure 4.49 shows variation of specific wear rate with the variation of TBHQ concentration in B100 and B20 blend. Figure 4.49 a and b show that the specific wear rate (*k*) decreases gradually with the increase of TBA concentration in both B100 and B20. Compared to B100, 30.01% reduction of specific wear rate is observed in 900 ppm TBHQ doped B100 while 22.67% reduction is seen in TBHQ doped B20 than B20. This finding can be explained by the procrastination of fuel deterioration in terms of fatty acid. This fatty acid enhances lubrication properties by film formation (M. Habibullah et al., 2015; Mosarof et al., 2016).

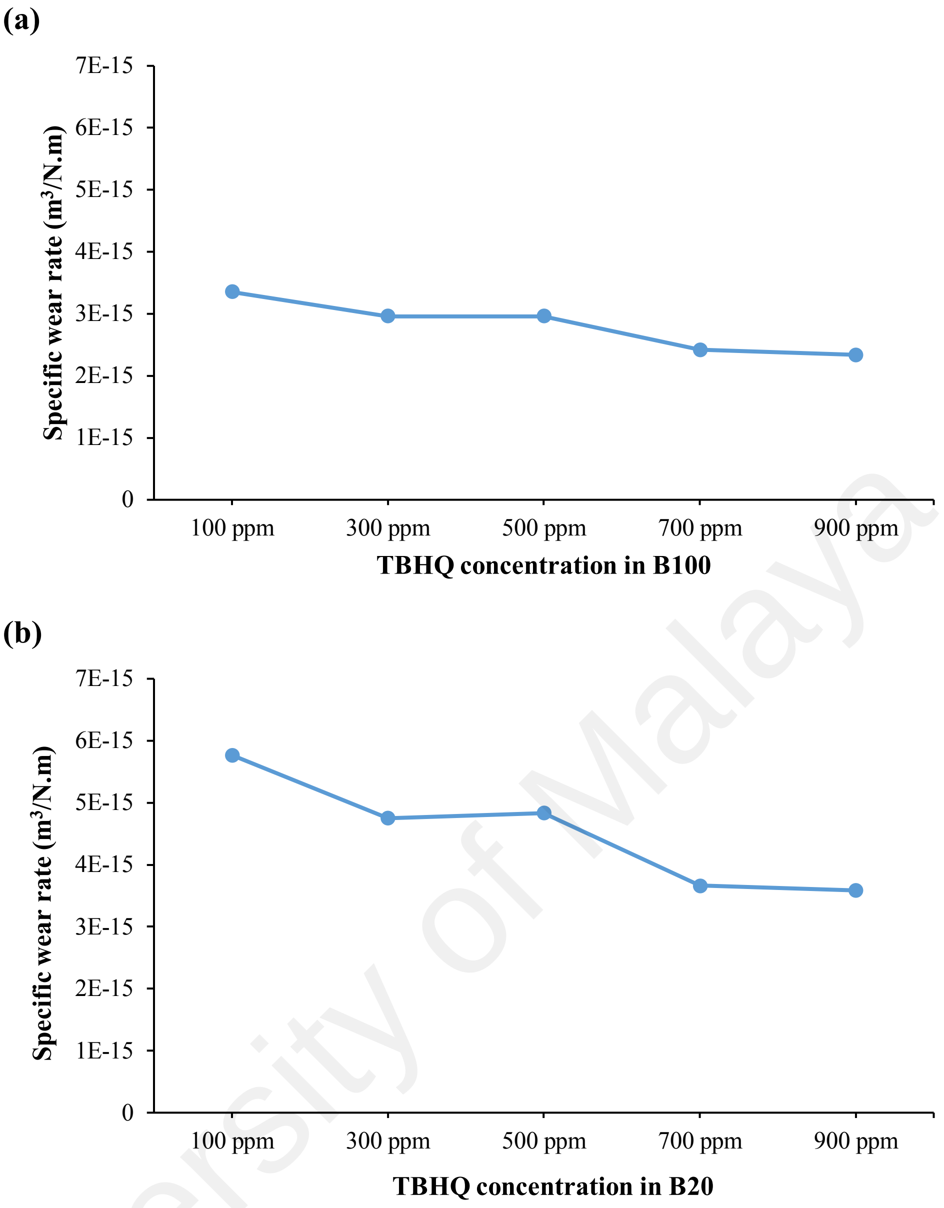

Figure 4.49: Specific wear rate of cast iron plate in different TBHQ concentrations in (a) B100 and (b) B20

4.7.2 Adsorption isotherm model and type of adsorption

Adsorption mechanism of additives on metal surface is vital in lubrication. Statistical analysis of gibbs free energy is helpful for the assumption on adsorption behavior. TBHQ additive consists of a polar hydroxyl group (-OH) at tow end of the molecule. The -OH group reacts with the polar molecule of biodiesel and attached on charged surfaces through an adsorption (adherence) mechanism. This adsorbed layer is responsible for supporting load, minimizing asperity contact and interfacial shear stress thereby, reduces friction and wear (Stachowiak & Batchelor, 2013).

Figure 4.50 a and b show the plot of 1/θ versus 1/C which represents the characteristic isotherm line of adsorption for different TBHQ concentrations in B100 and B20 respectively. Isotherm lines are close to unity, which indicates the agreement with the Langmuir adsorption isotherm model (M. A. Deyab, 2014). The inverse value of the intercept of the isotherm line implies to equilibrium constant of adsorption (K_{eqi}) which is essential for quantification of free energy of adsorption (ΔG_{addi}). It is necessary to find the spontaneity of the TBHQ adsorption process. The obtained values of ΔG_{addi} according to the Equation 3.11 are -26.15 kJ·mol^{-1} and -30.33 kJ·mol^{-1} for TBHQ doped in B100 and B20; the negative value implies the spontaneous adsorption of inhibitor molecules on metal surface (M. Deyab & Abd El-Rehim, 2013). In both conditions, ΔG_{addi} value confirms the physicochemical adsorption as it is in between the range of $-40 \leq \Delta G_{addi} \leq -20$ KJmol^{-1}. It can be attributed to the combination of electrostatic interaction between the charged additive molecules and the charged metal surface (M. Deyab & Abd El-Rehim, 2013; Tebbji et al., 2007). Adsorption of TBHQ on metal surface forms a protective layer and prevents further interaction between metal and biodiesel thereby reduces tribological degradation.

(a)

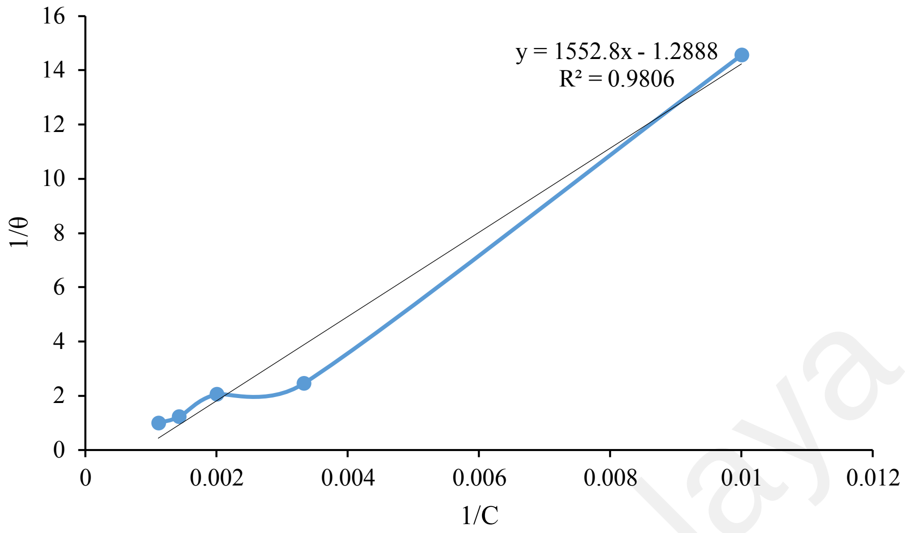

(b)

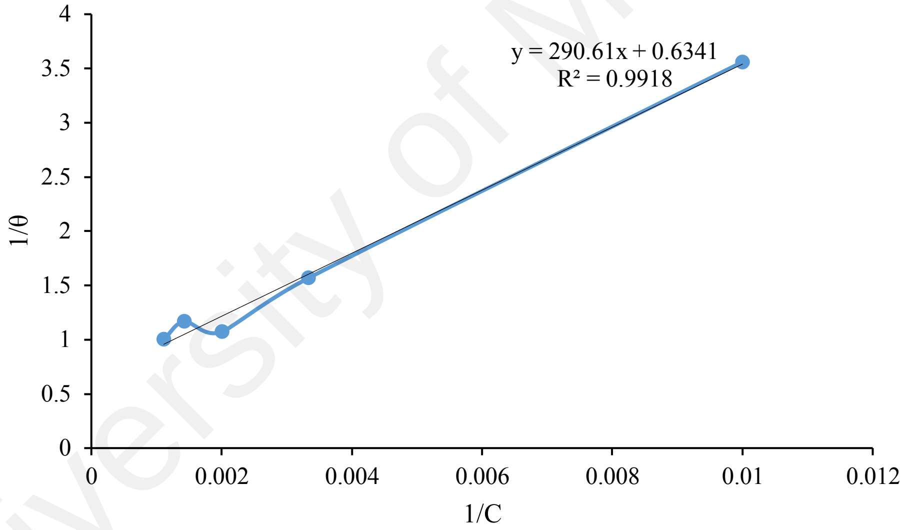

Figure 4.50: Plot of 1/θ versus 1/C for the isotherm line for different TBHQ concentrations added to (a) B100 and (b) B20

CHAPTER 5: CONCLUSIONS AND RECOMMENDATIONS

5.1 Conclusions

From the results and discussion of the present investigation, it can be concluded that severe corrosion attack was observed in biodiesel-exposed cast iron surface. Corrosion of cast iron in biodiesel is comparatively more than low carbon steel. TBA doped biodiesel has fairly good corrosion inhibiting properties for cast iron and low carbon steel followed by BTA doped biodiesel. TBA doped biodiesel shows efficiency of 86.54% and 86.71% in controlling the corrosion of cast iron and low carbon steel respectively. The material degradation rate caused by corrosion decreases with increasing TBA concentration. Corrosion rate of cast iron in biodiesel is significantly reduced because of the addition of TBA. The corrosion rates of low carbon steel in B100 and 500 ppm doped B100 are 2.266 µm/y and 0.135 µm/y respectively compared to the corrosion rate in pure biodiesel itself. Similar result is true for the corrosion rate of LCS. The highest corrosion inhibition efficiency (97.01%) was found for 500 ppm TBA doped biodiesel. It could be attributed to the formation of protective layer adherent to the metal surface. At the elevated temperature (353 K), corrosion attack on cast iron was severe in B20 compared to room temperature. It means, corrosion rate of cast iron in B20 increases with the increase of temperature. It could be the cause of insufficient surface coverage or desorption of additive from cast iron surface. In both temperatures corrosion inhibition performance of TBA is fairly good and it increases with the increase of TBA concentration in B20.

Metal surface characterization further clarify our results. AFM photographs exhibit rough surface with 30.012 nm and 20.59 nm for CI and LCS respectively due to corrosion attack immersed in B100. Roughness of materials exposed to TBA doped biodiesel confirms smoother surface indicating considerable reduction of corrosion. The formation of nitrogen-containing layer ($Fe(NO_3)_3.9H_2O$) was confirmed by XRD and XPS analysis. This layer seems to be more adherent with the metal surface and protect the surface from corrosion attack.

Corrosion inhibition mechanism of cast iron and low carbon steel surface confirmed physicochemical adsorption process. It is favorable, spontaneous and follows the Langmuir isotherm model. Regression coefficient of adsorption isotherm lines for TBA doped B20 also confirms the principle of Langmuir isotherm model in both temperatures (300 K and 353 K). For TBA doped B20, free energy value of adsorption confirms physicochemical at 300 K while probable initiation of chemical adsorption by endothermic reaction at elevated temperature.

In tribological study, specific wear rate of cast iron at Specific wear rate of cast iron at B0 and B20 are 1.6 and 1.4 times higher than B100. Except TBHQ doped biodiesel all doped B100 show higher specific wear rate. TBHQ doped B100 show 9.25% reduction of specific wear. TBHQ doped palm biodiesel shows 7.35% reduction in COF compared to pure B100. It may be due to the active antioxidant (TBHQ) which can make a faster complex bond with free radical of palm biodiesel to reduce oxidation and thus reduce biodiesel lubricity. Specific film thickness (λ) forms on contact surface exposed in TBHQ doped biodiesel ensures less COF and specific wear rate. The range of λ found in between 0.015 and 0.031for all tests which means the existence of boundary lubrication regime.

Both TBHQ doped B100 and B20 confirms the physicochemical adsorption. Adsorption of TBHQ on metal surface forms a protective layer and prevents further interaction between metal and biodiesel thereby reduces tribological degradation.

Two types of degradation mechanisms namely corrosion and wear has been studied with respect to additives. TBA exhibits better with respect to corrosion resistance, but

TBHQ fares well with respect to wear resistance. Therefore, the better choice of additive between TBA and TBHQ could depend on the application as the same additive cannot be effective for both. Further study could be done by blending of these two additives.

5.2 Recommendations for future work

- Change in fuel properties such as TAN, induction period, kinematic viscosity for additive doped could be investigated.
- Effect of different elevated temperature on corrosion inhibition efficiency of additive could be studied.
- Tribological study on elevated temperature could be a further studied.
- Research on retardation of materials degradation by blended TBA and TBHQ doped palm biodiesel could be another future study.

REFERENCES

A. Adhvaryu, Erhan, S., & Perez, J. (2004). Tribological studies of thermally and chemically modified vegetable oils for use as environmentally friendly lubricants. Wear, 257(3), 359-367.

Adam, N. (1928). The structure of thin films. Part XI. Oxygenated derivatives of benzene. Proceedings of the Royal Society of London. Series A, Containing Papers of a Mathematical and Physical Character, 119(783), 628-644.

Adebusoye, A, S., Ilori, M. O., Amund, O. O., Teniola, O. D., & Olatope, S. (2007). Microbial degradation of petroleum hydrocarbons in a polluted tropical stream. World Journal of Microbiology and Biotechnology, 23(8), 1149-1159.

Adhvaryu, A, Erhan, S.Z., Liu, Z.S. (2000). Oxidation kinetic studies of oils derived from unmodified and genetically modified vegetables using pressurized differential scanning calorimetry and nuclear magnetic resonance spectroscopy. Thermochimica Acta, 364(1), 87-97.

Adhvaryu, Atanu, Biresaw, Girma, Sharma, Brajendra, Z, S. (2006). Friction behavior of some seed oils: biobased lubricant applications. Industrial & engineering chemistry research, 45(10), 3735-3740.

Agarwal, A. K. (1999). Performance evaluation and tribological studies on a biodiesel-fuelled compression ignition engine. Ph. D. thesis, Center for Energy Studies, Indian Institute of Technology, Delhi, India.

Agarwal, A. K. (2007). Biofuels (alcohols and biodiesel) applications as fuels for internal combustion engines. Progress in energy and combustion science, 33(3), 233-271.

Agarwal, A. K., & Das, L. (2001). Biodiesel development and characterization for use as a fuel in compression ignition engines. Journal of engineering for gas turbines and power, 123(2), 440-447.

Albuquerque, d. R., Anderson, Maul, Jefferson, Dos Santos, Pereira, J., Gouveia, A. (2012). Estimation of the oxidation temperature of biodiesels from a limited number of chemical parameters. Fuel, 102, 585-591.

Ali, Yusuf, Hanna, A, M., Cuppett, & L, S. (1995). Fuel properties of tallow and soybean oil esters. Journal of the American Oil Chemists' Society, 72(12), 1557-1564.

Amin, A, M., EI-Rehim, Abd, S. S., El-Sherbini. (2009). Polyacrylic acid as a corrosion inhibitor for aluminium in weakly alkaline solutions. Part I: Weight loss, polarization, impedance EFM and EDX studies. Corrosion Science, 51(3), 658-667.

Arkoudeas, P., Kalligeros, S., Zannikos, F., Anastopoulos, G., Karonis, D., Korres, D., & Lois, E. (2003). Study of using JP-8 aviation fuel and biodiesel in CI engines. Energy Conversion and Management, 44(7), 1013-1025.

Ashnani, Mohammadi, M. H., Johari, Anwar, Hashim, Haslenda, Elham. (2014). A source of renewable energy in Malaysia, why biodiesel? Renewable and Sustainable Energy Reviews, 35, 244-257. doi: http://dx.doi.org/10.1016/j.rser.2014.04.001

Atadashi, M., I., Aroua, K., M., Abdul Aziz, R. (2012). The effects of water on biodiesel production and refining technologies: A review. Renewable and Sustainable Energy Reviews, 16(5), 3456-3470. doi: http://dx.doi.org/10.1016/j.rser.2012.03.004

Atadashi, M., I., Aroua, K., M., Abdul Aziz, R. (2013). The effects of catalysts in biodiesel production: A review. Journal of Industrial and Engineering Chemistry, 19(1), 14-26. doi: http://dx.doi.org/10.1016/j.jiec.2012.07.009

Atkins, P. W. (1978). Physical Chemistry. 1990: Oxford university press.

Balat, M., & Balat, H. (2010). Progress in biodiesel processing. Applied Energy, 87(6), 1815-1835.

Barmatov, Evgeny, Geddes, Jill, Hughes, Trevor, Michaela. (2012). Research on corrosion inhibitors for acid stimulation. Paper presented at the CORROSION 2012.

Barnwal, B., & Sharma, M. (2005). Prospects of biodiesel production from vegetable oils in India. Renewable and Sustainable Energy Reviews, 9(4), 363-378.

Bart, CJ, J., Cavallaro, Stefano, Gucciardi, & Emanuele. (2012). Biolubricants: Science and technology: Elsevier.

Bartels, T., Bock, W., Braun, J., Busch, C., Buss, W., Dresel, W., Hörner, D. (2005). Lubricants and lubrication. Ullmann's Encyclopedia of Industrial Chemistry.

Ben Hassen-Trabelsi, A., Kraiem, T., Naoui, S., & Belayouni, H. (2014). Pyrolysis of waste animal fats in a fixed-bed reactor: Production and characterization of bio-oil and bio-char. Waste Management, 34(1), 210-218. doi: http://dx.doi.org/10.1016/j.wasman.2013.09.019

Benjumea, P., Agudelo, J., & Agudelo, A. (2008). Basic properties of palm oil biodiesel–diesel blends. Fuel, 87(10), 2069-2075.

Bessee, G., & Hutzler, S. (2009). The effects of diesel fuel additives on water separation performance: SAE Technical Paper.

Bhushan, B. (2013a). Introduction to tribology: John Wiley & Sons.

Bhushan, B. (2013b). Principles and applications of tribology: John Wiley & Sons.

Blau, P. J., & Pollard, M. (2009). Materials for High Pressure Fuel Injection Systems.

Bouaid, Abderrahim, Martinez, Mercedes, Aracil, & José. (2007). Long storage stability of biodiesel from vegetable and used frying oils. Fuel, 86(16), 2596-2602.

Brophy, J., & Zisman, W. A. (1951). Surface chemical phenomena in lubrication. Annals of the New York Academy of Sciences, 53(4), 836-861.

Burton, R., & Biofuels, P. (2008). An overview of ASTM D6751: biodiesel standards and testing methods. Alternative Fuels Consortium.

Cao, Peigang, Tremblay, Y, A., Dubé, A, M., Katie. (2007). Effect of membrane pore size on the performance of a membrane reactor for biodiesel production. Industrial & engineering chemistry research, 46(1), 52-58.

Chen, Y.-H., & Luo, Y.-M. (2011). Oxidation stability of biodiesel derived from free fatty acids associated with kinetics of antioxidants. Fuel processing technology, 92(7), 1387-1393.

Chew, KV, Haseeb, ASMA, Masjuki, HH, M. (2013). Corrosion of magnesium and aluminum in palm biodiesel: A comparative evaluation. Energy, 57, 478-483.

Cole, G. M. (1994). Assessment and remediation of petroleum contaminated sites: CRC Press.

Connors, K. A. (1990). Chemical kinetics: the study of reaction rates in solution: John Wiley & Sons.

Cook, E. L., & Hackerman, N. (1951). Adsorption of polar organic compounds on steel. The Journal of Physical Chemistry, 55(4), 549-557.

Cosgrove, P, J., Church, F, D., Pryor, & A, W. (1987). The kinetics of the autoxidation of polyunsaturated fatty acids. Lipids, 22(5), 299-304.

Crouse, W., & Angle, D. (1993). Automotive mechanics. 10th international ed: New York: Macmillan/McGraw-Hill.

Cui, Y., Liu, S., Smith, K., Yu, K., Hu, H., Jiang, W., & Li, Y. (2015). Characterization of corrosion scale formed on stainless steel delivery pipe for reclaimed water treatment. Water research.

Ćurković, Lidija, Rastovčan-Mioč, Alenka, Majić, Marijana, Josip. (2011). APPLICATION OF DIFFERENT ISOTHERM MODELS ON LEAD IONS SORPTION ONTO ELECTRIC FURNACE SLAG. The Holistic Approach to Environment, 1(1), 13-18.

Cursaru, Diana-Luciana, Brănoiu, Gheorghe, Ramadan, Ibrahim, Florin. (2014). Degradation of automotive materials upon exposure to sunflower biodiesel. Industrial Crops and Products, 54, 149-158.

Daugulis, A. J., & McCracken, C. M. (2003). Microbial degradation of high and low molecular weight polyaromatic hydrocarbons in a two-phase partitioning bioreactor by two strains of Sphingomonas sp. Biotechnology letters, 25(17), 1441-1444.

De Mello, A, J., Carmichael, A, C., Peacock, E, E. (2007). Biodegradation and environmental behavior of biodiesel mixtures in the sea: An initial study. Marine Pollution Bulletin, 54(7), 894-904.

De Silva, PR, Priest, M., Lee, P., Coy, R., & Taylor, R. (2011). Tribometer investigation of the frictional response of piston rings when lubricated with the separated phases of lubricant contaminated with the gasoline engine biofuel ethanol and water. Tribology Letters, 43(2), 107-120.

DeMello, A, J., Carmichael, A, C., Peacock, E. (2007). Biodegradation and environmental behavior of biodiesel mixtures in the sea: An initial study. Marine Pollution Bulletin, 54(7), 894-904.

Demirbas, & Ayhan. (2007). Importance of biodiesel as transportation fuel. Energy Policy, 35(9), 4661-4670.

Demirbas, A. (2009). Progress and recent trends in biodiesel fuels. Energy Conversion and Management, 50(1), 14-34.

Deng, Xin, Fang, Zhen, Liu, Yun-hu, Chang-Liu. (2011). Production of biodiesel from Jatropha oil catalyzed by nanosized solid basic catalyst. Energy, 36(2), 777-784.

Deyab, M. (2015). Application of nonionic surfactant as a corrosion inhibitor for zinc in alkaline battery solution. Journal of Power Sources, 292, 66-71.

Deyab, M. (2016). The inhibition activity of butylated hydroxytoluene towards corrosion of carbon steel in biodiesel blend B20. Journal of the Taiwan Institute of Chemical Engineers, 60, 369-375.

Deyab, M., & Abd El-Rehim, S. (2013). Influence of polyethylene glycols on the corrosion inhibition of carbon steel in butyric acid solution: weight loss, EIS and theoretical studies. Int J Electrochem Sci, 8, 12613-12627.

Deyab, M. A. The inhibition activity of butylated hydroxytoluene towards corrosion of carbon steel in biodiesel blend B20. Journal of the Taiwan Institute of Chemical Engineers. doi: http://dx.doi.org/10.1016/j.jtice.2015.10.035

Deyab, M. A. (2014). Adsorption and inhibition effect of Ascorbyl palmitate on corrosion of carbon steel in ethanol blended gasoline containing water as a contaminant. Corrosion Science, 80(0), 359-365. doi: http://dx.doi.org/10.1016/j.corsci.2013.11.056

Deyab, M. A. (2016). Corrosion inhibition of aluminum in biodiesel by ethanol extracts of Rosemary leaves. Journal of the Taiwan Institute of Chemical Engineers, 58, 536-541. doi: http://dx.doi.org/10.1016/j.jtice.2015.06.021

dos Reis Albuquerque, Anderson, Maul, J., Dos Santos, J. P., Dos Santos, I. M. G., & De Souza, A. G. (2012). Estimation of the oxidation temperature of biodiesels from a limited number of chemical parameters. Fuel, 102, 585-591.

Drown, DC, Harper, K, Frame, & E. (2001). Screening vegetable oil alcohol esters as fuel lubricity enhancers. Journal of the American Oil Chemists' Society, 78(6), 579-584.

Dunn, R. O. (2005). Effect of antioxidants on the oxidative stability of methyl soyate (biodiesel). Fuel processing technology, 86(10), 1071-1085. doi: http://dx.doi.org/10.1016/j.fuproc.2004.11.003

Dunn, R. O. (2007). Effect of temperature on the oil stability index (OSI) of biodiesel. Energy & fuels, 22(1), 657-662.

El Qada, N, E., Allen, J, S., Walker, & M, G. (2008). Influence of preparation conditions on the characteristics of activated carbons produced in laboratory and pilot scale systems. Chemical Engineering Journal, 142(1), 1-13.

Elayyachy, M., Hammouti, B., El Idrissi, A., & Aouniti, A. (2011). Adsorption and corrosion inhibition behavior of C38 steel by one derivative of quinoxaline in 1 M HCl. Portugaliae Electrochimica Acta, 29(1), 57-68.

Fattah, Rizwanul, I., Masjuki, HH, Kalam, M.A. (2014). Effect of antioxidants on oxidation stability of biodiesel derived from vegetable and animal based feedstocks. Renewable and Sustainable Energy Reviews, 30, 356-370.

Fattah, R., M., I., Masjuki, H., H., Kalam, A. (2014). Effect of antioxidant on the performance and emission characteristics of a diesel engine fueled with palm biodiesel blends. Energy Conversion and Management, 79(0), 265-272. doi: http://dx.doi.org/10.1016/j.enconman.2013.12.024

Fazal, M.A, Haseeb, A.S.M.A., Masjuki, & H.H. (2011). Effect of different corrosion inhibitors on the corrosion of cast iron in palm biodiesel. Fuel processing technology, 92(11), 2154-2159.

Fazal, MA, Haseeb, ASMA, Masjuki, H.H. (2010). Comparative corrosive characteristics of petroleum diesel and palm biodiesel for automotive materials. Fuel processing technology, 91(10), 1308-1315.

Fazal, MA, Haseeb, ASMA, Masjuki, H.H. (2011a). Biodiesel feasibility study: An evaluation of material compatibility; performance; emission and engine durability. Renewable and Sustainable Energy Reviews, 15(2), 1314-1324.

Fazal, MA, Haseeb, ASMA, Masjuki, H.H. (2011b). Effect of temperature on the corrosion behavior of mild steel upon exposure to palm biodiesel. Energy, 36(5), 3328-3334.

Fazal, MA, Haseeb, ASMA, Masjuki, H.H. (2012). Degradation of automotive materials in palm biodiesel. Energy, 40(1), 76-83.

Fazal, MA, Haseeb, ASMA, Masjuki, H.H. (2013a). Corrosion mechanism of copper in palm biodiesel. Corrosion Science, 67, 50-59.

Fazal, MA, Haseeb, ASMA, Masjuki, H.H. (2013b). Investigation of friction and wear characteristics of palm biodiesel. Energy Conversion and Management, 67, 251-256.

Fazal, MA, Jakeria, MR, Haseeb, ASMA. (2014). Effect of copper and mild steel on the stability of palm biodiesel properties: A comparative study. Industrial Crops and Products, 58, 8-14.

Fazal, MA. Haseeb, A.S.M.A, Masjuki H.H. (2014). A critical review on the tribological compatibility of automotive materials in palm biodiesel. Energy Conversion and Management, 79, 180-186.

Felizardo, P., Correia, M. J. N., Raposo, I., Mendes, J. F., Berkemeier, R., & Bordado, J. M. (2006). Production of biodiesel from waste frying oils. Waste Management, 26(5), 487-494.

Fernandes, D. M., Montes, R. H., Almeida, E. S., Nascimento, A. N., Oliveira, P. V., Richter, E. M., & Muñoz, R. A. (2013). Storage stability and corrosive character of stabilised biodiesel exposed to carbon and galvanised steels. Fuel, 107, 609-614.

Finšgar, M., & Jackson, J. (2014). Application of corrosion inhibitors for steels in acidic media for the oil and gas industry: A review. Corrosion Science, 86, 17-41.

Foo, K., & Hameed, B. (2009). An overview of landfill leachate treatment via activated carbon adsorption process. Journal of Hazardous Materials, 171(1), 54-60.

Foo, K., & Hameed, B. (2010). Insights into the modeling of adsorption isotherm systems. Chemical Engineering Journal, 156(1), 2-10.

Fox, N., & Stachowiak, G. (2007). Vegetable oil-based lubricants—a review of oxidation. Tribology International, 40(7), 1035-1046.

Fujita, S., & Mizuno, D. (2007). Corrosion and corrosion test methods of zinc coated steel sheets on automobiles. Corrosion Science, 49(1), 211-219.

Geller, P., D., Adams, T., T., Goodrum, W., J., Joshua. (2010). Storage stability of poultry fat and diesel fuel mixtures: Part II – Chemical properties. Fuel, 89(3), 792-796. doi: http://dx.doi.org/10.1016/j.fuel.2009.09.021

Geller., P., D., Adams, T., T., Goodrum, W., J., Joshua. (2008). Storage stability of poultry fat and diesel fuel mixtures: Specific gravity and viscosity. Fuel, 87(1), 92-102. doi: http://dx.doi.org/10.1016/j.fuel.2007.03.043

Ghazali, W., Maawa, W. N., Mamat, Rizalman, Masjuki, H. H., Gholamhassan. (2015). Effects of biodiesel from different feedstocks on engine performance and emissions: A review. Renewable and Sustainable Energy Reviews, 51, 585-602. doi: http://dx.doi.org/10.1016/j.rser.2015.06.031

Gitte Sørensen, Pedersen, V, D., Nørgaard, K, A., Sørensen, D. S. (2011). Microbial growth studies in biodiesel blends. Bioresource Technology, 102(8), 5259-5264.

Goldstein, J. (2012). Practical scanning electron microscopy: electron and ion microprobe analysis: Springer Science & Business Media.

Goodrum, J. W., & Geller, D. P. (2005). Influence of fatty acid methyl esters from hydroxylated vegetable oils on diesel fuel lubricity. Bioresource Technology, 96(7), 851-855.

Gopi, D., Bhuvaneswaran, N., Rajeswarai, S., & Ramadas, K. (2000). Synergistic effect of thiourea derivatives and non-ionic surfactants on the inhibition of corrosion of carbon steel in acid environments. Anti-Corrosion Methods and Materials, 47(6), 332-339.

Gopinath, A, Sairam, K, Velraj, R.G. (2015). Effects of the properties and the structural configurations of fatty acid methyl esters on the properties of biodiesel fuel: a review. Proceedings of the Institution of Mechanical Engineers, Part D: Journal of Automobile Engineering, 229(3), 357-390.

Grzesik, Z, Smoła, G, Adamaszek, K.S. (2013). Thermal shock corrosion of valve steels utilized in automobile industry. Oxidation of Metals, 80(1-2), 147-159.

Guthrie, Jeffrey, Battat, Bridgitte, Grethlein, & Chris. (2002). Accelerated corrosion testing. AMPTIAC Quarterly, 6(3), 11-15.

Habibullah, M, Rizwanul Fattah, IM, Masjuki, H.H. (2015). Effects of Palm–Coconut Biodiesel Blends on the Performance and Emission of a Single-Cylinder Diesel Engine. Energy & fuels, 29(2), 734-743.

Habibullah, M., Masjuki, H. H., Kalam, M. A., Zulkifli, N. W. M., Masum, B. M., Arslan, A., & Gulzar, M. (2015). Friction and wear characteristics of Calophyllum inophyllum biodiesel. Industrial Crops and Products, 76, 188-197. doi: http://dx.doi.org/10.1016/j.indcrop.2015.05.042

Hackerman, N., & Roebuck, A. (1954). Adsorption of polar organic compounds on steel. Industrial & Engineering Chemistry, 46(7), 1481-1485.

Hamrock, B. J., & Dowson, D. (1981). Ball bearing lubrication: the elastohydrodynamics of elliptical contacts.

Haque, M., & Sharif, A. (2001). Study on wear properties of aluminium–silicon piston alloy. Journal of materials processing technology, 118(1), 69-73.

Hardalupas, Y., Taylor, P., A. M. K., Whitelaw, & H., J. (1992). Characteristics of the spray from a diesel injector. International Journal of Multiphase Flow, 18(2), 159-179. doi: http://dx.doi.org/10.1016/0301-9322(92)90080-Z

Haseeb, ASMA, Fazal, MA, Jahirul, MI, HH. (2011). Compatibility of automotive materials in biodiesel: a review. Fuel, 90(3), 922-931.

Haseeb, ASMA, Sia, SY, Fazal, MA, Masjuku H.H. (2010). Effect of temperature on tribological properties of palm biodiesel. Energy, 35(3), 1460-1464.

Haseeb A.S.M.A, Masjuki, H.H, Ann, LJ, Fazal, & MA. (2010). Corrosion characteristics of copper and leaded bronze in palm biodiesel. Fuel processing technology, 91(3), 329-334.

Hashemi, T., & Hogarth, C. (1988). The mechanism of corrosion inhibition of copper in NaCl solution by benzotriazole studied by electron spectroscopy. Electrochimica acta, 33(8), 1123-1127.

Haşimoğlu, C., Ciniviz, M., Özsert, İ., İçingür, Y., Parlak, A., & Salman, M. S. (2008). Performance characteristics of a low heat rejection diesel engine operating with biodiesel. Renewable energy, 33(7), 1709-1715.

Havet, L., Blouet, J., Valloire, F. R., Brasseur, E., & Slomka, D. (2001). Tribological characteristics of some environmentally friendly lubricants. Wear, 248(1), 140-146.

He, C., Ge, Y., Tan, J., You, K., Han, X., & Wang, J. (2010). Characteristics of polycyclic aromatic hydrocarbons emissions of diesel engine fueled with biodiesel and diesel. Fuel, 89(8), 2040-2046.

He, C., Tian, Z., Zhang, B., Lin, Y., Chen, X., Wang, M., & Li, F. (2015). Inhibition Effect of Environment-Friendly Inhibitors on the Corrosion of Carbon Steel in Recirculating Cooling Water. Industrial & engineering chemistry research, 54(7), 1971-1981.

Herrag, L., Hammouti, B., Elkadiri, S., Aouniti, A., Jama, C., Vezin, H., & Bentiss, F. (2010). Adsorption properties and inhibition of mild steel corrosion in hydrochloric solution by some newly synthesized diamine derivatives: experimental and theoretical investigations. Corrosion Science, 52(9), 3042-3051.

Hill, P. D. (2002). Biodiesel Basics. Collinsville, IL, USA.

Hoekman, Kent, S., Broch, Amber, Robbins, Curtis, Mani. (2012). Review of biodiesel composition, properties, and specifications. Renewable and Sustainable Energy Reviews, 16(1), 143-169.

Holmberg, Kenneth, Andersson, Peter, Erdemir, & Ali. (2012). Global energy consumption due to friction in passenger cars. Tribology International, 47, 221-234.

Höök, M., & Tang, X. (2013). Depletion of fossil fuels and anthropogenic climate change—A review. Energy Policy, 52, 797-809. doi: http://dx.doi.org/10.1016/j.enpol.2012.10.046

Horel, A. A. (2009). Biodegradation of petroleum and alternative fuel hydrocarbons in moderate to cold climate: University of Alaska Fairbanks.

Hosseini, SMA, Salari, M, Jamalizadeh, E, & Jafari, A. (2012). Electrochemical and quantum chemical studies of aromatic amines on the steel corrosion in acid solution. Corrosion, 68(7), 600-609.

Hu, Enzhu, Xu, Yufu, Hu, Xianguo, Shaotong. (2012). Corrosion behaviors of metals in biodiesel from rapeseed oil and methanol. Renewable energy, 37(1), 371-378.

Hu, Jianbo, Du, Zexue, Li, Changxiu, Enze. (2005). Study on the lubrication properties of biodiesel as fuel lubricity enhancers. Fuel, 84(12–13), 1601-1606. doi: http://dx.doi.org/10.1016/j.fuel.2005.02.009

Jahanmir, S., & Beltzer, M. (1986a). An adsorption model for friction in boundary lubrication. ASLE transactions, 29(3), 423-430.

Jahanmir, S., & Beltzer, M. (1986b). Effect of additive molecular structure on friction coefficient and adsorption. Journal of Tribology, 108(1), 109-116.

Jain, S., & Sharma, M. (2010). Stability of biodiesel and its blends: a review. Renewable and Sustainable Energy Reviews, 14(2), 667-678.

Jain, S., & Sharma, M. (2012). Oxidation, thermal, and storage stability studies of Jatropha curcas biodiesel. ISRN Renewable Energy, 2012.

Jakeria, MR, Fazal, MA, Haseeb, ASMA. (2014). Influence of different factors on the stability of biodiesel: A review. Renewable and Sustainable Energy Reviews, 30, 154-163.

Jayadas, N., & Prabhakaran Nair, K. (2007). Tribological evaluation of coconut oil as an environment-friendly lubricant. Tribology International, 40(2), 350-354.

Jin, Dingfeng, Zhou, Xuehua, Wu, Panpan, Hongliang. (2015). Corrosion behavior of ASTM 1045 mild steel in palm biodiesel. Renewable energy, 81, 457-463.

Johari, A., Nyakuma, B. B., Mohd Nor, S. H., Mat, R., Hashim, H., Ahmad, A., Tuan Abdullah, T. A. (2015). The challenges and prospects of palm oil based biodiesel in Malaysia. Energy, 81, 255-261. doi: http://dx.doi.org/10.1016/j.energy.2014.12.037

Kabir, MA, Higgs, Fred, C., Lovell, & R, M. (2008). A pin-on-disk experimental study on a green particulate-fluid lubricant. Journal of Tribology, 130(4), 041801.

Kajdas, C., & Majzner, M. (2001). The influence of fatty acids and fatty acids mixtures on the lubricity of low-sulfur diesel fuels: SAE Technical Paper.

Kalam, , MA, Husnawan, , M, . . . HH. (2003). Exhaust emission and combustion evaluation of coconut oil-powered indirect injection diesel engine. Renewable energy, 28(15), 2405-2415.

Kalam, MA., & Masjuki., H. (2008). Testing palm biodiesel and NPAA additives to control NOx and CO while improving efficiency in diesel engines. Biomass and Bioenergy, 32(12), 1116-1122.

Kapilan, N, Ashok Babu, TP, Reddy, & RP. (2009). Technical aspects of biodiesel and its oxidation stability. Int J ChemTech Res, 1, 278-282.

Karamangil, M., & Taflan, R. (2013). Experimental investigation of effect of corrosion on injected fuel quantity and spray geometry in the diesel injection nozzles. Fuel, 112, 531-536.

Karavalakis, Georgios, Hilari, Despina, Givalou, Lida, Stamos. (2011). Storage stability and ageing effect of biodiesel blends treated with different antioxidants. Energy, 36(1), 369-374.

Kaul, S., Saxena, R., Kumar, A., Negi, M., Bhatnagar, A., Goyal, H., & Gupta, A. (2007). Corrosion behavior of biodiesel from seed oils of Indian origin on diesel engine parts. Fuel processing technology, 88(3), 303-307.

Kaya, C., Hamamci, C., Baysal, A., Akba, O., Erdogan, S., & Saydut, A. (2009). Methyl ester of peanut (Arachis hypogea L.) seed oil as a potential feedstock for biodiesel production. Renewable energy, 34(5), 1257-1260. doi: http://dx.doi.org/10.1016/j.renene.2008.10.002

Kegl, Breda, Kegl, Marko, Pehan, & Stanislav. (2013). Green Diesel Engines: Biodiesel Usage in Diesel Engines: Springer.

Klofutar, B., Golob, J., Likozar, B., Klofutar, C., Žagar, E., & Poljanšek, I. (2010). The transesterification of rapeseed and waste sunflower oils: Mass-transfer and kinetics in a laboratory batch reactor and in an industrial-scale reactor/separator setup. Bioresource Technology, 101(10), 3333-3344.

Knothe, G. (2005). Dependence of biodiesel fuel properties on the structure of fatty acid alkyl esters. Fuel processing technology, 86(10), 1059-1070.

Knothe, G. (2006). Analyzing biodiesel: standards and other methods. Journal of the American Oil Chemists' Society, 83(10), 823-833.

Knothe, G. (2008). “Designer” biodiesel: optimizing fatty ester composition to improve fuel properties†. Energy & fuels, 22(2), 1358-1364.

Knothe, G., & Steidley, K. R. (2005a). Kinematic viscosity of biodiesel fuel components and related compounds. Influence of compound structure and comparison to petrodiesel fuel components. Fuel, 84(9), 1059-1065.

Knothe, G., & Steidley, K. R. (2005b). Lubricity of components of biodiesel and petrodiesel. The origin of biodiesel lubricity. Energy & fuels, 19(3), 1192-1200.

Kousoulidou, Marina, Fontaras, Georgios, Ntziachristos, Leonidas, Zissis. (2010). Biodiesel blend effects on common-rail diesel combustion and emissions. Fuel, 89(11), 3442-3449.

Kousoulidou, Marina, Ntziachristos, Leonidas, Fontaras, Georgios, Samaras, Z. (2012). Impact of biodiesel application at various blending ratios on passenger cars of different fueling technologies. Fuel, 98, 88-94.

Kovács, A., Tóth, J., Isaák, Gy. (2015). Aspects of storage and corrosion characteristics of biodiesel. Fuel processing technology, 134, 59-64. doi: http://dx.doi.org/10.1016/j.fuproc.2015.01.014

Kumar, A., & Sharma, S. (2008). An evaluation of multipurpose oil seed crop for industrial uses (Jatropha curcas L.): A review. Industrial Crops and Products, 28(1), 1-10. doi: http://dx.doi.org/10.1016/j.indcrop.2008.01.001

Kumar, N., & Chauhan, S. (2014). Analysis of tribological performance of biodiesel. Proceedings of the Institution of Mechanical Engineers, Part J: Journal of Engineering Tribology, 1350650114532452.

Lapuerta, Magin, Armas, Octavio, Rodriguez-Fernandez, & Jose. (2008). Effect of biodiesel fuels on diesel engine emissions. Progress in energy and combustion science, 34(2), 198-223.

Lee, S, J., Ray, I, R., Little, & J, B. (2010). An assessment of alternative diesel fuels: microbiological contamination and corrosion under storage conditions. Biofouling, 26(6), 623-635.

Lenauer, Claudia, Tomastik, Christian, Wopelka, Thomas, Martin. (2014). Piston ring wear and cylinder liner tribofilm in tribotests with lubricants artificially altered with ethanol combustion products. Tribology International.

Lenauer, Claudia, Tomastik, Christian, Wopelka, Thomas, & Jech, M. (2015). Piston ring wear and cylinder liner tribofilm in tribotests with lubricants artificially altered with ethanol combustion products. Tribology International, 82, 415-422.

Li, P, Lin, JY, Tan, KL. (1997). Electrochemical impedance and X-ray photoelectron spectroscopic studies of the inhibition of mild steel corrosion in acids by cyclohexylamine. Electrochimica acta, 42(4), 605-615.

Li, W., Kong, X., Ruan, M., Ma, F., Jiang, Y., Liu, M., Zuo, X. (2012). Green waxes, adhesives and lubricants. Philosophical Transactions of the Royal Society of London A: Mathematical, Physical and Engineering Sciences, 370(1970), 3269-3269.

Li, X., Deng, S., & Fu, H. (2012). Inhibition of the corrosion of steel in HCl, H2SO4 solutions by bamboo leaf extract. Corrosion Science, 62(0), 163-175. doi: http://dx.doi.org/10.1016/j.corsci.2012.05.008

Lin, Bai-Fu, Huang, Jyun-Han, Huang, & Dao-Yi. (2009). Experimental study of the effects of vegetable oil methyl ester on DI diesel engine performance characteristics and pollutant emissions. Fuel, 88(9), 1779-1785.

Lin, Yuan-Chung, Hsu, Kuo-Hsiang, Chen, & Chung-Bang. (2011). Experimental investigation of the performance and emissions of a heavy-duty diesel engine fueled with waste cooking oil biodiesel/ultra-low sulfur diesel blends. Energy, 36(1), 241-248.

Lin, C.-Y., & Chiu, C.-C. (2010). Burning characteristics of palm-oil biodiesel under long-term storage conditions. Energy Conversion and Management, 51(7), 1464-1467.

Lin, C.-Y., & Lin, H.-A. (2006). Diesel engine performance and emission characteristics of biodiesel produced by the peroxidation process. Fuel, 85(3), 298-305.

Lin, Y.-C., Kan, T.-H., Chen, J.-N., Tsai, J.-C., Ku, Y.-Y., & Lin, K.-W. (2013). Tribological performance of engine oil blended with various diesel fuels. Tribology Transactions, 56(6), 997-1010.

Lopez, D., Schreiner, W., De Sánchez, S., & Simison, S. (2003). The influence of carbon steel microstructure on corrosion layers: an XPS and SEM characterization. Applied Surface Science, 207(1), 69-85.

Lovell, M., & Deng, Z. (1999). Experimental investigation of sliding friction between hard and deformable surfaces with application to manufacturing processes. Wear, 236(1), 117-127.

Lu, X, Cotter, J, Eadie, & DT. (2005). Laboratory study of the tribological properties of friction modifier thin films for friction control at the wheel/rail interface. Wear, 259(7), 1262-1269.

M Bento, F., & C Gaylarde, C. (2001). Biodeterioration of stored diesel oil: studies in Brazil. International biodeterioration & biodegradation, 47(2), 107-112.

Maleque, MA, Masjuki, HH, Haseeb, & ASMA. (2000). Effect of mechanical factors on tribological properties of palm oil methyl ester blended lubricant. Wear, 239(1), 117-125.

Mall, Deo, I., Srivastava, Chandra, V., Agarwal, Kumar, N., Mani, I. (2005). Adsorptive removal of malachite green dye from aqueous solution by bagasse fly ash and activated carbon-kinetic study and equilibrium isotherm analyses. Colloids and Surfaces A: Physicochemical and Engineering Aspects, 264(1), 17-28.

Mankowski, G., Duthil, P., J., Giusti, & A. (1997). The pit morphology on copper in chloride- and sulphate-containing solutions. Corrosion Science, 39(1), 27-42. doi: http://dx.doi.org/10.1016/S0010-938X(96)00100-X

Martinez, S., & Štern, I. (2001). Inhibitory mechanism of low-carbon steel corrosion by mimosa tannin in sulphuric acid solutions. Journal of Applied Electrochemistry, 31(9), 973-978.

Maru, Marie, M., Lucchese, Maria, M., Legnani, Cristiano, Carreteiro, J. (2009). Biodiesel compatibility with carbon steel and HDPE parts. Fuel processing technology, 90(9), 1175-1182.

Maru, M. M., Trommer, R. M., Cavalcanti, K. F., Figueiredo, E. S., Silva, R. F., & Achete, C. A. (2014). The Stribeck curve as a suitable characterization method of the lubricity of biodiesel and diesel blends. Energy, 69, 673-681. doi: http://dx.doi.org/10.1016/j.energy.2014.03.063

Masjuki, HH, Maleque, MA, Kubo, Aizoh, Tetsuya. (1999). Palm oil and mineral oil based lubricants—their tribological and emission performance. Tribology International, 32(6), 305-314.

Masjuki, HH., & Maleque, M. (1996). The effect of palm oil diesel fuel contaminated lubricant on sliding wear of cast irons against mild steel. Wear, 198(1), 293-299.

McCormick, L, R., Graboski, S, M., Alleman, L, T., Shaine, K. (2001). Impact of biodiesel source material and chemical structure on emissions of criteria pollutants from a heavy-duty engine. Environmental science & technology, 35(9), 1742-1747.

Melero, J. A., Calleja, G., Garcia, A., Clavero, M., Hernandez, E. A., Miravalles, R., & Galindo, T. (2010). Storage stability and corrosion studies of renewable raw materials and petrol mixtures: A key issue for their co-processing in refinery units. Fuel, 89(3), 554-562. doi: http://dx.doi.org/10.1016/j.fuel.2009.09.026

Minami, I., & Mitsumune, S. (2002). Antiwear properties of phosphorous-containing compounds in vegetable oils. Tribology Letters, 13(2), 95-101.

Mistry, K, K., Morina, Ardian, Neville, & Anne. (2011). A tribochemical evaluation of a WC–DLC coating in EP lubrication conditions. Wear, 271(9), 1739-1744.

Mofijur, M., Masjuki, H. H., Kalam, M. A., Atabani, A. E., Shahabuddin, M., Palash, S. M., & Hazrat, M. A. (2013). Effect of biodiesel from various feedstocks on combustion characteristics, engine durability and materials compatibility: A review. Renewable and Sustainable Energy Reviews, 28, 441-455. doi: http://dx.doi.org/10.1016/j.rser.2013.07.051

Mohsin, R, Majid, ZA, Shihnan, AH, . . . Z. (2014). Effect of biodiesel blends on engine performance and exhaust emission for diesel dual fuel engine. Energy Conversion and Management, 88, 821-828.

Monyem, A., & H Van Gerpen, J. (2001). The effect of biodiesel oxidation on engine performance and emissions. Biomass and Bioenergy, 20(4), 317-325.

Monyem, A., & Van Gerpen, J. H. (2001). The effect of biodiesel oxidation on engine performance and emissions. Biomass and Bioenergy, 20(4), 317-325.

Morris, N, Rahmani, Ramin, Rahnejat, Homer, Brian. (2013). Tribology of piston compression ring conjunction under transient thermal mixed regime of lubrication. Tribology International, 59, 248-258.

Mosarof, M. H., Kalam, M. A., Masjuki, H. H., Alabdulkarem, A., Habibullah, M., Arslan, A., & Monirul, I. M. (2016). Assessment of friction and wear characteristics of Calophyllum inophyllum and palm biodiesel. Industrial Crops and Products, 83, 470-483. doi: http://dx.doi.org/10.1016/j.indcrop.2015.12.082

Mosarof, M. H., Kalam, M. A., Masjuki, H. H., Ashraful, A. M., Rashed, M. M., Imdadul, H. K., & Monirul, I. M. (2015). Implementation of palm biodiesel based on economic aspects, performance, emission, and wear characteristics. Energy Conversion and Management, 105, 617-629. doi: http://dx.doi.org/10.1016/j.enconman.2015.08.020

Moser, R, B., Eller, J, F., Tisserat, H, B., Alan. (2011). Preparation of fatty acid methyl esters from osage orange (Maclura pomifera) oil and evaluation as biodiesel. Energy & fuels, 25(4), 1869-1877.

Moser, B. R., & Vaughn, S. F. (2010). Evaluation of alkyl esters from Camelina sativa oil as biodiesel and as blend components in ultra low-sulfur diesel fuel. Bioresource Technology, 101(2), 646-653.

Muik, Barbara, Lendl, Bernhard, Molina-Díaz, Antonio, José, M. (2005). Direct monitoring of lipid oxidation in edible oils by Fourier transform Raman spectroscopy. Chemistry and physics of lipids, 134(2), 173-182.

Munson, W, J., Hertz, Barry, P., Dalai, K, A., J, M. (1999). Lubricity Survey of Low–Level Biodiesel Fuel Additives Using the "Munson ROCLE" Bench Test: SAE Technical Paper.

Murugesan, A, Umarani, C, Subramanian, R. N. (2009). Bio-diesel as an alternative fuel for diesel engines—a review. Renewable and Sustainable Energy Reviews, 13(3), 653-662.

Musa, A. Y., Kadhum, A. A. H., Mohamad, A. B., Daud, A. R., Takriff, M. S., & Kamarudin, S. K. (2009). A comparative study of the corrosion inhibition of mild steel in sulphuric acid by 4, 4-dimethyloxazolidine-2-thione. Corrosion Science, 51(10), 2393-2399.

Nakasa, M. (1995). Engine friction overview. Paper presented at the Proceedings of International Tribology Conference, Yokohama, Japan.

Neff, W., Selke, E., Mounts, T., Rinsch, W., Frankel, E., & Zeitoun, M. (1992). Effect of triacylglycerol composition and structures on oxidative stability of oils from selected soybean germplasm. Journal of the American Oil Chemists' Society, 69(2), 111-118.

Norouzi, Shahrouz, Eslami, Farshad, Wyszynski, L, M., Athanasios. (2012). Corrosion effects of RME in blends with ULSD on aluminium and copper. Fuel processing technology, 104, 204-210.

Oğuz, Hidayet, Düzcükoğlu, Hayrettin, Ekinci, & Şerafettin. (2011). The investigation of lubrication properties performance of Euro-diesel and biodiesel. Tribology Transactions, 54(3), 449-456.

Onions, R., & Archard, J. (1973). The contact of surfaces having a random structure. Journal of Physics D: Applied Physics, 6(3), 289.

Palash, S. M., Kalam, M. A., Masjuki, H. H., Arbab, M. I., Masum, B. M., & Sanjid, A. (2014). Impacts of NOx reducing antioxidant additive on performance and emissions of a multi-cylinder diesel engine fueled with Jatropha biodiesel blends. Energy Conversion and Management, 77(0), 577-585. doi: http://dx.doi.org/10.1016/j.enconman.2013.10.016

Papavinasam, S, Revie, RW, Attard, M. (2003). Comparison of techniques for monitoring corrosion inhibitors in oil and gas pipelines. Corrosion, 59(12), 1096-1111.

Pasqualino, C, J., Montane, Daniel, Salvado, & Joan. (2006). Synergic effects of biodiesel in the biodegradability of fossil-derived fuels. Biomass and Bioenergy, 30(10), 874-879.

Pasqualino, C., J., Montané, Daniel, Salvadó, & Joan. (2006). Synergic effects of biodiesel in the biodegradability of fossil-derived fuels. Biomass and Bioenergy, 30(10), 874-879. doi: http://dx.doi.org/10.1016/j.biombioe.2006.03.002

Pehan, Stanislav, Jerman, Svoljšak, M., Kegl, Marko, Breda. (2009). Biodiesel influence on tribology characteristics of a diesel engine. Fuel, 88(6), 970-979.

Prieto, Gonzalez, L., Sorichetti, PA, Romano, & SD. (2008). Electric properties of biodiesel in the range from 20Hz to 20MHz. Comparison with diesel fossil fuel. International Journal of Hydrogen Energy, 33(13), 3531-3537.

Qi, D., Geng, L., Chen, H., Bian, Y., Liu, J., & Ren, X. (2009). Combustion and performance evaluation of a diesel engine fueled with biodiesel produced from soybean crude oil. Renewable energy, 34(12), 2706-2713.

Rashid, Umer, Anwar, Farooq, Moser, R, B.,Gerhard. (2008). A possible source of biodiesel, Bioresource Technology. Bioresource Technology, 99(17), 8175-8179.

Reeves, J, C., Menezes, L, P., Jen, Tien-Chien,R. M. (2012). Evaluating the tribological performance of green liquid lubricants and powder additive based green liquid lubricants. Paper presented at the Proceedings of 2012 STLE Annual Meeting & Exhibition, STLE.

Reeves, C. J. (2013). An Experimental Investigation Characterizing the Tribological Performance of Natural and Synthetic Biolubricants Composed of Carboxylic Acids for Energy Conservation and Sustainability.

Ren, Siming, Zheng, Shaoxian, Pu, Jibin, Guangan. (2015). Study of tribological mechanisms of carbon-based coatings in antiwear additive containing lubricants under high temperature. RSC Advances, 5(81), 66426-66437.

Rizwanul, IM, Masjuki, HH, Kalam, M., Mofijur, M., & Abedin, M. (2014). Effect of antioxidant on the performance and emission characteristics of a diesel engine fueled with palm biodiesel blends. Energy Conversion and Management, 79, 265-272.

Rizwanul Fattah, I., Masjuki, H., Liaquat, A., Ramli, R., Kalam, M., & Riazuddin, V. (2013). Impact of various biodiesel fuels obtained from edible and non-edible oils on engine exhaust gas and noise emissions. Renewable and Sustainable Energy Reviews, 18, 552-567.

Romero, M., Pizzi, A., Toscano, G., Busca, G., Bosio, B., & Arato, E. (2015). Deoxygenation of waste cooking oil and non-edible oil for the production of liquid hydrocarbon biofuels. Waste Management.

Ryu, K. (2009). Effect of antioxidants on the oxidative stability and combustion characteristics of biodiesel fuels in an indirect-injection (IDI) diesel engine. Journal of mechanical science and technology, 23(11), 3105-3113.

Saad, Bahruddin, Wai, Tatt, W., Lim, & Peng, B. (2008). Comparative study on oxidative decomposition behavior of vegetable oils and its correlation with iodine value using thermogravimetric analysis. Journal of oleo science, 57(4), 257-261.

Salaheldeen, M., Aroua, M. K., Mariod, A. A., Cheng, S. F., Abdelrahman, M. A., & Atabani, A. E. (2015). Physicochemical characterization and thermal behavior of biodiesel and biodiesel–diesel blends derived from crude Moringa peregrina seed oil. Energy Conversion and Management, 92(0), 535-542. doi: http://dx.doi.org/10.1016/j.enconman.2014.12.087

Sarin, Amit, Arora, Rajneesh, Singh, N.P. (2009). Influence of metal contaminants on oxidation stability of Jatropha biodiesel. Energy, 34(9), 1271-1275.

Sarvi, Arto, Fogelholm, Carl-Johan, Zevenhoven, & Ron. (2008). Emissions from large-scale medium-speed diesel engines: 2. Influence of fuel type and operating mode. Fuel processing technology, 89(5), 520-527.

Sarvi, Arto, Kilpinen, Pia, Zevenhoven, & Ron. (2009). Emissions from large-scale medium-speed diesel engines: 3. Influence of direct water injection and common rail. Fuel processing technology, 90(2), 222-231.

Shafiee, S., & Topal, E. (2009). When will fossil fuel reserves be diminished? Energy Policy, 37(1), 181-189. doi: http://dx.doi.org/10.1016/j.enpol.2008.08.016

Shahabuddin, M., Masjuki, H., H., Kalam, A., M. (2012). Effect of Additive on Performance of C.I. Engine Fuelled with Bio Diesel. Energy Procedia, 14(0), 1624-1629. doi: http://dx.doi.org/10.1016/j.egypro.2011.12.1143

Shahabuddin M, Liaquat, AM, Masjuki, HH, Kalam, M.A. (2013). Ignition delay, combustion and emission characteristics of diesel engine fueled with biodiesel. Renewable and Sustainable Energy Reviews, 21, 623-632.

Shahir, A., S., Masjuki, H., H., Kalam, A., M. (2015). Performance and emission assessment of diesel–biodiesel–ethanol/bioethanol blend as a fuel in diesel engines: A review. Renewable and Sustainable Energy Reviews, 48, 62-78. doi: http://dx.doi.org/10.1016/j.rser.2015.03.049

Shahir, K., V., Jawahar, P., C., Suresh, & R., P. (2015). Comparative study of diesel and biodiesel on CI engine with emphasis to emissions—A review. Renewable and Sustainable Energy Reviews, 45, 686-697. doi: http://dx.doi.org/10.1016/j.rser.2015.02.042

Sharma, K, B., Adhvaryu, A, Erhan, & Z, S. (2009). Friction and wear behavior of thioether hydroxy vegetable oil. Tribology International, 42(2), 353-358.

Sharma, YC, Singh, B, Upadhyay, & SN. (2008). Advancements in development and characterization of biodiesel: a review. Fuel, 87(12), 2355-2373.

Sharma, B. K., Doll, K. M., & Erhan, S. Z. (2008). Ester hydroxy derivatives of methyl oleate: tribological, oxidation and low temperature properties. Bioresource Technology, 99(15), 7333-7340.

Shay, E. G. (1993). Diesel fuel from vegetable oils: status and opportunities. Biomass and Bioenergy, 4(4), 227-242.

Shiotani, H., & Goto, S. (2007). Studies of fuel properties and oxidation stability of biodiesel fuel: SAE Technical Paper.

Singh, B, Korstad, John, Sharma, & YC. (2012). A critical review on corrosion of compression ignition (CI) engine parts by biodiesel and biodiesel blends and its inhibition. Renewable and Sustainable Energy Reviews, 16(5), 3401-3408.

Singh, A., Singh, V., & Quraishi, M. (2010). Aqueous extract of kalmegh (Andrographis paniculata) leaves as green inhibitor for mild steel in hydrochloric acid solution. International Journal of Corrosion, 2010.

Singh, S., & Singh, D. (2010). Biodiesel production through the use of different sources and characterization of oils and their esters as the substitute of diesel: a review. Renewable and Sustainable Energy Reviews, 14(1), 200-216.

Smith, W. F., & Hashemi, J. (2011). Foundations of materials science and engineering: McGraw-Hill.

Sorate, K., & Bhale, P. (2013). Impact of biodiesel on fuel system materials durability. Journal of Scientific and Industrial Research, 72, 48-57.

Sorate, K. A., & Bhale, P. V. (2015). Biodiesel properties and automotive system compatibility issues. Renewable and Sustainable Energy Reviews, 41, 777-798.

Sørensen, , G., Pedersen, V, D., Nørgaard, K, A. (2011). Microbial growth studies in biodiesel blends. Bioresource Technology, 102(8), 5259-5264.

Sørensen, Gitte, Pedersen, V, D., Nørgaard, K, A. (2011). Microbial growth studies in biodiesel blends. Bioresource Technology, 102(8), 5259-5264.

Spearot, J. (2000). May 2000. Paper presented at the Friction, wear, health, and environmental impacts tribology in the new millennium. A keynote lecture at the STLE Annual Meeting. Nashville, Tennessee.

Sperring, T., & Nowell, T. (2005). SYCLOPS—a qualitative debris classification system developed for RAF early failure detection centres. Tribology International, 38(10), 898-903.

Squarcialupi, Cristina, M., Bernardini, Piero, G., Faso, Valentina, Gianfranco. (2002). Characterisation by XPS of the corrosion patina formed on bronze surfaces. Journal of Cultural Heritage, 3(3), 199-204.

Srivastava, A., & Prasad, R. (2000). Triglycerides-based diesel fuels. Renewable and Sustainable Energy Reviews, 4(2), 111-133.

Stachowiak, G., & Batchelor, A. W. (2013). Engineering tribology: Butterworth-Heinemann.

Standard, A. (2003). G1-03. Standard Practice for preparing, cleaning, and evaluating corrosion test specimens, Annual Book of ASTM Standards, 3, 17-25.

Standard, A. (2004). D6079: Standard Test Method for Evaluating Lubricity of Diesel Fuels by the High-Frequency Reciprocating Rig (HFRR). American Society for Testing and Materials, West Conshohocken, PA (USA).

Stanfel, C. (2009). Fuel filtration: Protecting the diesel engine. Filtration & Separation, 46(3), 22-25.

Stedile, T., Ender, L., Meier, F., H. (2015). Comparison between physical properties and chemical composition of bio-oils derived from lignocellulose and triglyceride sources. Renewable and Sustainable Energy Reviews, 50, 92-108. doi: http://dx.doi.org/10.1016/j.rser.2015.04.080

Sulek, W., M., Kulczycki, A., Malysa, & A. (2010). Assessment of lubricity of compositions of fuel oil with biocomponents derived from rape-seed. Wear, 268(1–2), 104-108. doi: http://dx.doi.org/10.1016/j.wear.2009.07.004

Szybist, P, J., Song, Juhun, Alam, Mahabubul, L. A. (2007). Biodiesel combustion, emissions and emission control. Fuel processing technology, 88(7), 679-691.

Tang, H., Abunasser, N., Wang, A., Clark, B. R., Wadumesthrige, K., Zeng, S., Wilson, J. (2008). Quality survey of biodiesel blends sold at retail stations. Fuel, 87(13), 2951-2955.

Tebbji, K., Faska, N., Tounsi, A., Oudda, H., Benkaddour, M., & Hammouti, B. (2007). The effect of some lactones as inhibitors for the corrosion of mild steel in 1M hydrochloric acid. Materials Chemistry and Physics, 106(2), 260-267.

Thamsiriroj, T., & Murphy, J. D. (2011). A critical review of the applicability of biodiesel and grass biomethane as biofuels to satisfy both biofuel targets and sustainability criteria. Applied Energy, 88(4), 1008-1019.

Tsuchiya, Takehiro, Shiotani, H., Goto, S., Sugiyama, G., & Maeda, A. (2006). Japanese standards for diesel fuel containing 5% FAME: Investigation of acid generation in FAME blended diesel fuels and its impact on corrosion: SAE Technical Paper.

Tsuchiya, T., Shiotani, H., Goto, S., Sugiyama, G., & Maeda, A. (2006). Japanese standards for diesel fuel containing 5% FAME: Investigation of acid generation in FAME blended diesel fuels and its impact on corrosion: SAE Technical Paper.

Tung, S. C., & McMillan, M. L. (2004). Automotive tribology overview of current advances and challenges for the future. Tribology International, 37(7), 517-536.

Tyson, K. (2009). Biodiesel handling and use guidelines: DIANE Publishing.

Vohrer, U, Blomfield, C, Page, S. A. (2005). Quantitative XPS imaging—new possibilities with the delay-line detector. Applied Surface Science, 252(1), 61-65.

Von Wallbrunn, Angelika, Richnow, H. H., Neumann, G., Meinhardt, F., & Heipieper, H. J. (2003). Mechanism of cis-trans isomerization of unsaturated fatty acids in Pseudomonas putida. Journal of bacteriology, 185(5), 1730-1733.

Wain, S., K., Perez, M., J., Chapman, Elana, L. A. (2005). Alternative and low sulfur fuel options: boundary lubrication performance and potential problems. Tribology International, 38(3), 313-319. doi: http://dx.doi.org/10.1016/j.triboint.2004.08.014

Wang, Wei, Jenkins, E, P., Ren, & Zhiyong. (2011). Heterogeneous corrosion behaviour of carbon steel in water contaminated biodiesel. Corrosion Science, 53(2), 845-849.

Williams, J. (2005). Engineering tribology: Cambridge University Press.

Xu, Y. F., Yu, H. Q., Wei, X. Y., Cui, Z., Hu, X. G., Xue, T., & Zhang, D. Y. (2013). Friction and Wear Behaviors of a Cylinder Liner–Piston Ring with Emulsified Bio-Oil as Fuel. Tribology Transactions, 56(3), 359-365.

Yaakob, Zahira, Narayanan, N, B., Padikkaparambil, & Silija. (2014). A review on the oxidation stability of biodiesel. Renewable and Sustainable Energy Reviews, 35, 136-153.

Yamane, K, Kawasaki, K, Sone, K. T. (2007). Oxidation stability of biodiesel and its effects on diesel combustion and emission characteristics. International Journal of Engine Research, 8(3), 307-319.

Yıldırım, A., & Cetin, M. (2008). Synthesis and evaluation of new long alkyl side chain acetamide, isoxazolidine and isoxazoline derivatives as corrosion inhibitors. Corrosion Science, 50(1), 155-165.

Yufu Xu, Wang, Qiongjie, Hu, Xianguo, Li, Xifeng. (2010). Characterization of the lubricity of bio-oil/diesel fuel blends by high frequency reciprocating test rig. Energy, 35(1), 283-287.

Zhang, Xiulin, Peterson, Charles, Reece, Daryl, G. (1998). Biodegradability of biodiesel in the aquatic environment. Transactions of the ASAE, 41(5), 1423.

Zhang, B., He, C., Wang, C., Sun, P., Li, F., & Lin, Y. (2015). Synergistic corrosion inhibition of environment-friendly inhibitors on the corrosion of carbon steel in soft water. Corrosion Science, 94, 6-20. doi: http://dx.doi.org/10.1016/j.corsci.2014.11.035

Zulkifli, , N., Kalam, M., Masjuki, H., Shahabuddin, M., & Yunus, R. (2013). Wear prevention characteristics of a palm oil-based TMP (trimethylolpropane) ester as an engine lubricant. Energy, 54, 167-173.

LIST OF PUBLICATION AND PAPERS PRESENTED

Accepted articles in journals

i. **Sazzad, B.S.,** Fazal, M.A., Haseeb, A.S.M.A. Masjuki, H.H. (2016). Retardation of oxidation and material degradation in biodiesel: A review, *RSC Advance Review* **[ISI indexed; Quartile 1]**

ii. Fazal, M.A., **Sazzad, B.S.,** Haseeb, A.S.M.A. Masjuki, H.H. (2016). Inhibition study of additives towards corrosion of ferrous metal in palm biodiesel, *Energy Conversion and Management* **[ISI indexed; Quartile 1]**

Submitted articles in journals

i. Inhibition performance and adsorption properties of tert-butylamine against corrosion of cast iron in palm biodiesel, **Renewable energy/ Under review**.

ii. Adsorption Kinetics of tert-butylamine on cast iron exposed to B20, **Journal of the Taiwan Institute of Chemical Engineers / Under review**.

iii. Tribological performance of B20 biodiesel-diesel blend, **Journal of Mechanical Science and Technology / Under review**.

iv. Lubricity assessment of the biodiesel in presence of different additives, **Energy Conversion and Management/ Submitted.**

Accepted article in conferences

i. **Sazzad, B.S.,** Fazal, M.A., Haseeb, A.S.M.A. Masjuki, H.H. (2016). Corrosion retardation of low carbon steel in palm biodiesel, *17th Asian Pacific Corrosion Control Conference*, 2016, IIT Bombay, India.

ii. **Sazzad, B.S.,** Fazal, M.A., Haseeb, A.S.M.A. Masjuki, H.H. (2016). Effect of Additive Concentrations on Retardation of Tribological Degradation of

Cast Iron Metal in Palm Biodiesel, *Advances in Materials and Processing Technologies Conference (AMPT 2016)*, 08-11th November 2016, Kuala Lumpur, Malaysia.

Award

i. **Sazzad, B.S.,** Fazal, M.A., Haseeb, A.S.M.A. Masjuki, H.H. (2016). Corrosion retardation of low carbon steel in palm biodiesel, **got 3rd prize in** *17th Asian Pacific Corrosion Control Conference*, 2016, IIT Bombay, India.